Fundamentals of SPME extraction of tissue and plasma: experimental and in-silico approaches

by

Mohammad Huq

A thesis
presented to the University of Waterloo
in fulfillment of the
thesis requirement for the degree of
Doctor of Philosophy
in
Chemistry

Waterloo, Ontario, Canada, 2021

# Examining Committee Membership

The following served on the Examining Committee for this thesis. The decision of the Examining

Committee is by majority vote.

External Examiner                             Professor Rainer Bischoff

University of Groningen

Netherlands

Supervisor                                       Prof. Janusz Pawliszyn

University Professor and Canada Research Chair

Department of Chemistry, University of Waterloo

Internal Member                            Prof. Michael Palmer

Associate Professor

Department of Chemistry, University of Waterloo

Internal Member                            Prof. Wojciech Gabryelski

Associate Professor

Department of Chemistry, University of Guelph

Internal-external Member                Prof. Luis Ricardez-Sandoval.

Professor

Department of Chemical Engineering

University of Waterloo

# Author Declaration

I hereby declare that I am the sole author of this thesis. This is a true copy of the thesis, including

any required final revisions, as accepted by my examiners.

I understand that my thesis may be made electronically available to the public.

# Abstract

Over the last three decades, solid-phase microextraction (SPME) has continuously evolved and received recognition as a useful tool in various scientific fields. Notable applications have been published including environmental analysis, in vivo drug monitoring, direct coupling to mass spectrometers, and analysis of complex biological samples such as tissue matrix, etc. Much of this success stems from the intrinsic simplicity of SPME's use, variable configurational geometry to promote experimental suitability, and most prominently, the ability to extract target analytes selectively via the free concentration. However, the theory and concept of SPME are much more complex than its simple practical handling. Rigorous fundamental and experimental studies are required before optimizing SPME to facilitate the simplification of many analytical applications. Computational models are required to reduce the extent of experimental studies and refine theoretical concepts. In this regard, numerical models have been increasingly used in SPME over the last six years. In particular, understanding how the mass transfer is controlled by the thickness of the extraction phase, the shape of the SPME device, and the important effect of the presence of binding matrices in samples. In this thesis, computational models were developed to demonstrate how binding matrices contribute to the mass transfer of analytes to the SPME extraction phase.

Chapter 1 provides an overview of matrix components, SPME, and the use of computational modeling. Chapter 2 describes the SPME mass transfer kinetics in the biological tissue matrix. The anticancer drug doxorubicin (DOX) was chosen as a model for this study. Its activity is controlled by the free concentration in the extracellular space that crosses the cell membrane to bind with a specific receptor. However, the distribution of DOX in the tissue matrix

is very dynamic as it binds heavily with human serum albumin (HSA), cell membrane, and other macromolecules. It is cleared from the body through renal excretion. Therefore, the total concentration measurement followed by conventional analytical methods does not represent the bioactivity of DOX in the tissue matrix. Accordingly, a suitable analytical technique was developed for the determination of the free in situ concentration of DOX in the extracellular space where it is bound to multiple binding matrix components. Commercially available mixed-mode bio-SPME fibers using coating consisting of C8 and weak cation exchange (WCX) materials were used to extract DOX via the free form from a surrogate tissue matrix – bovine lung tissue. Computational models were developed to determine the mass transfer of DOX during extraction and how binding matrices control the distribution of DOX in the tissue matrix as well as the mass transfer onto the extraction phase. The investigations revealed that DOX is 99.97% bound to the tissue matrix, with its free concentration profoundly depleted in the extracellular space. The free concentration was not affected by the mass transfer to the extraction phase due to instant release from binding matrices, which indicated that binding matrices serve as a reservoir of DOX. 3D computational models were developed in COMSOL Multiphysics based on experimentally obtained physical parameters and available literature values to demonstrate the mass transfer between different reservoirs in the tissue matrix. The development of computational models involved experiment-based simulation of DOX extraction in matrix-free solid medium (agar gel) at static conditions, followed by extraction of DOX spiked in PBS solution to demonstrate how convection contributes to the mass transfer. Finally, a computational model was developed to demonstrate the effect of the HSA binding matrix on the mass transfer of DOX under agitation conditions. Results showed that mass transfer in tissue was faster than during extraction from even agitated PBS solution

without HSA binding matrix, implying that binding matrix contributes to the mass transfer through releasing bound analyte within the boundary layer. Furthermore, a computational model was developed to demonstrate the mass transfer in the tissue matrix. The results showed that mass transfer in tissue is profoundly faster than agitated extraction in PBS solution with HSA binding matrix, even though it takes place in static conditions. This study demonstrated how the binding matrix controls the mass transfer and distribution of free analyte that is of interest to quantitative pharmacokinetics and pharmacodynamics.

In Chapter 3, SPME was used to investigate the complex binding equilibrium between fatty acids (FA) and HSA. HSA is the main cargo molecule for FAs in the human body and in normal physiological conditions, almost 99% of FAs are bound to it. HSA has multiple FA binding sites, which are heterogeneously distributed in three structurally similar domains of HSA. The affinities of these binding sites are not identical, which results in multiple binding equilibria with FAs, dependent on the ligands' initial concentration. The binding characteristics of FAs with HSA could be altered by the allosteric modification which is related to important pathological information. The requirement of accurate measurement of free FAs has been fulfilled in this study by SPME, due to the technique's capability to determine the free concentration in complex matrices. Both site-oriented and stoichiometric approaches were used to analyze the binding characteristics. Computational models were developed to demonstrate the mass transfer kinetics of FA within the HSA binding matrix. The apparent binding constant of FAs to HSA was determined followed by a Scatchard plot and used to simulate the extraction kinetics of FAs. In-silico results demonstrated good fitting with experimental data, which indicates the reliability of this method. Also,

stoichiometric binding constants were determined using a nonlinear least-square regression model.

The overall work reported in this thesis reflects on experimental and computational approaches of SPME techniques to measure the mass transfer of free analyte from complex matrices where the analyte is involved in multiphase equilibria with binding components that control the rate of mass transfer to the extraction phase.

# Acknowledgments

First of all, I am grateful to the Almighty Creator and Sustainer for helping me all the way to accomplish this thesis.

I would like to thank my supervisor, Professor Janusz Pawliszyn, for his guidance throughout my Ph.D. studies for this inspiring and challenging project.

I am thankful to all my committee members, Professor Michael Palmer, Professor Wojciech Gabryelski, and Professor Luis Ricardez Sandoval for their effort to improve my research journey by providing thoughtful suggestions. I would also like to thank my internal-external examiner, Professor Luis Ricardez-Sandoval, for his constructive suggestion to improve the thesis.

Dedication

To my parents:

Md Fazlul Huq & Akter Zahan

# Table of Contents

# List of figures

# List of Tables

# List of Abbreviations

| | |
|---|---|
| ACN | Acetonitrile |
| aLA | Alpha linoleic acid |
| BET | Brunauer, Emmett and Teller |
| BSA | Bovine serum albumin |
| CAD | Computer aided design |
| CMC | Critical micelle concentration |
| CW | Carbowax |
| DOX | Doxorubicin |
| ECM | Extracellular matrix |
| ED | Equilibrium dialysis |
| EPR | Electron paramagnetic resonance |
| ESI | Electrospray ionization |
| FA | Fatty acid |
| FEM | Finite element method |
| IM | Intramuscular |
| IPA | Isopropanol |
| IRS | Insulin receptor substrate |
| ITC | Isothermal titration calorimetry |
| IVLP | In vivo lung perfusion |
| LA | Linoleic acid |
| LC | Liquid chromatography |
| LCMS | Liquid chromatography mass spectrometry |
| LLE | Liquid liquid extraction |
| LOQ | Limit of quantification |
| LSF | Least square fitting |
| MD | Microdialysis |
| MS | Mass spectrometry |
| MW | Molecular weight |
| NEFA | Non-esterified fatty acids |
| NMR | Nuclear magnetic resonance |
| PAN | Polyacrylonitrile |
| PBS | Phosphate buffer saline |
| PD | Pharmacodynamics |
| PDMS | Polydimethylsiloxane |
| PK | Pharmacokinetic |
| PUFA | Polyunsaturated fatty acid |
| RA | Rheumatoid arthritis |
| RBC | Red blood cell |
| RNA | Ribonucleic acid |

| | |
|---|---|
| SC | Subcutaneous |
| SPE | Solid-phase extraction |
| SPME | Solid-phase microextraction |
| SPR | Surface plasmon resonance |
| SRM | Single reaction monitoring |
| SSR | Square sum of residuals |
| T2DM | Type 2 diabetes mellitus |
| UF | Ultrafiltration |
| UHPLC | Ultra-high performance liquid chromatography |
| WBC | White blood cell |
| WCX | Weak cation exchange |

# List of Symbols

| | |
|---|---|
| $a$ | Time constant |
| $A$ | Surface area |
| $b$ | Boundary layer thickness |
| C18 | Octadecyl |
| C8 | Octane |
| $D$ | Diffusion coefficient |
| $K_A$ | Binding association constant |
| $N$ | Flux |

# Chapter 1 Introduction

## 1.1. An overview of blood plasma and tissue components

Blood plasma is the acellular fraction of whole blood which looks light yellowish in color. It is obtained by adding an anticoagulant to whole blood and then removing the blood cells (RBC, WBC, and platelets) by centrifugation (Figure 1). It is the liquid part of whole blood which makes up to 55% of total blood volume. It contains 90-92% water and 7-8% of solid ingredients and <1% dissolved gases. Solid components of plasma can be categorized broadly into two groups- large and small molecules. Among large molecules most notable are plasma proteins such as serum albumin (50-60%), immunoglobulins (35-38%), enzymes, and some hormones, etc. Among small molecules, glucose, lipids, amino acids, neurotransmitters, electrolytes, drug metabolites, nutrients, etc.[1,2,3] Beside plasma another important derivative of blood is serum, which is obtained by coagulation of blood followed by centrifugation. In other words, the serum is the fluid part of the plasma which is basically without fibrinogen - a key blood coagulation factor.
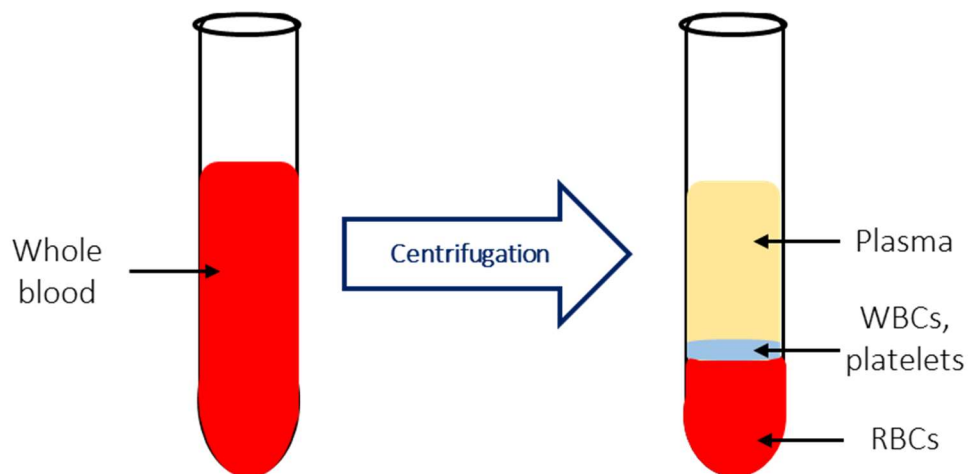
Figure 1. 1 A schematic diagram of whole blood and plasma

The plasma essentially serves as the transport medium which carries all the nutrients to the cells, and it also maintains the intravascular osmotic pressure that controls the balance of electrolytes.[4] Plasma contains numerous different components with a wide dynamic range of abundance. The most abundant plasma component is the human serum albumin (HSA), a large protein (585 amino acid residues) that serves as a transport vehicle for many small molecules including fatty acids, amino acids, bilirubin, hemin, drugs, etc.[5] It binds small molecules through specific or nonspecific interactions and carries them to their respective site of action. Therefore, it works as a reservoir for many small molecules (drugs and fatty acids for example) and plays a vital role by maintaining their bioactive concentrations.[6] Characterization of the binding interaction of drug molecules with albumin is of paramount interest in clinical research for drug development. The binding interaction of analytes with HSA will be described in detail later in chapter 2 and chapter 3.

On the other hand, biological tissue is a complex network structure that is composed of three basic components: cells, extracellular matrix (ECM), and signaling components.[7] From the analytical standpoint adopted in this study, only extracellular matrix components will be discussed here. ECM is a three-dimensional dynamic cross-linked network that is composed of minerals and macromolecules, such as collagen, glycoproteins, polysaccharides, drug molecules, etc. ECM provides physical and mechanical support to the tissue. It regulates all cellular functions such as cell growth, cell proliferation, cell differentiation, and cell homeostasis, etc. All necessary components to maintain cellular functions are available in ECM. However, ECM components are highly dynamic due to continuous cellular processes.[8,9] Therefore, ECM components can provide valuable information on many biological functions. This requires appropriate analytical

techniques to investigate with minimal invasion of the native environment. Chapter 2 will describe detailed ideal analytical techniques to characterize ECM components.

## 1.2. Characterization of plasma components: impact of binding matrices

Blood plasma is the most widely used analytical sample in many biological research fields. Since plasma contains plenty of components that play key roles in cellular and physiological activities such as metabolic reactions and cell signaling, identification and characterization of these components are of great interest in biomedical research fields. For example, characterization of regulatory proteins (enzymes, hormones, etc.) provides information about intra and extracellular reaction pathways, identification of biomarkers is necessary for disease prognosis and diagnosis, characterization of drug molecules and their metabolites is required for pharmacokinetic (PK) and pharmacodynamic (PD) studies in clinical research, and characterization of illicit drugs and poisons in forensic and toxicological studies, etc.[10–16]

Since blood plasma is one of the most complex biological sample matrices, most often characterizations require very sophisticated and tedious analytical techniques to attain accurate information. Due to the presence of a wide range of components with highly variably abundance, separation of low abundant components from the matrix is tremendously challenging – yet it is crucial for quantification.[3] In the case of small molecules, the characterization is made difficult by the presence of highly abundant binding matrices such as HSA. Of particular interest to this thesis are the cases in which the analytes are small molecules, which are heavily bound to the large matrix components - mostly serum albumin.

The extent of such binding interactions results in the perturbation of analytes into matrix-bound and unbound (free) states. The fraction of the analyte that remains unbound (free) participates in physiochemical reactions and is therefore considered the bioactive concentration. Most of the small drug molecules bind with HSA, and the measurement of free/bioactive concentration is an integral part of PK/PD studies in clinical research for drug development. In general, the abundance of binding components (such as HSA, immunoglobulins, etc.) in plasma is significantly higher than that of target analytes (such as pharmaceutical drugs). In such cases, the free analyte concentration predominantly depends on their binding affinities towards the matrix components. Analytes with higher nonpolar character (logP) show stronger binding affinity with matrix components.[17,18] This active concentration is dynamic and subject to changes concerning physiological conditions.[19] We can write the binding reaction between analyte and matrix component as follows:

$$A + M <=> AM \tag{1.1}$$

Where: $A$, is the free analyte, M is the binding matrix component and AM is the matrix-bound analyte. At equilibrium the binding constant for this equilibrium can be defined by the following equation:

$$K_A = \frac{k_f}{k_r} = \frac{[AM]}{[A]^{eq} * [M]} \tag{1.2}$$

Where: $K_A$ is the binding association constant for the analyte $A$, $k_f$ and $k_r$ are the forward (matrix association) and backward (matrix dissociation) rate constants, $[A]^{eq}$ is the free unbound concentration of the analyte when equilibrium is established. This unbound state is the subject of many analytical studies since it represents the active (bioavailable) concentration that

participates in biological activities.

## 1.3. Characterization of plasma components: analytical methods

Most analytical process essentially includes three stages – sampling, sample preparation, and detection. Among these, sample preparation is the bottleneck of the whole analytical process because It is time consuming and tedious.[20] Due to the complex nature of plasma, sample preparation requires multiple experimental steps- sample pretreatment, separation/extraction, sample clean-up, enrichment, and analyte transfer to a detection device, such as liquid chromatography coupled with mass spectrometry (LC-MS). The most popular sample preparation techniques used for plasma components analysis are - liquid-liquid extraction (LLE), solid-phase extraction (SPE), dispersive solid-phase extraction (dSPE), membrane-based separations, such as ultrafiltration (UF) and microdialysis (MD), etc.[21] LLE uses organic solvents to extract or isolate the target analytes, which partition between aqueous and organic phase. For example, extraction of fatty acids (FAs) from blood plasma according to the Bligh-Dyer (BD) method involves the addition of a mixture of chloroform-methanol (1:2). The separation takes place *via* partition between the aqueous and organic phases.[22,23] The organic phase which is enriched with FAs due to their high partition coefficient is separated and then analyzed. SPE uses a solid sorbent for the extraction of a target analyte. The sorbent is packed in a small cartridge through which the sample containing analytes of interest is passed. The separation takes place based on the affinity of the analyte to the sorbent material.[10] In dispersive SPE, the sorbent is dispersed into the sample matrix and separated from the matrix by centrifugation.[24] While the separation in LLE, SPE, and dSPE involves exhaustive extraction, the membrane-based separation technique provides nonexhaustive extraction of analyte *via* free/unbound concentration. Both ultrafiltration and microdialysis use

porous membranes with a low molecular weight cut-off, allowing the permeation of small but not of large molecules. In addition, microdialysis permits *in vivo* analysis.[25] Albeit microdialysis (MD) and ultrafiltration are capable of determining the free concentration, they possess several shortcomings; in particular, their application is limited molecules which are both polar and low molecular weight. The analysis is time consuming, and suffers from low recovery of solutes with low abundance.[24,26]

## 1.4. SPME

To overcome the limitations of traditional sample preparation methods for separating free/unbound analytes from complex biofluids like plasma sample, researchers around the world endeavored to innovate new sample preparation tools that can mitigate the complexities associated with existing techniques. With that mindset a researcher might aim to develop such a novel technique which will be facile, faster, nonexhaustive, noninvasive and also nondestructive which means the sample can be reused. Moreover, such new methods might sample free concentration analyte only. However, no analytical technique can meet all requirements and each analytical technique has its strength and weakness. Nonetheless the best choice would be the one which meets most of the requirements. Such and endeavor was made by Arthur and Pawliszyn in 1990 with the invention of a microextraction device named as solid-phase microextraction (SPME).[20] SPME is a nonexhaustive, noninvasive and solvent free (sample matrix does not require organic solvent) sample preparation technique that extracts analytes *via* free concentration. SPME is able to integrate both sampling and sample preparation steps through development of *in vivo* sample extraction.[21] The recent advancement of SPME directly to mass spectrometry, has further reduced the time and cost of analysis.[27–29]  Although SPME demonstrated great advantages over

traditional sample preparation techniques in many cases, particularly extraction of small molecules from complex biological samples, it is still limited with respect to large molecules; applications to the latter is still at the stage of exploration.[30]

## 1.5. General aspects of solid-phase microextraction (SPME)

Solid-phase microextraction (SPME) is a separation technique developed by Arthur and Pawliszyn in 1990,[31] which includes a micro extraction device to selectively separate the analytes of interest from sample matrices via negligible depletion of free concentration. The extraction device consists of small volume/amount of sorbent (extraction phase) which is essentially a semi-liquid (absorptive) or solid (adsorptive) material such as polydimethylsiloxane (PDMS), C8, C18, carbowax (CW), etc. coated onto a solid support. The rate of mass transfer of analytes is controlled by the diffusion to the boundary layer (Figure 1.2) which is theoretically treated as a stagnant layer of sample matrix. The thickness of the boundary layer can be minimized by applying convection to the sample matrix.[20] The diffusion of analyte in the extraction phase is insignificant compared to the thickness of the coating. SPME is an equilibrium based non-exhaustive extraction technique where the analyte of interest partitions (for absorptive coating such as PDMS) between sample matrix and extraction phase. At equilibrium the distribution of analyte can be expressed as:

$$K_{es} = \frac{c_e^\infty}{c_s^\infty} \tag{1.3}$$
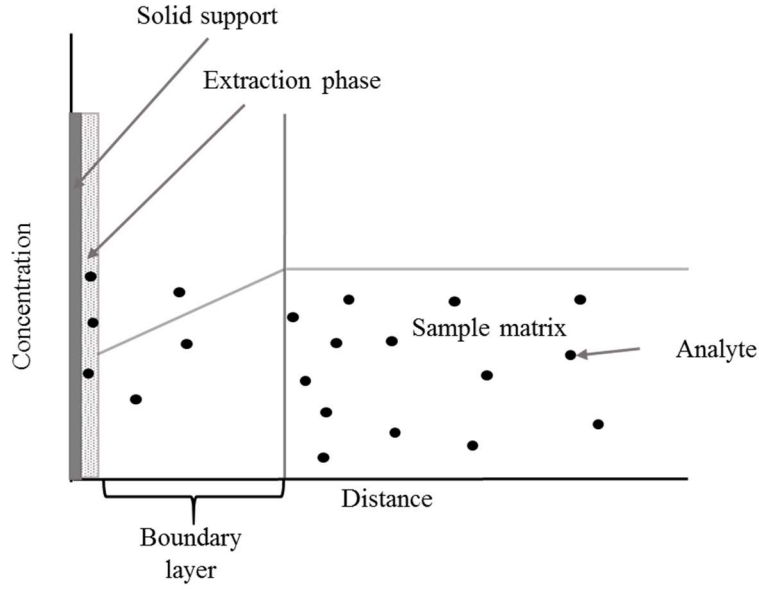
Figure 1. 2 Boundary layer model configuration of SPME extraction in pre-equilibrium stage demonstrating the mass transfer of analytes in different regions in terms of concentration versus distance profile

Where: $K_{es}$ is the distribution constant at equilibrium also known as partition coefficient when the extraction phase is absorptive (semi-liquid such as PDMS), $C_e^\infty$ and $C_s^\infty$ are the concentrations of analyte in the extraction phase and sample matrix respectively. The amount of analyte extracted ($n_e$) under equilibrium can be correlated with the concentration of analyte in the sample matrix by the following equation:

$$n_e = \frac{K_{es}V_eV_s}{K_{es}V_e+V_s} C_s^0 \tag{1.4}$$

Where: $n_e$ is the amount of analyte extracted at equilibrium, $V_e$ is the volume of extraction phase, $V_s$ is the volume of the sample matrix and $C_s^0$ is the initial concentration of analyte in the sample matrix. Since the volume of the extraction phase, $V_e$ is significantly smaller than the sample volume $V_s$, depletion of analyte from the sample matrix is negligible. Under these conditions, $V_s \gg K_{es}V_e$, and eq. (1.4) can be simplified into:

$$n_e = K_{es}V_eC_s^0 \tag{1.5}$$

Eq. (1.5) demonstrates that the amount extracted $(n_e)$ is independent of sample volume $V_s$, which makes it suitable quantitative technique where measurements of sample volume is difficult to determine such as *in vivo* experiments.

## 1.6. Mass transfer in SPME

The driving forces of mass transfer in SPME can be categorized into three factors- diffusion of the analyte in the bulk sample, convection, and matrix assisted mass transfer. The dynamics of mass transfer mechanism can be illustrated as follows:
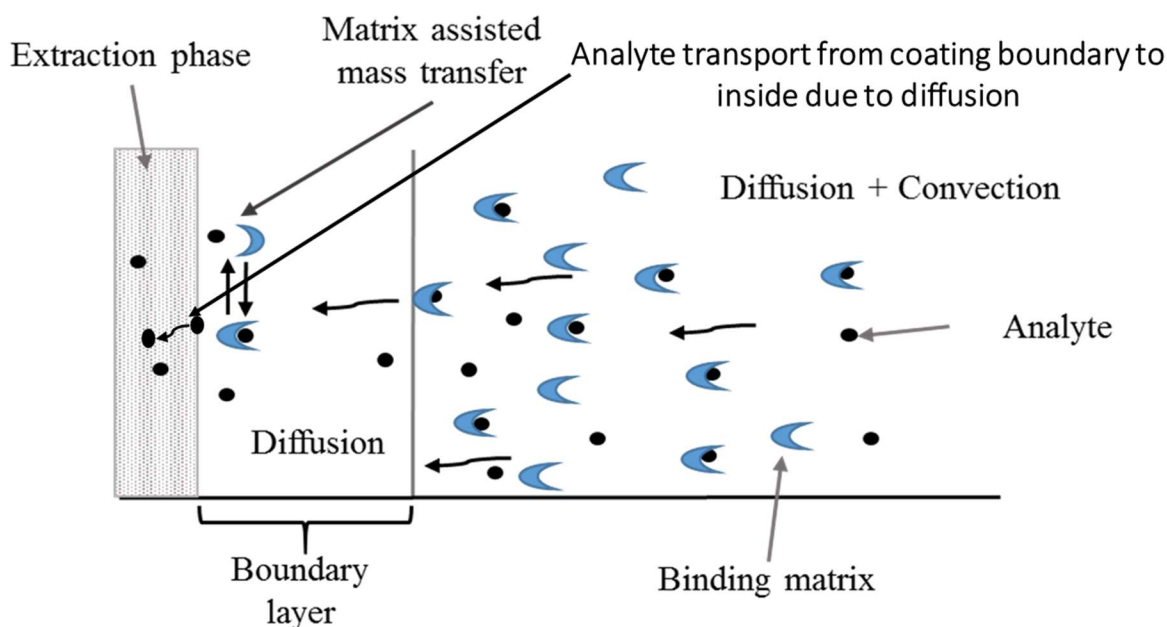


**Figure 1. 3 A schematic diagram shows the factors that contribute to the analyte mass transfer in SPME process**

When an SPME device is immersed in an aqueous sample, mass transfer of the analyte takes place from bulk (high concentration) towards the extraction phase (low concentration) via diffusion in the absence of other external force (such as, convection or reaction). In that case the only driving

for mass transport is diffusion which can be described by Fick's law. The time dependent mass balance equation for diffusion controlled mass transport can be described as:[32]

$$\frac{\partial c}{\partial t} - \nabla * (D_s \nabla c_s) = 0 \tag{1.6}$$

Where: $\frac{\partial c}{\partial t}$ (mol m$^2$ s$^{-1}$) is the molar flux of the species (analyte in this case) $i$, $c_s$ (mol m$^{-3}$) is the total **free** analyte concentration (not total initial concentration) in the sample matrix, $D_s$ (m$^2$ s$^{-1}$) is the diffusivity of analyte $i$ in the sample matrix.

Under agitated condition, mass transport is controlled by both diffusion and convection. The mass balance equation for convective-diffusive mass transfer can be derived as:

$$\frac{\partial c}{\partial t} - \nabla * (D_s \nabla c_s) + \boldsymbol{u} * \nabla c_s = 0 \tag{1.7}$$

Where: $\boldsymbol{u}$ (m s$^{-1}$) is the velocity field of analyte due to convection. When there is any reaction involved in the system, it also contributes to the overall mass transfer by consuming or producing analyte species in the system. In such case, the mass balance equation can be formulated as:

$$\frac{\partial c}{\partial t} - \nabla * (D_s \nabla c_s) + \boldsymbol{u} * \nabla c_s = R \tag{1.8}$$

Where: $R$ is the source term which is the result of either generation or elimination of analyte $i$ in the system. In this case, $R$ corresponds to the matrix assisted mass transfer. The matrix components adjacent to the extraction phase (which are inside the boundary layer) release the bound analyte into the extraction phase due to high affinity of the extraction phase to the target analyte. Since the concentration of the binding matrix components is significantly higher than the concentration of free analyte, the contribution of matrix assisted mass transfer leads the extraction phase to reach equilibrium faster. Therefore $R > 0$ in eq (1.8). The analyte is also transported from the extraction phase to the sample matrix. Since there is no convection in the

extraction phase, and ideally no matrix component is present in the extraction phase (SPME extraction phase is selective and restricts the access of binding matrices) the source term $R = 0$. Therefore, the mass transfer is only governed by the diffusion.

$$\frac{\partial c}{\partial t} - \nabla * (D_e \nabla c_e) = 0 \tag{1.9}$$

Where, $D_e$ is the diffusion coefficient of analyte in the extraction phase and $c_e$ is the analyte concentration in the extraction phase.

## 1.7. Significance of the partition coefficient ($K_{es}$ )

$K_{es}$ is a crucial thermodynamic parameter for analyte under given extraction conditions which depends on mode of extraction (such as headspace or direct immersion), physicochemical properties of the extraction phase material, geometry of the SPME device as well as temperature and pH of the extraction conditions. In typical SPME terminology, $K_{es}$ refers to the affinity of the analyte towards the extraction phase for a given set of extraction conditions. In such case, the net mass transfer kinetics of the analyte can be expressed as:[17]

$$\frac{dc_e^t}{dt} = k_f C_s^t - k_r C_e^t \tag{1.10}$$

Where: $C_s^t$ and $C_e^t$ and are the time dependent concentrations of the analyte in the sample matrix and extraction phase, respectively; $k_f$ and $k_r$ are the forward (uptake) and reverse (release) rate constants of analyte. At equilibrium $k_f C_s = k_r C_e$, therefore the net mass transfer equals zero and eq. (1.10) is reduced to:

$$\frac{C_e^\infty}{C_s^\infty} = \frac{k_f}{k_r} = K_{es} \tag{1.11}$$

Eq. (1.11) states the empirical formula to estimate $K_{es}$. When the initial concentration of the analyte $C_s^0$ is known, one can simply derive the value of $K_{es}$ by measuring the value $C_e^\infty$ followed

by desorption, since $C_s^\infty = C_s^0 - C_e^\infty$. The higher the affinity of the analyte towards the extraction phase, the higher the $C_e^\infty$ value, and the resulting increased $K_{es}$ value requires longer extraction time for the analyte to reach equilibrium (Figure 1.4). Since $K_{es}$ is a thermodynamic constant, it is not affected by the presence of binding matrix components (such as humic materials in water, proteins and nucleic acids in blood plasma, etc.) in samples which are ubiquitous in most analytical samples. The reliance of measurements at equilibrium enables SPME technique to estimate the **free analyte concentration** in the presence of binding matrix components - one of the most exclusive SPME features that makes it unique and allows it to stand out amongst many contemporary sample preparation techniques.
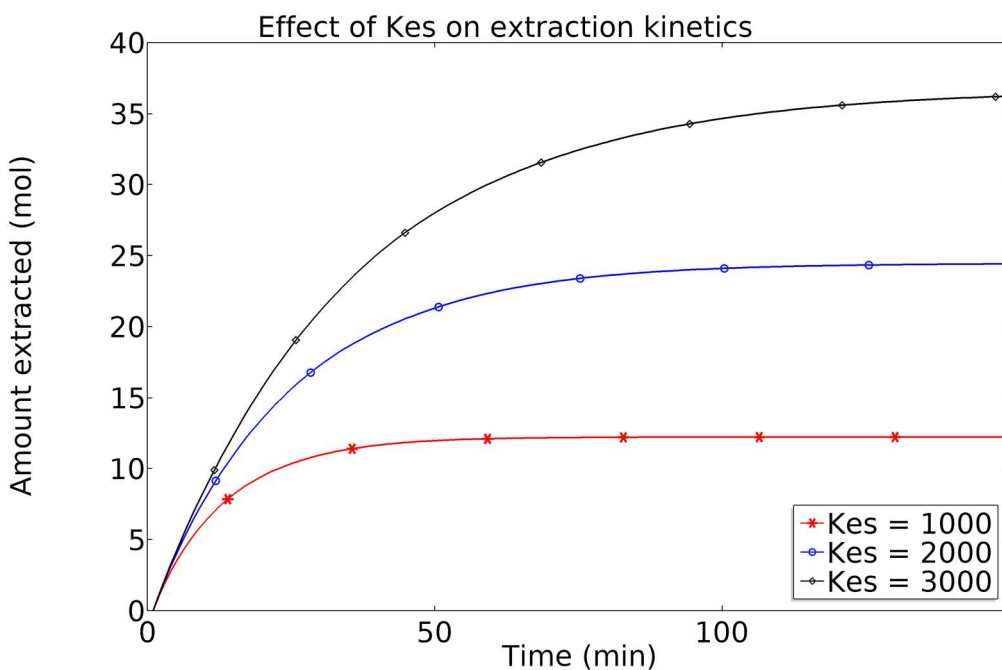


Figure 1. 4 Simulated SPME extraction profile generated by COMSOL Multiphysics using comprehensive physicochemical parameters demonstrates how K_esaffects the extraction time to reach equilibrium, provided all other experimental conditions are kept constant

The 'free' concentration refers to the fraction of the analyte which is unbound to the sample matrix constituents and thus able to participate in the mass transfer through the boundary layer.

12

The binding matrices are usually suspended solids or macromolecules to which free analytes (which are assumed to be small molecules) bind. To acquire extraction via free analyte concentration, it is necessary to restrict the extraction of matrix macromolucules or matrix-bound analytes, which has been achieved by using biocompatible extraction phase (coated with PAN or Teflon binders). The biocompatibility is defined by the immunogenic or toxicological inertness of a material when placed in a biological system. For example, PAN coated SPME fiber demonstrated less interaction with biological matrix components like proteins or macromolecules.[33] This increases the stability of the extraction phase, also produces better analytical results. One of the reasons for biocompatibility is the smoothness of the surface which is enhanced using PAN. Biocompatible coating also can be prepared using restricted access material (RAM) such as, alkyl-diol-silica (ADS).[34,35]

## 1.8. SPME kinetics and quantitation

The fundamental aspects of SPME kinetics are necessary to understand for accurate quantitative analysis. In defined extraction conditions, the amount of the analyte extracted ($n$) over time ($t$) can be expressed by the following equation:[20]

$$n = (1 - e^{-at}) \frac{K_{es} V_e V_s}{K_{es} V_e + V_s} C_s^0 \qquad (1.12)$$

Where: $a$ is a rate constant which depends on the physical properties of the extraction phase, agitation, sample volume, mass transfer coefficient, and distribution coefficient. Eq. (1.12) can be simplified by combining with eq. (1.4):

$$n = n_e(1 - e^{-at}) \qquad (1.13)$$

The kinetic profile of the extraction based time profile in eq. (1.13) has been depicted in Figure 1.5.
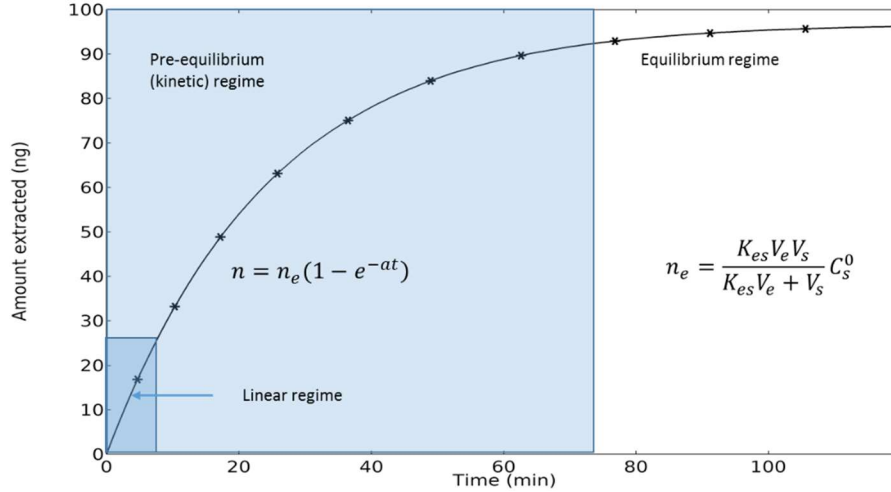
**Figure 1. 5 Schematic SPME time profile with equations providing basis for quantitation at different kinetic regimes**

From a kinetic perspective, quantification of the analyte can be performed following two approaches - equilibrium extraction and pre-equilibrium extraction in the kinetic regime. Quantification using equilibrium extraction provides higher sensitivity and reproducibility, because the maximum possible partition of analyte is reached and the dynamic conditions (agitation) of the extraction process do not affect the amount extracted. The pre-equilibrium-based quantification is affected by the convection/agitation conditions. While equilibrium-based quantification method may be preferable for achieving better precision and accuracy, the major constraint of this method remains the time necessary to reach equilibrium. The equilibration time is defined as the time required to extract ≥95% of the amount that would be obtained at t = ∞. It can be calculated according to the equation 1.11:

$$t_e \approx t_{95\%} = \frac{3\delta K_{es}b}{D_s} \tag{1.14}$$

Where: $b$ is the extraction phase (coating) thickness, $\delta$ is the boundary layer thickness and $D_s$ is the diffusion coefficient of the analyte in the bulk sample. Eq. (1.14) indicates at the factors that

modulate the extraction equilibrium time ($t_e$). Faster equilibration can be achieved by optimizing those parameters. For example, equilibrium time can be shortened by decreasing the coating thickness and increasing the agitation speed. To enhance the sensitivity it is necessary to increase the $K_{es}$ value, which can be achieved by using appropriate coating chemistry.

## 1.9. The use of computational modeling in SPME

Understanding of the fundamental concepts of SPME requires in-depth knowledge of physics, mathematics and thermodynamics. For example, the extraction kinetics or mass transfer of anlyte in SPME is influenced by the of partition coefficient (Figure 1.4), coating thickness, convection, and the presence of binding matrix components (Figure 1.6).[17,18,26,36]
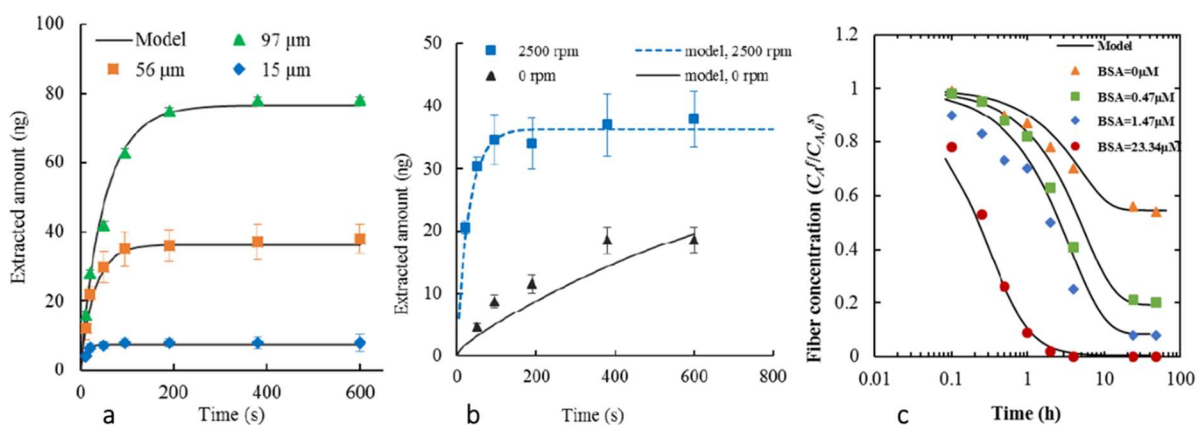


Figure 1. 6 Extraction of benzene using PDMS SPME fiber with different coating thickness (a), at different agitation speed (b), and effect of BSA (bovine serum albumin) binding matrix on pyrene extraction (c)

Figure 1.6 (a) demonstrates how the extraction reaches equilibrium faster with decrease in coating thickness. This gives a valuable information to optimize coating thickness for specific experiments where the sample size is very small and agitation is difficult to perform for example biofluids. Figure 1.6 (b) shows how equilibrium reaches faster with agitation, and Figure 1.6 (c)

shows how the concentration of binding matrix component contributes to faster equilibrium time.

Besides fundamental concepts, computational model can be used to understand some in-depth

SPME concepts such as – radial diffusion and balanced coverage. The mass transfer of analyte is

heavily depended on the geometry (size and shape) of SPME device. The mass flux increases

significantly due to radial diffusion when the radius of the device is below 10 μm (Figure 1.7).[36]
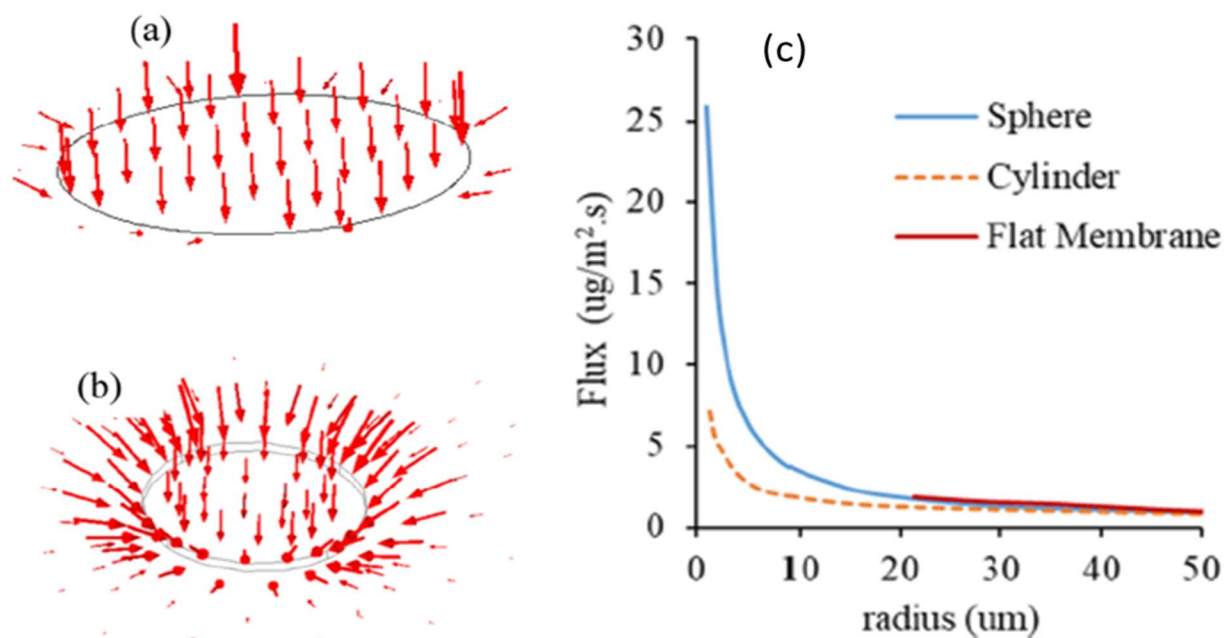


**Figure 1. 7 Simulation of total flux for two different radii of circular coating surfaces (a) 100 μm and (b) 2 μm, and effect of radius length on total flux for different SPME geometries (c)**

The radial diffusion of analyte plays a vital role to develop efficient miniaturized SPME

geometries for many applications such as, SPME fiber tip for extraction in small volume, magnetic

nanoparticles for dispersive extraction.[37,38] Figure 1.7 (a) and (b) indicate the enhanced total flux

induced by the smaller radius (2 μm) due to radial diffusion. While the Figure 1.7 (c) demonstrates

how the radial diffusion is governed by the shape of the SPME device. The spherical geometry

induces higher degree of radial diffusion compared to other geometries like cylindrical and flat

membrane.

There are many SPME applications where extraction of multiple analytes in complex samples is essential for both quantitative and qualitative (metabolites) aspects. In this regard, appropriate SPME coating chemistry is required to attain a balanced coverage of analytes with wider range of properties.[18] The 'balanced coverage' or distribution of analytes in the extraction phase heavily depends on the affinity of particular analyte to the extraction phase (partition coefficient, $K_{es}$) which can be optimized by changing the coating chemistry. Well known C-18 and PDMS extraction phases show higher affinity towards nonpolar analytes, whereas, ionic extraction phases show higher affinity towards polar analytes. Therefore, a suitable coating material such as, HLB (hydrophilic and lipophilic balance) can be used to develop SPME extraction phase which can attain balanced coverage of analytes. In addition to $K_{es}$, the binding affinity of analytes to the matrix components $K_a$ is another important parameter to attain the balanced coverage. The correlation between $K_{es}$ and $K_a$ in balanced coverage SPME extraction can be explained comprehensively using computational a model (Figure 1.8).
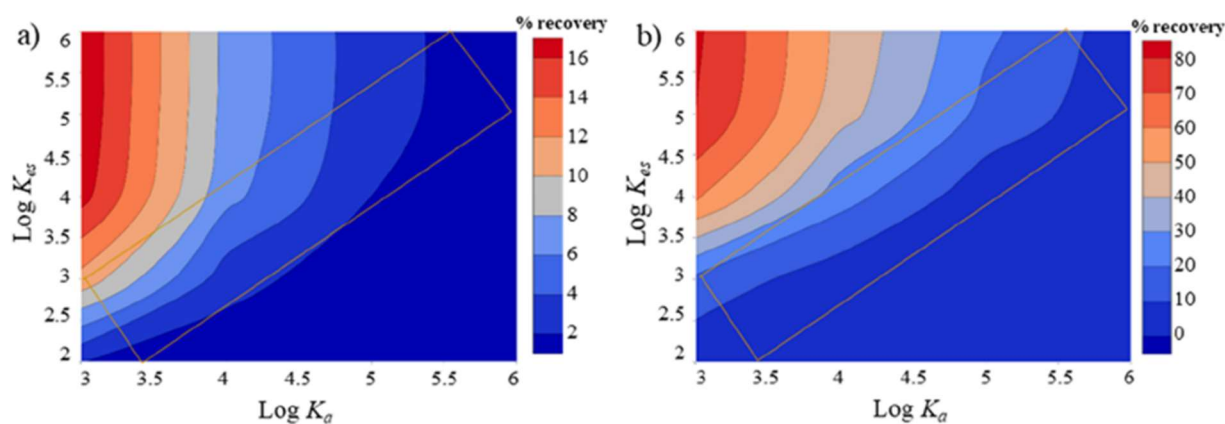


Figure 1. 8 Effects of partition coefficient ($K_{es}$) and matrix binding constant ($K_a$) on analyte enrichment in the extraction phase after 5 min (a) and 500 min (b)

Figure 1.8 shows the distribution of analytes in the extraction phase with variation of $K_{es}$ and $K_a$ values. The recovery of analytes rises with the increase of $K_{es}$, and reduces with the decrease of $K_{es}$. While the $K_a$ value of analytes contribute to the free concentration. With higher $K_a$ value the free concentration decreases and vice versa. In reality, most SPME experiments involve extraction of analytes which are heavily bound (high $K_a$ value) to the matrix components (such as, diazepam, tranexamic acid and doxorubicin in blood plasma). In order to obtain a balanced coverage of multiple analytes HLB coating is preferable. In a tentative case, Figure 1.8 (a) demonstrates that analytes with lower $K_{es}$ and $K_a$ values will be close to equilibrium in a short period of time while other will be in linear extraction kinetic regime. This indicates that, the extraction. While Figure 1.8 (b) shows the coverage of analytes with higher $K_{es}$ and $K_a$ values. This is because of displacement of analytes with low $K_{es}$ values by the ones with high $K_{es}$ values. Therefore, computational models can be used to optimize the experimental conditions where the balanced coverage of wider range of analytes is required.

Overall, the use of computational models in SPME technique demonstrates as a powerful analytical tool for in-depth understanding and investigation of experimental process. It can be used to minimize the cost of analysis through optimization of experimental steps using computational data. In addition, it provides the explicit explanation for many complex phenomena which are otherwise difficult to comprehend.

## 1.10.    An Overview of COMSOL Multiphysics

Over the last couple of years COMSOL Multiphysics software has been used as a computational tool to calculate analyte mass transfer kinetics in many SPME applications. COMSOL Multiphysics has been frequently used in our research group over the last six years because of its intrinsic simplicity for non-expert users. Other computational platforms like MATLAB require in-depth knowledge of mathematics. This computational platform offers users a comprehensive model builder template for various physics interfaces such as chemical species transport, heat transfer, fluid dynamics, etc. An overview of this software is described in this section. Firstly, the user develops a preliminary model template by selecting space dimensions (such as 3D, 2D or 1D, etc.), physics interfaces (such as chemical species physics interface for mass transport phenomena) and study type (such as time dependent study or stationary study). The basic model template contains some classified nodes – 'Global Definitions', 'Components', 'Study' and 'Results'.

**Definitions:** The 'Global Definitions' node includes user defined variables, functions, material descriptions, etc., which are applicable to all components in the model. Multiple components may require defining multiple physics, such as 'reaction engineering' and 'chemical species transport' physics (Figure 1.9). 'Definitions' branch is available under component node as well. Definitions
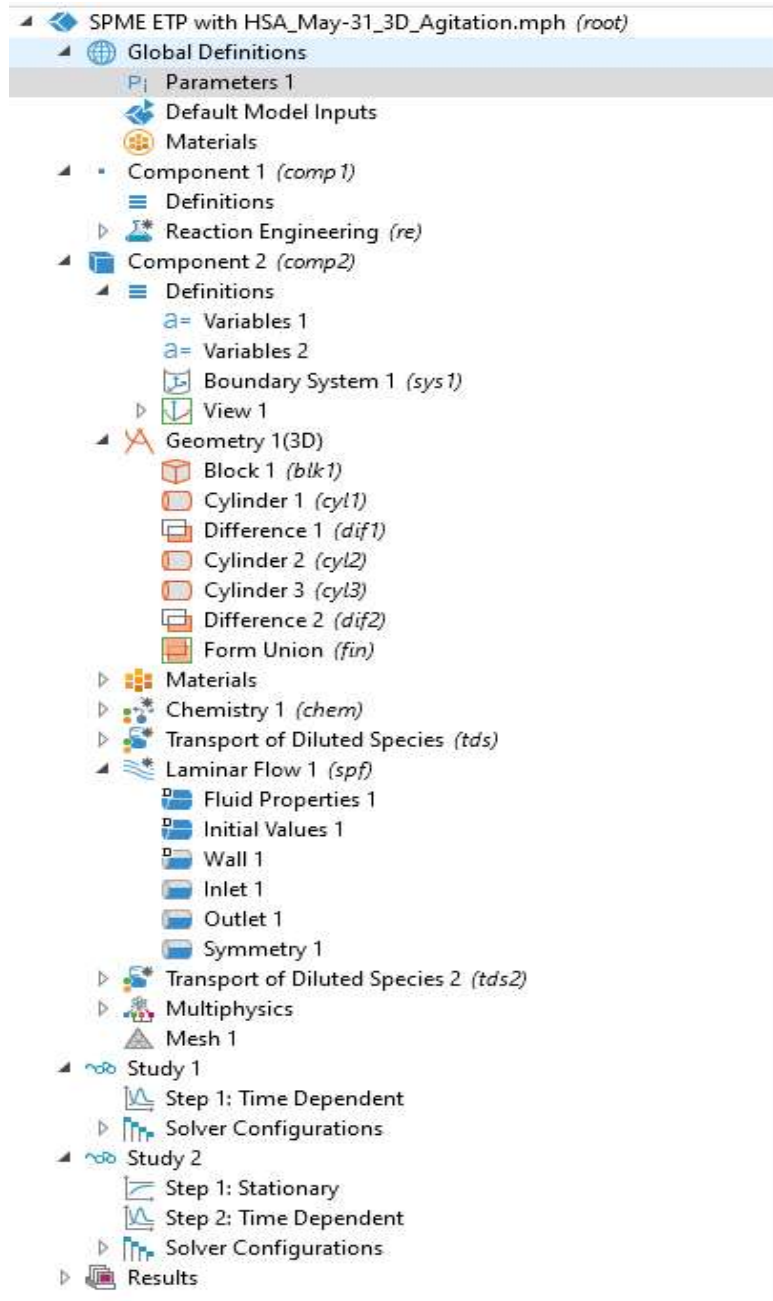
**Figure 1. 9 Snapshot of model build-up sequence in COMSOL Multiphysics 5.2 software**

The component branch also provides user defined variables, parameters and functions, boundary system, etc., which are restricted to the respective component (in figure 1.9 functions are not selected but can be obtained from model builder).

**Geometry:** Another important section of the 'Component' node is 'Geometry'. It offers the user the option to define and develop the geometry of the component model using either COMSOL kernel or CAD (computer-aided design) kernel. In case of CAD kernel, the user needs to import the design developed in CAD module. The COMSOL kernel module includes all basic geometric shapes of objects (such as, blocks, cylinder, cone, sphere, etc.) and all geometric operations to build a component model (Figure 1.10). The user also needs to define the units (length and angular units). The geometric operations such as, Booleans and Partitions are noteworthy. These geometric operations define the partition of domains and boundaries of the geometric entity. For example, the 'Difference' Boolean operation is used to subtract one geometric object from another. At the end of the sequence, the user needs to perform 'Form Union or, Form Assembly'. 'Form Union' combines all geometric entities in a single object with different domains and boundaries, whereas 'Form Assembly' treats different entities as a collection instead of a single entity. In latter case, the user needs to pair boundaries or domains to perform special mathematical operations such as – special boundary pairs are required in 'rotatory machine' geometry where blades and fluid of the rotatory machine work as moving mesh (such as meshing of fluid) with respect to the stationary wall.
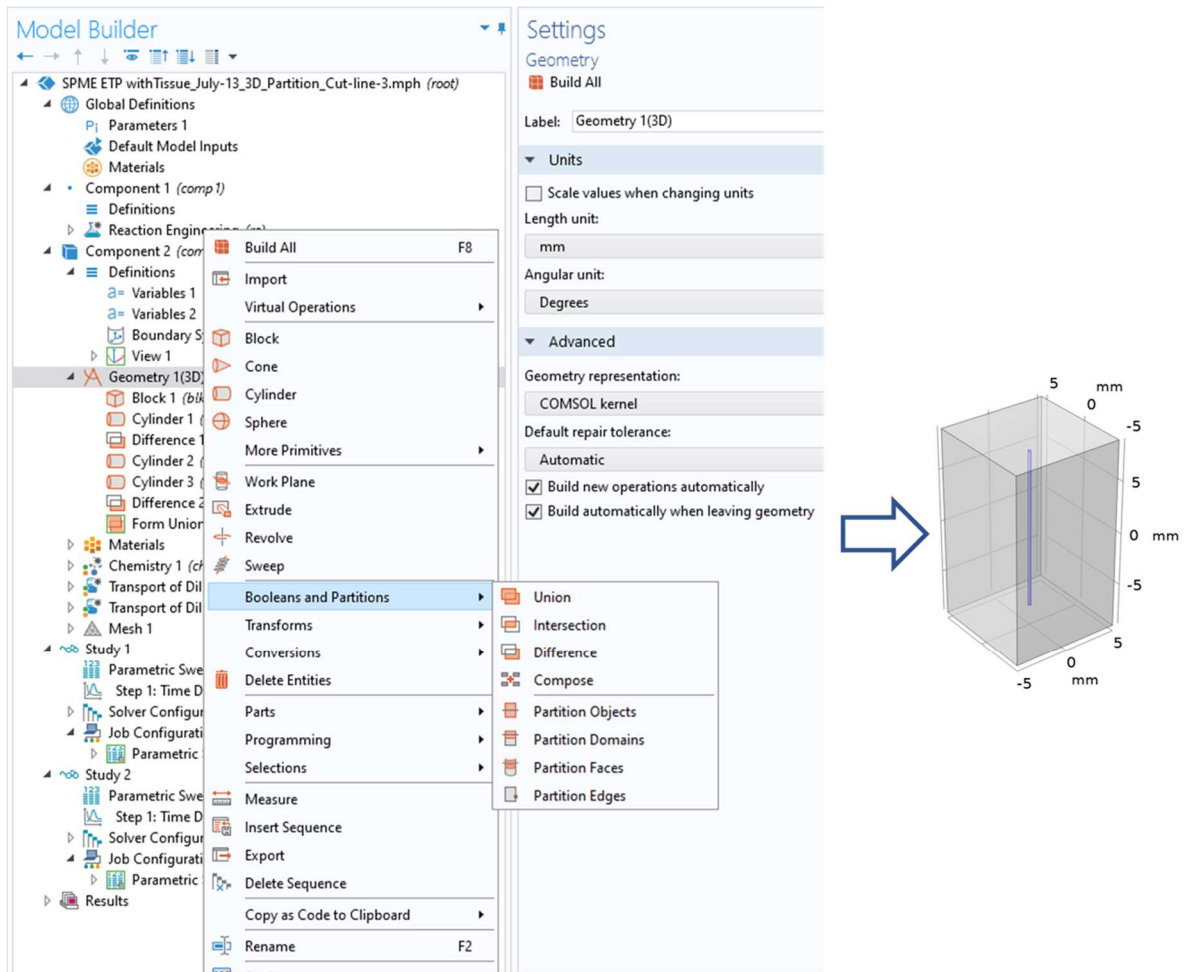
Figure 1. 10 A 3D geometry of SPME extraction experiment built in COMSOL kernel using different shapes and operational functions under 'Geometry' node in COMSOL Multiphysics 5.2

**Materials:** The material section includes a library of various materials such as, polymers, alloys, rocks, air, different types of liquid, etc. This section is particularly important if investigation of material properties is required. However, the objective of this study is mainly focused on mass transport properties of analytes. To obtain a comprehensive mathematical model, someone might consider material properties as an important factor in case of mass transfer of analyte in complex sample matrices like biological tissue. However, COMSOL provides specific physics components (explained later in this section) which include the necessary properties of a specific mass transport

type, for example 'transported diluted species in porous medium'. Nevertheless, 'water-liquid' material is mostly used as a medium to study the mass transfer in SPME.

Physics: COMSOL Multiphysics provide various physics template to simulate mass transfer properties, such as 'transported diluted species (*tds*)' which has already been used in many SPME applications. to simulate mass transport of analyte in aqueous matrix when the properties are not of interest. *tds* is used to calculate concentration of a solute in air, liquid or solid (SPME). The driving force for mass transport in this physics is controlled by the Fick's law of diffusion, as well as convection when coupled with fluid dynamics, and reaction engineering (detailed explanation was given in chapter 2). The dependent variable of this physics interface is molar concentration (c). This interface is applicable to simulate mass transport in 1D, 2D and 3D as well as axisymmetric components in 1D and 2D. Besides *tds,* some other commonly used physics interfaces in SPME are reaction engineering (re) and fluid flow (such as laminar flow, *spf*).

Mesh: The purpose of 'Mesh' node in COMSOL Multiphysics is to discretize the geometry through meshing sequence into small units which are referred to as mesh elements.
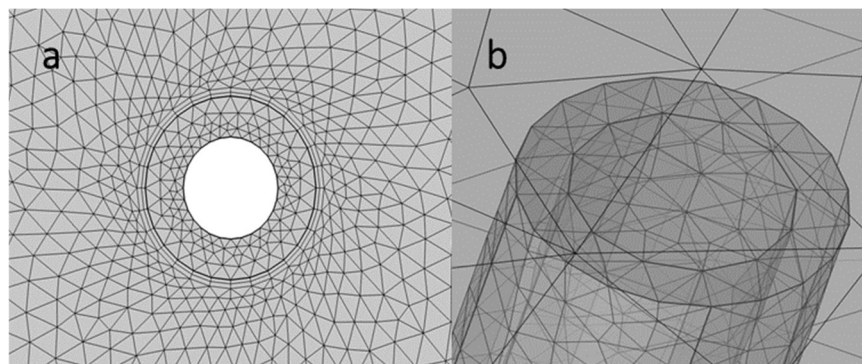


Figure 1. 11 Meshing of 2D (a) and 3D (b) geometry in COMSOL Multiphysics 5.2 using 'trigonal' and 'tetrahedral' shape meshing elements

Meshing sequence corresponds to meshing 'operation' and 'attribute' nodes (see Figure 1.12). Operation node creates or modifies the mesh of the defined geometry according to the selected properties. For example, 'Free Tetrahedral' and 'size' are two operation nodes. Attribute nodes are subnodes of operational nodes which corresponds to local operation node and overrides the global properties of operation nodes.
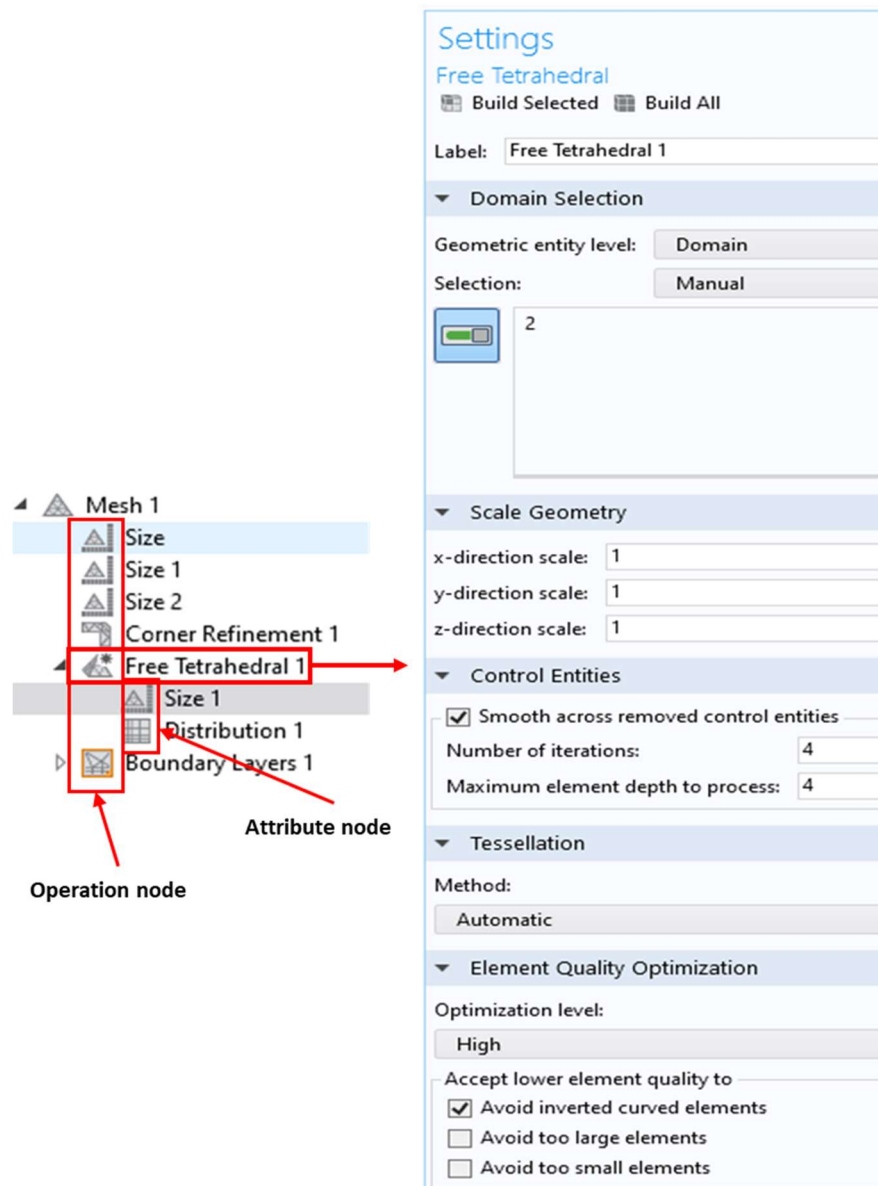


Figure 1. 12 Meshing sequence and meshing nodes in COMSOL Multiphysics 5.2

In COMSOL Multiphysics, meshing operation can be performed either by 'physics controlled' or, 'user-controlled' meshing. Under 'physics-controlled' meshing operation, the software creates and modifies a mesh according to the default values set by the physics interfaces. In that case, the user needs to select the predefined element size (see Figure 1.13). However, physics-controlled setting may result in poor meshing resolution due to the complex shape of the geometry which will affect the outcome of modeling. The 'user-controlled' meshing operation allows the user to develop meshing sequence and customize respective properties of meshing nodes. User-controlled meshing operation is the preferred choice to obtain better simulation results.

| ICON | NAME | ICON | NAME |
|------|------|------|------|
| | Extremely Fine | | Normal |
| | Extra Fine | | Coarse |
| | Finer | | Coarser |
| | Fine | | Extra Coarse |
| | | | Extremely Coarse |

Figure 1. 13 Predefined element size in COMSOL Multiphysics 5.2[32]

**Studies and Solvers:** COMSOL Multiphysics software follows a hierarchy approach for solving a problem. The 'Study' node is at the top level (see Figure 1.14) which contains a least amount of detail and a Study branch.
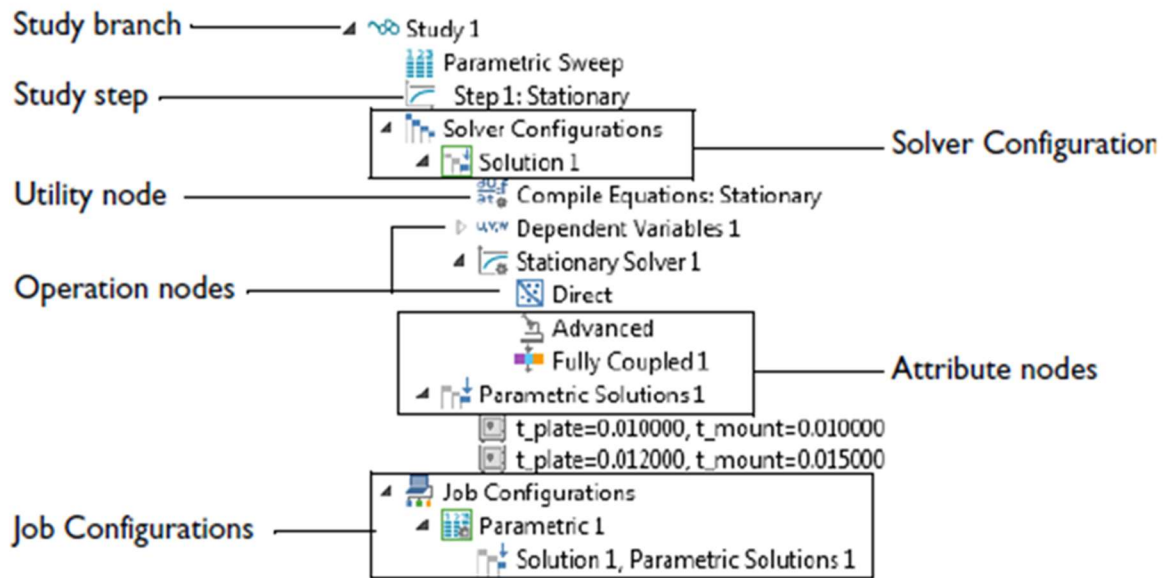
**Figure 1. 14 The hierarchy sequence of 'Study' node in COMSOL Multiphysics 5.2** [32]

The 'Study' node corresponds to a 'study step' which is added while creating a new model in the model builder. A study step defines the type of study such as, 'Stationary' or 'Time-dependent'. Multiple study steps can be included under same branch of 'Study' node. A study step corresponds to 'Solver Configurations' and 'Job Configurations' nodes. Solver configuration includes the solver to solve for the dependent variables in the physics interface, and intermediate storage of solutions. While the job configurations node contains all jobs defined for a particular study such as, parametric jobs, batch jobs, etc. Although there are different types of solvers available in COMSOL Multiphysics, 'linear' and 'nonlinear' types of solvers were mostly used in this study. COMSOL automatically detects the nonlinearity of the problem and switches to a nonlinear solver.
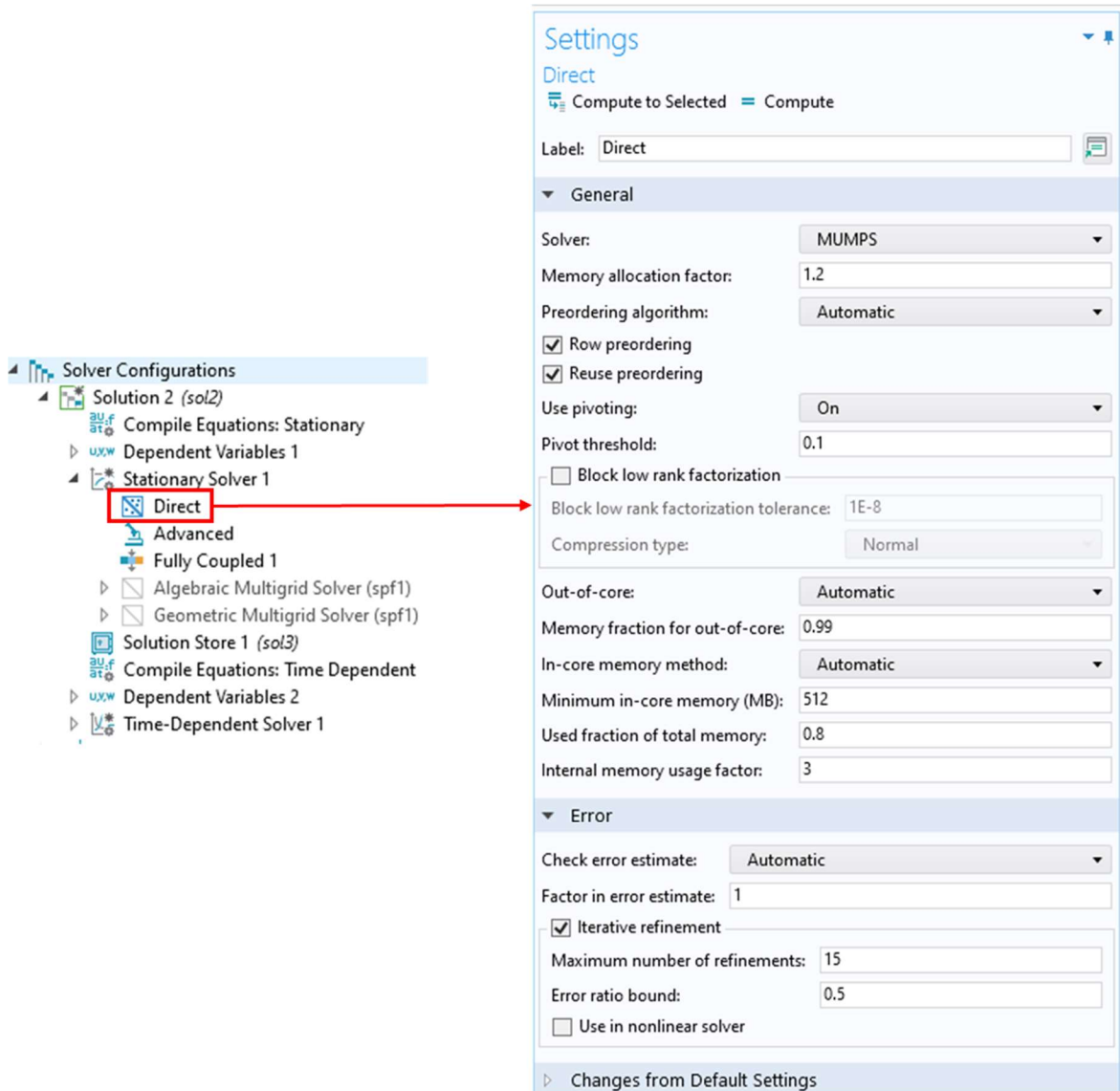
**Figure 1. 15 'Direct' linear solver configuration is COMSOL Multiphysics 5.2**

Since this section is based purely on mathematics and COMSOL provides very limited information

about solver configuration, only a few customized operations were performed for our study. Most

notably, selection of 'Direct' linear solver (see Figure 1.15) instead of 'Iterative' linear solver.

'Direct' contains MUMPS (multifunctional massively parallel sparse direct solver) as a default, or

PARDISO (parallel sparse direct solver), or SPOOLES (sparse object-oriented linear equations

solver). All these solvers use default settings.

**Results Analysis:** This section of COMSOL Multiphysics provides mathematical and analytical tools for post processing and analyzing results derived from simulations – examples include data plotting in 1D (line plots), 2D (surface plots) and 3D (volume plots). Visualization and animation of the results are also available.

## 1.11.    Research objectives

Over the last two decades SPME technique has been extensively used for characterization analytical components in many complex biological matrices including blood, serum, urine, tissue, etc. This widespread adoption of SPME has been achieved due to its intrinsic simplicity, and ability to measure free analyte concentration from complex sample matrices where multiple binding matrices exist. The continuous evolution of SPME techniques enables it to diversify into numerous applications, such as *in vivo* applications in clinical research, direct extraction from biological tissues like liver, lungs, brains, etc. For example, measurement of free drug concentration in blood plasma and solid tissue is a critical analytical step in clinical trials. However, the concentration of heavily binding matrix components (such as albumins, immunoglobulins, etc.) present in the biological samples significantly reduces the free analyte concentration of drug, leading to inaccurate analytical results. Since SPME extracts negligible amounts of analyte via free concentration, it enables the determination of free drug concentration in complex biological samples. However, knowledge of the characteristics of mass transfer kinetics in the presence of binding matrix components is necessary in order to understand important SPME attributes, such as extraction equilibrium time, matrix assisted mass transfer, and local depletion. In these aspects, the computational model is considered as an effective analytical tool to demonstrate comprehensive knowledge about the mass transfer kinetics. In-silico approach can also be applied

to reduce experimental steps in analytical method optimization, helping to save time and cost of analysis. Previous efforts of computational studies for SPME extraction kinetics primarily focused on single binding matrix component system, containing only albumins. This simplified approach demonstrated how HSA binding matrix influences the mass transfer of the analyte to the extraction phase.[17]   Such computational studies onset the journey to investigate more complicated sample matrices like blood plasma or solid tissue, where analytes are bound with different components (albumins, immunoglobulins, cell membrane, etc.). This intricate binding nature of the matrix components complicates the efforts to investigate the mass transfer kinetics, because the binding matrix components also contribute to the mass transfer the of analyte. Thus, the apparent binding constant (which is assumed to be the true binding affinity of analyte to the matrix components) of the target analyte for respective matrix components needs to be estimated in order to investigate the mass transfer kinetics. In this regard, the study documented in this thesis aimed to achieve the following objectives:

- SPME method development and optimization using computational models to determination the free concentration of target analyte in complex biological samples, such as tissue and blood plasma.

- To demonstrate critical SPME attributes, such as matrix assisted mass transfer, local depletion, etc. using computational models.

- Develop 3D computational models based on adsorption kinetics in solid coating which are more practical to the experimental conditions (in many SME experiments the extraction kinetics is followed by adsorption on solid coating). It should be noted that computational models using 2D axisymmetric approach can be used in many SPME experiments (usually

all experimental conditions applied here are compatible for 2D axisymmetric) where 3D models are not necessary in order to simplify mathematical calculations. However, the 3D models are particularly required in some experimental conditions, such as *in vivo*, or where the sample geometries are mostly asymmetric for example in a living organism. Therefore, the objective of using 3D models is to achieve the computational expertise for such applications.

**Chapter 2** documents the development of an SPME approach to determine free doxorubicin (DOX) concentration in bovine lung tissue, using solid extraction phase. 3D computational models were developed based on experimental data, which demonstrated the mass transfer of DOX to the solid extraction phase in lung tissue. **Chapter 3** demonstrates the use of 3D mathematical models to determine free fatty acid (alpha linoleic acid and linoleic acid) concentration and subsequent application of the experimental data to monitor the dynamic ligand-receptor interactions between the fatty acid and the HAS.

# Chapter 2    Investigation of mass transfer kinetics of drugs in biological tissue by SPME
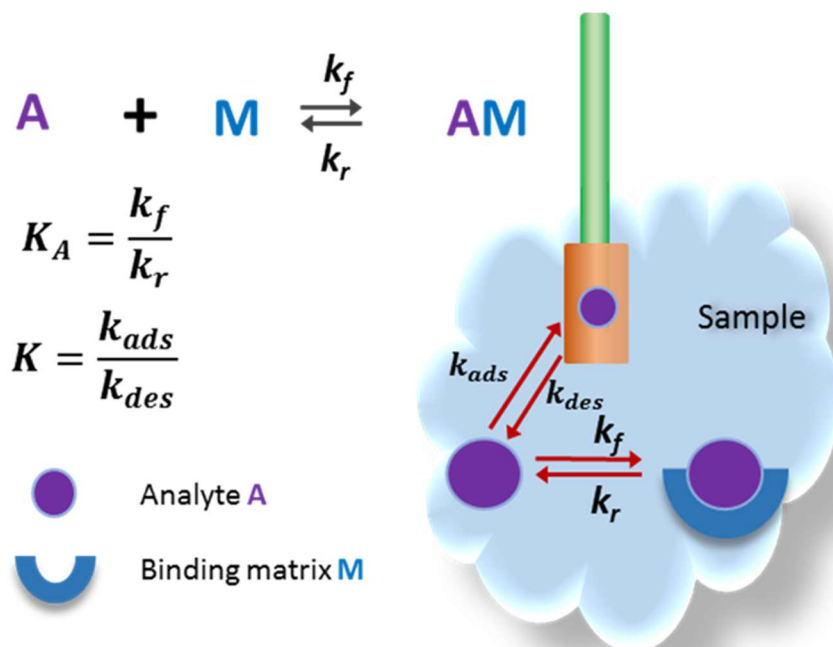


## 2.1. Preamble

This chapter has been published in the journal Analytical Chemistry. Mohammad Huq, Marcos Tascon, Emir Nazdrajic, Anna Roszkowska, Janusz Pawliszyn; *Measurement of free drug concentration from biological tissue by Solid-phase Microextraction: In-Silico and Experimental Study*, Anal. Chem., 2019, 91 (12), pp 7719–7728. All the figures and data for all sections of this chapter were reprinted from this article with the permission from the American Chemical Society (Copyright 2019). Copyright for this work remains the property of ACS and any permission for further re-use of this information should be requested directly from them (DOI: 10.1021/acs.analchem.9b00983).

The contribution of co-authors Marcos Tascon and Anna Roszkowska to the work described in this chapter was involved in experimental characterization from tissue. Emir Nazdrajic helped with mathematical equations used for mass transfer (the assistance was just discussion). All the assistance from co-authors were merely enough to include them in publishing the work. All major works – developing mathematical models, performing simulations and experimental designs were done by the main author. All the listed co-authors were asked for their permission to use this material for writing this thesis.

## 2.2. Introduction

One of the main aims of clinical pharmacology studies is to provide the most accurate measurements of drug concentrations in living systems, a task most likely to succeed via in vivo assessments of free drug concentrations at receptor sites (the biophase). Given that the majority of drug-receptor interactions take place in tissue, determining free drug concentrations in the intracellular space would be a more rational way to investigate the pharmacokinetics/pharmacodynamics (PK/PD) of a given drug, as compared to its measurement in blood plasma.[39,40] These concerns are of particular importance in PK/PD studies involving drugs that are administered subcutaneously (SC) or intramuscularly (IM). In such cases, the in vivo free concentration of the administered drug in the intracellular space would be the most appropriate indicator of therapeutic efficiency.[41] However, given the complex nature of drug distribution in tissue matrix as well as the limitations of traditional analytical techniques available for such measurements, in vitro measurement of free drug concentrations in blood plasma is oftentimes adopted as a surrogate technique to study PK/PD.[42–44]While a variety of analytical methods are available for measurement of free drug concentrations in tissue matrix, such as equilibrium

dialysis, ultrafiltration, and microdialysis,[45,46] few of them are capable of in vivo measurement. Microdialysis (MD) is the method most widely used to monitor free analyte concentrations in the extracellular space of tissue. However, the MD technique encounters some limitations, such as low recovery for highly protein-bound nonpolar drugs, and low temporal resolution of fast changing tissue components. The electrochemical biosensors technique, on the other hand, is highly efficient for measurement of rapidly changing tissue components, since it promotes fast detection via chemical or biochemical reactions. However, this technique, already limited to the detection of electroactive analytes only, is also characterized by low specificity due to the presence of non-electroactive interferences.[47,48] Due to technical difficulties, equilibrium dialysis and ultrafiltration are only used for in vitro analysis in blood plasma and other biological fluids.[49,50] The major limitations of equilibrium dialysis encounters are longer equilibration times (typically 4 – 28 h), volume shifts and poor drug solubility. On the other side, the ultrafiltration technique prone to nonspecific interactions with matrix components and equilibrium displacements, producing in this way a bias stemming from overestimations of the free concentration value.[51] Given the various shortcomings associated with MD and electrochemical biosensors, a simpler and more robust analytical technique is thus needed to tackle measurements of free drug concentrations in tissue. Solid-phase microextraction (SPME), developed in 1990,[31] stands as particularly suitable for this application given its unique characteristics. In vivo SPME for analysis of tissue can be performed by placing a biocompatible microextraction phase coated onto a thin fiber into tissue matrix with minimal invasiveness. Here, unbound analytes are selectively extracted from the matrix by diffusion through the boundary layer. Due to negligibly depletive nature of the microextraction phase, SPME does not disturb the

binding equilibrium between the analyte and the matrix. Further, SPME allows for extractions to be carried out either in the equilibrium or pre-equilibrium regime.[,17,20] These qualities of SPME render the technique an ideal choice for measurements of free concentration of analytes from complex biological matrices, as supported by its many successful applications in the biological field, both in vivo and ex vivo.[52–54] In 2003, Lord et al. first reported the use of fiber SPME for in vivo monitoring of benzodiazepines in the systemic blood circulation of dogs.[55] Since then, *in vivo* SPME applications have been widely exploited to study drug biomarkers and metabolomes due to the advantages associated with its minimally invasive direct extraction capabilities, as well as its ability to extract analytes with wide range of polarity, which is often referred to as balanced coverage [22-25].[53,56–58] From a theoretical point of view, Musteata et al. explained the mechanism of SPME extraction of free analytes in the presence of a binding matrix under equilibrium conditions, where the unbound portion of the analyte partitions to the liquid extraction phase of the SPME fiber.[[59]] In addition to the use of experimental techniques, mathematical modelling has proven as an excellent tool to determine the kinetics of SPME extraction in the presence of a binding matrix, as it allows for better predictions of results while minimizing the number of experiments that must be carried out during method development and routine analysis [17, 27, 28].[17,18,60] Alam et al. first successfully the effects of a binding matrix on the extraction kinetics of SPME liquid coatings via development of a 2D model in COMSOL Multiphysics.[17] Gorecki et al. and Zhou et al., in turn, demonstrated the extraction kinetics of solid coatings with the use of Langmuir's isotherms, which approach assumes isotropy of the fiber surface.[61,62] Since most of the biocompatible microextraction phases currently employed in SPME experiments for biological applications consist of a solid coating, the current work has

focused on developing mathematical simulations of SPME kinetics in tissue matrix for solid coatings. To the best of our knowledge, this is the first time a mathematical model to measure free drug concentrations from tissue matrix via SPME is reported in the literature. Of note, the developed model, which allows for calculations of binding constants and free concentrations of relevant drugs directly from tissue, opens an exciting new area of study in bioanalytical chemistry.

### 2.2.1.  Doxorubicin case study

Doxorubicin (DOX) is a widely known chemotherapeutic agent that has been used for over 40 years in the treatment of many different types of cancers. The mode of action involves the binding of DOX which causes potential cytotoxic effects and limits the proliferation of malignant tissue by intercalating with DNA base pairs. However, this drug is nonselective in nature, for which it inherits adverse side-effects by damaging healthy tissue. To reduce such side-effect, in most cases, DOX is administered locally to the site of action. Since the site of action of DOX is intracellular and it enters into the cell through passive diffusion like most other small molecules, the drug has been commonly administered intravenously (IV).[63,64] Pharmacokinetic studies have shown that DOX has a plasma half-life of 3-5 min, and a tissue half-life of 24-36 h. This indicates rapid uptake of DOX by tissue matrix. However, passive diffusion of DOX depends on the free form of DOX in the extracellular matrix, where it is heavily bound to multiple extracellular species. To the best of our knowledge, no studies have been reported estimating the free concentration of DOX in tissue matrix.[65] More recently, DOX has been under preclinical study for treatment of metastatic lung cancer through in vivo lung perfusion (IVLP), where DOX concentration in lung tissue was determined by measurement of total drug concentrations in perfusate solution and serum.[66] In these scenarios, it is of great bioanalytical interest to develop a novel technique

capable of determining the free concentration of a drug in biological tissue by direct sampling, with minimum invasiveness so as to also enable in vivo applications. The current work presents the SPME extraction kinetics for solid coatings in tissue using numerical and experimental models. As a proof of concept, DOX was selected as a model drug, while bovine lung tissue was selected as the biological matrix. The physics of the biological matrix was also modeled based on fundamental and biological parameters, such as tortuosity and intracellular space of the tissue matrix, since these factors control drug diffusion and distribution. Experimental results were then attained and compared with the developed numerical simulations. Once optimized, the model enabled calculations of free drug concentrations as well as relevant concepts for in vivo sampling, such as sampled area, depleted area, and spatial resolution.

### 2.2.2. Theoretical considerations

SPME extraction takes place via free concentration. If the amount extracted is negligible, then the equilibrium concentration of the analyte in the sample matrix is equivalent to the free concentration, which is measured according to eq. 1.5:

$$n = K_{es}V_f[A]^{free}$$

Where: $n$ is the amount of analyte extracted on the fiber coating at equilibrium, $K_{es}$ is the partition coefficient and $V_f$ is volume of the extraction phase. Since $K_{es}$ and $V_f$ are constants for particular analyte and specific extraction phase, then the above equation can be formulated as below:

$$n = f * [A]^{free} \tag{2.1}$$

Where, $f = K_{es} * V_f$ is the fiber constant. The partition coefficient $K_{es}$ is derived from the equilibrium extraction Eq. (2.):

$$K_{es} = \frac{[A]_{fiber}^{eq}}{[A]_{sample}^{eq}} \tag{2.2}$$

However, when solid coatings are employed in SPME, analytes are adsorbed on the active surface area rather than partitioned, making the above eq. (2.2) inadequate for measurements of free concentrations under these conditions. A theoretical approach based on Langmuir's theory for the extraction kinetics of solid coating SPME has been previously proposed in the literature [18,67]. In brief, the amount of solute adsorbed to the solid coating at equilibrium $cs^{eq}$ (mol m$^{-2}$) is given by:

$$cs^{eq} = \frac{\gamma_s * K * [A]^{eq}}{1 + K * [A]^{eq}} \tag{2.3}$$

Where $\gamma_s$ is the maximum free active-site concentration in the fiber (mol m$^{-2}$), $K$ is the adsorption equilibrium constant (m$^3$ mol$^{-1}$), and [A]$^{eq}$ is the free concentration of analyte in the matrix at equilibrium (mol m$^{-3}$).

The mass transfer in solid coatings is defined by Langmuir's isotherm, which is defined as:

$$r_{ads} - r_{des} = k_{ads} * [A] * (1 - \theta) - k_{des} * \theta \tag{2.4}$$

Where, $r_{ads}$ is the rate of adsorption of analyte onto the coating surface (mol m$^{-2}$ s$^{-1}$); $r_{des}$ is the rate of desorption (mol m$^{-2}$ s$^{-1}$); $k_{ads}$ is the adsorption rate constant (m s$^{-1}$), and $k_{des}$ is the desorption rate constant (mol m$^{-2}$ s$^{-1}$). For solid coatings, the rates of adsorption and desorption are dependent on the fraction of vacant sites available on the solid surface, which is defined as θ. The fraction of occupied sites on the solid surface is defined as:

$$\theta = \frac{cs}{\gamma_s}$$

Where $cs$ is the amount extracted on the fiber at a given time t, and $\gamma_s$ (mol m$^{-2}$) is the maximum active surface concentration. The latter can be defined as follows:

$$\gamma_s \left(\frac{mol}{m^2}\right) = \frac{\text{saturated amount extracted on the fiber}}{\text{active surface area per fiber}} = \frac{cs_{sat}}{A} \tag{2.5}$$

Eq. (2.4) can be rearranged as:

$$r_{ads} - r_{des} = k_{ads} * [A] * \left(1 - \frac{cs}{\gamma_s}\right) - k_{des} * \frac{cs}{\gamma_s}$$
(2.6)

At equilibrium, the rates of adsorption and desorption are equal. Therefore, eq. (2.6) can be

expressed as:

$$K = \frac{k_{ads}}{k_{des}} = \frac{cs^{eq}/\gamma_s}{[A]^{eq}*(1-cs/\gamma_s)}$$
(2.7)

Eq. (2.6) provides the partition coefficient value for an analyte in a given solid coating. However,

if the extracted amount is significantly high, significant depletion of the free concentration of the

analyte in the local area of the fiber will occur after the system reaches equilibrium. If we consider

the extraction of analyte without any binding matrix present in the system, the free concentration

will be same as the total concentration. Therefore, eq. (2.1) can be expressed as follows:

$$[A]^{free} = [A]^{eq} + \frac{n}{V_s}; \text{ where } \frac{n}{V_s} \text{ is the depletion of concentration}$$
(2.8)

And eq. (2.6) and eq. (2.7) can be rewritten as:

$$[A]^{free} = [A]^{eq} + \frac{n}{V_s} = \frac{cs^{eq}/\gamma_s}{K*(1-cs/\gamma_s)} + \frac{n}{V_s}$$
(2.9)

$$[A]^{free} = \frac{cs^{eq}}{K*(\gamma_s-cs)} + \frac{n}{V_s}$$
(2.10)

Eq. (2.10) provides the free concentration of analyte extracted by a solid coating without the

presence of a binding matrix.

### 2.2.3. Mass transfer kinetics in presence of binding matrix

In the presence of a binding matrix with univalent binding sites of uniform affinity, analyte $A$

is in equilibrium with the matrix component M, where the binding association constant $K_A$ is given

by the eq. (2.11)

$$A + M <=> AM$$
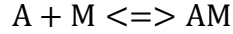
$$K_A = \frac{k_f}{k_r} = \frac{[AM]}{[A]^{eq}*[M]} \tag{2.11}$$

Where: $k_f$, $k_r$, and $[A]^{eq}$ are the rate of association, rate of dissociation, and concentration of $A$ at equilibrium, respectively. $[M]$ is the concentration of the binding matrix, and $[AM]$ is the concentration of analyte bound to the matrix. Eq. (2.11) can be expressed as:

$$K_A = \frac{[AM]}{[A]*[M]} = \frac{[A]^{tot}-[A]^{free}}{[A]^{free}*([M]^{tot}-[A]^{tot}+[A]^{free})} \tag{2.12}$$

Where, $[A]^{tot}$ is the total concentration of analyte or initial concentration, $[A]^{free}$ is the free concentration of analyte, and $[M]^{tot}$ is the total matrix concentration.

If the binding matrix concentration [M] $\gg$ [A]$^{tot}$, then eq. (2.12) can be rearranged as:

$$K_A * [M]^{tot} = \frac{[A]^{tot}}{[A]^{free}} - 1 \tag{2.13}$$

A linear regression line can be obtained from eq. (2.14), where the slope gives the value of the binding association constant $K_A$. Eq. (2.8) determines the amount of free analyte extracted by the extraction phase in absence of any binding matrix. However, in the presence of a binding matrix the amount extracted into the extraction phase can be derived from eq. (2.8) and eq. (2.13):

$$K_A * [M]^{tot} = \frac{[A]^{tot}}{([A]^{eq} + \frac{n}{V_s})} - 1$$

$$\frac{1}{[A]^{free}} = (K_A * [M]^{tot} + 1) * \frac{1}{[A]^{tot}} \tag{2.14}$$

The binding association constant can thus be calculated by using eq. (2.13). Interestingly, the product of $K_A.[M]^{tot}$ from eq. (2.14) is a unitless constant, which we can consider as the apparent binding constant $K_{App} = K_A.[M]^{tot}$. In this chapter, eq. (2.14) was used for the binding study of DOX with tissue binding matrix. For mathematical simplification, we assumed that DOX binds

univalently to a single site of HSA in this case study. However, we justified the mathematical limitations by fitting the experimental results with simulations. For experimental results we extended the equilibrium conditions described above by the exact equations to transient situations prior to equilibrium using numerical modeling.

## 2.3. Experimental

### 2.3.1. Materials and supplies

Human Serum Albumin (HSA), doxorubicin hydrochloride (DOX), formic acid (FA), and ammonium acetate (LC-MS grade) were purchased from Sigma–Aldrich (Oakville, ON, Canada). Agar gel, methanol (MeOH), and water were LC-MS grade and purchased from Fisher Scientific (Mississauga, ON, Canada). C-8 mixed mode SPME fibers were kindly provided by Millipore-Sigma (Oakville, ON, Canada). A phosphate-buffered saline solution (PBS) at pH 7.4 was prepared followed by standard procedure available in many literatures. Standard stock solutions were prepared in methanol at a concentration of 2000 µg·mL-1 and stored at -80 ºC. Bovine lung tissue was purchased from a local meat shop, and the respective experiments were conducted with the approval of the University of Waterloo's Office of Research Ethical Board.

### 2.3.2. Measurement of maximum surface concentration of DOX ($\gamma_s$)

According to eq. (2.5), the maximum site concentration of doxorubicin on the fiber coating is attained once equilibrium is reached. To determine the value of $\gamma_s$ of DOX on a C-8 mixed mode SPME fiber, equilibrium extractions were performed at 0.5, 1, 2, 3, 4, and 5 µg·mL-1 initial concentrations in PBS under agitation at 1500 rpm. The amount of DOX extracted at equilibrium was determined using LC-MS method. The active surface area of the fiber coating was determined

via Brunauer–Emmett–Teller (BET) analysis.

BET is the most widely used method for measurement of surface area of porous materials (solids).

In BET analysis, an inert gas typically pure nitrogen is purged onto solid material surface under isothermal condition, while the pressure of the gas is increased. Therefore, the gas molecules will be adsorbed onto the solid surface and occupy the pores of the material. With respect to the Langmuir's isotherm which is limited to the monolayer, BET theory extends to the multilayers. Since the cross-section of the gas molecule is known, the specific surface area and pore volume can be calculated using BTE equation as follows:

$$\frac{1}{X[\left(\frac{P_0}{P}\right)-1]} = \frac{1}{X_m C} + \frac{C-1}{X_m C}\left(\frac{P}{P_0}\right)$$
(2.15)

Where $X$ is the weight of gas molecule (typically $N_2$) adsorbed at a given relative pressure $\frac{P_0}{P}$. $\frac{1}{X_m C}$ is the monolayer capacity according to the Langmuir's isotherm, and $C$ is a constant. Eq. (2.15) is a linear equation. The isotherm obtained for SPME coating materials in BET analysis is given below:
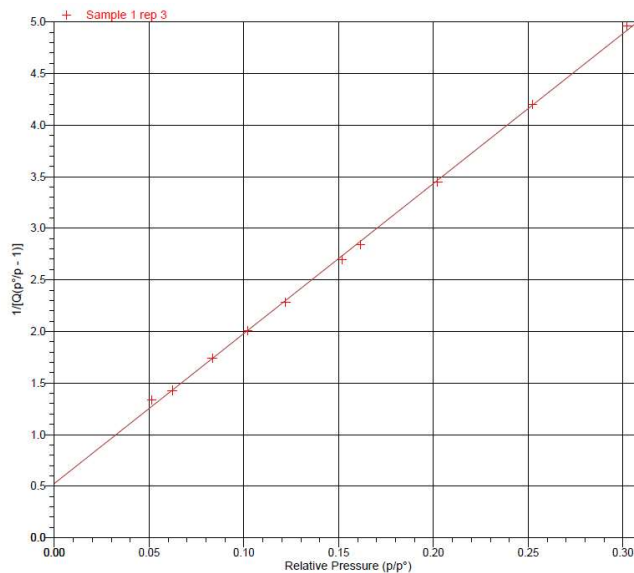


Figure 2. 1  BET isotherm of C-8 mixed mode SPME fiber.

41

The surface area from BET isotherm is calculated by the following equation:

$$Surface\ Area\ (SA) = \frac{1}{slope+intercept} * CSA\ (Crossectional\ area\ of\ N_2) \qquad (2.16)$$

The surface area of porous material provides the information about pore size distribution.
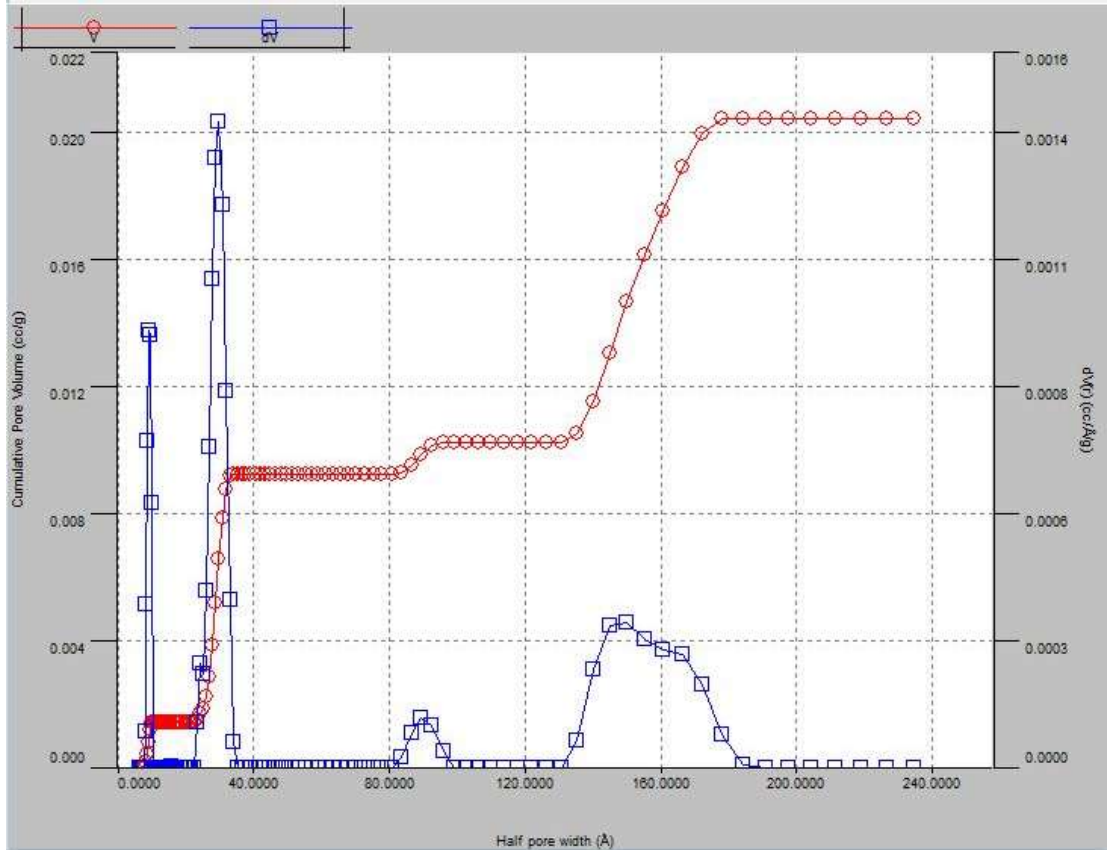


**Figure 2. 2** Physical characterization of active surface area of commercial mixed mode C-8 SPME fiber using BET (Brunauer, Emmett and Teller) method

In Fig. 2.1, X axis describes the different sizes of pores distributed onto the C-8 mixed mode material. We assumed that the interaction of DOX with extraction phase takes place on the outer surface of the material and the porous surface. To calculate the approximate specific surface area of the extraction phase, we ignored the pores smaller than 80Å considering the fact that it is difficult for DOX molecule to accesses such small pores. Based on this assumption, the active

42

surface area was measured as 1.98 m2/g. The value of maximum surface concentration ($\gamma_s$) can

be obtained from eq. (2.5).
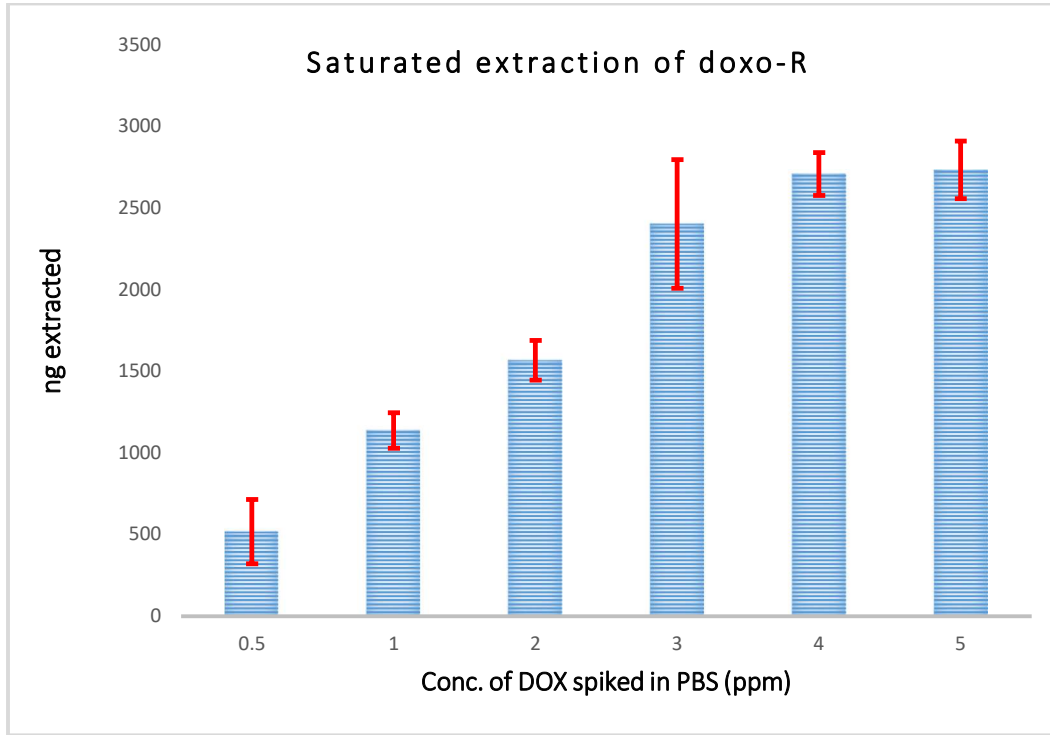


**Figure 2. 3** Amount of extract (in ng) with variation in initial concentration of DOX (ppm) from PBS solution spiked with standard DOX

**Table 2. 1** Experimentally measured physical parameters of SPME extraction phase

| Parameters | Measured |
|---|---|
| Specific surface area of SPME fiber coating (m$^{-2}$/g) | 1.98 |
| Amount of particles per fiber (g) | 2.30E-05 |
| Specific surface area per fiber (m$^2$) | 4.55E-05 |

Using eq. (2.5) we can estimate the value of $\gamma_s$ as below:

$$\gamma_s \left( \frac{mol}{m^2} \right) = \frac{5.1\text{e} - 9(\text{mol})}{4.55\text{e} - 4(\text{m}^2)} = 1.12e - 5 \left( \frac{mol}{m^2} \right)$$

### 2.3.3. Measurement of the adsorption equilibrium constant ($K$)

For DOX The adsorption equilibrium constant (K) for doxorubicin onto a C8 mixed mode SPME extraction phase was attained by carrying out extractions under the following conditions: agitated equilibrium extractions from PBS were carried out using two different initial concentrations (Table 2.2). Doxorubicin was spiked at 100 ng·mL$^{-1}$ and 50 ng·mL$^{-1}$ in PBS at pH 7.4. Extractions were performed at 1500 rpm with preconditioned SPME C-8 mixed mode fibers. Fibers were preconditioned with ACN/H2O (80/20) for 30 mins. An extraction time profile was obtained at eight different time points by independent triplicates, within a 120 min period. After each extraction time step, fibers were gently cleaned with Kim wipes and rinsed with 300 µL of LC-MS grade water for 10 s to remove salts and unspecific attachments from the coating. Desorption was performed with 300 µL of ACN/H2O (80/20 + 0.1% FA) for 60 min in a shaker at 1500 rpm. The estimated value of $K$ was determined using eq. (2.9).

**Table 2. 2 Experimentally calculated adsorption equilibrium constant $K$**

| $[A]^{init}$ (mol m$^{-3}$) | cs$^{eq}$ (ng) | $[A]^{eq}$ (mol m$^{-3}$) | cs$^{eq}$ (mol m$^{-2}$) | K (m$^3$ mol$^{-1}$) | K (m$^3$ mol$^{-1}$)<br><br>Average |
|---|---|---|---|---|---|
| 9.20E-05 | 49.2 | 3.87E-05 | 1.99E-06 | 466.7 | |
| 1.84E-04 | 97.98 | 7.79E-05 | 3.96E-06 | 469.9 | **≈ 468** |

### 2.3.4. Development of 3D mathematical models in COMSOL Multiphysics

3D models of different extraction conditions using C8 mixed mode SPME fiber immersed directly into the sample matrix were designed in to COMSOL Multiphysics 5.3 (Figure 2.4). The

shape of the sample matrix was considered rectangular with respect to the equivalent volume of cylindrical glass vial, in order to simplify the mathematical calculation. The volume of the sample matrix was 17 mL. The 3D geometry is shown in Figure 2.4. The shape of the sample matrix was designed s a rectangular shape instead of vial for simplicity, however the total volume remains same. The whole system was divided into two domains – the sample matrix and the solid extraction phase. The solid support (the fiber) was excluded from the simulation since it doesn't take part in the mass transfer of analyte. The extraction kinetics takes place at the boundary between the extraction phase and sample matrix, which is defined as the mass flux according to the Fick's law of diffusion. The mass transfer in both domains (sample matrix and extraction phase) was defined by the 'transported diluted species (tds)' physics interface in COMSOL Multiphysics. This physics interface simulates the transport of diluted chemical species in a solvent driven by the diffusion and convection (when coupled with fluid flow). The transport media could be a liquid solvent, a gel, or a porous solid immersed in a liquid solvent. 'Laminar flow (spf)' physics was used in COMSOL Multiphysics to simulate the convection in the sample domain. This 'laminar flow (spf)' physics couples the functionalities of 'transported diluted species (tds)' of sample domain with the single phase fluid flow (convection). The fluid flow of the sample domain was defined as a single phase because of the Reynolds number ($Re$) calculated for the experimental conditions ( vortex speed of the sample during the extraction) was way below the threshold value ($Re <$ 2000; $laminar\ flow$). The Reynolds number can be obtained by the following equation:

$$R_e = \frac{\rho UL}{\mu} \qquad (2.17)$$

Where,

$R_e$    = Reynolds number;    $\rho$    = density of the fluid;  U    = linear flow velocity

$L$    = characteristic linear length scale;    $\mu$    = dynamic viscosity of the fluid

We can convert the vortex speed into linear velocity of the fluid using following equation:

$$v = \omega r$$

Where $v$ is the linear velocity (m s$^{-1}$); $\omega$ is the angular speed ($\omega = 2\pi \times rotation\ per\ minute$),

which is the vortex speed in this case; and $r$ is the radius of the sample vial. The linear velocity of

fluid is calculated app. 0.5 (m s$^{-1}$) for 1500 rpm in a vial with 0.5 cm radius. Using this linear velocity

in computational model, the cell Reynolds number was obtained <40 which satisfy the selection of

'laminar flow (spf)' physics interface.
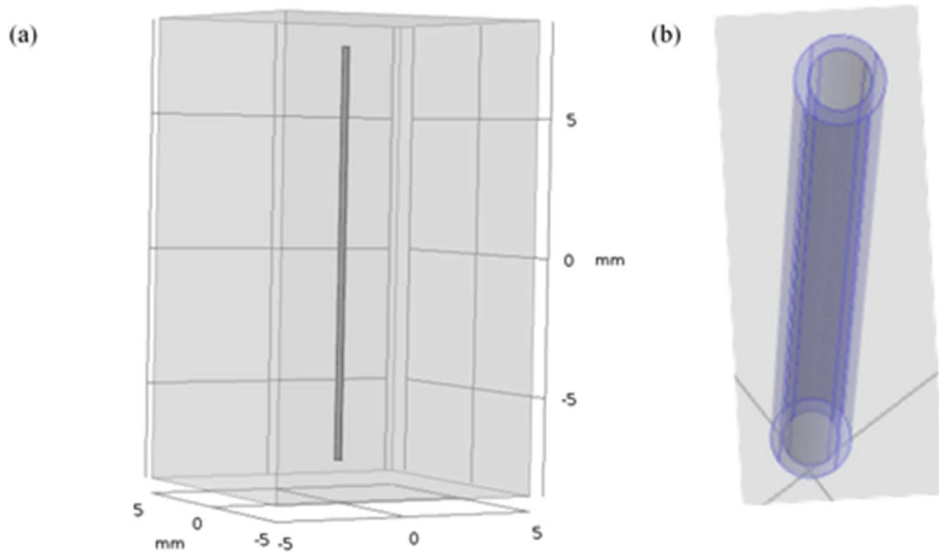


Figure 2. 4 (a) 3D geometry of an SPME fiber in rectangular box. The volume (W: D: H = 10mm x 10mm x 17mm) of the box is equivalent to the experimental sample volume. (b) A close view of SPME fiber coating. The thickness of the fiber is 45 µm

The physical parameters used for extraction simulation in bovine lung tissue are given Table 2.3.

The details of the extraction kinetics are discussed in Results and Discussion section.

Table 2. 3  Parameters used for all computational modeling in COMSOL Multiphysics

| Paremeter name | Expression | unit | Description |
|---|---|---|---|
| A_init | 4.60E-05 | mol/L | Initial concentration of DOX |
| B_init | 2.00E-01 | mol/L | Adjusted binding matrix concentration in tissue |
| Ds_A | 6.54E-06 | cm^-2/s | Diffusion coefficient of DOX in tissue matrix |
| Ds_B | 6.54E-07 | cm^-2/s | Adjusted diffusion coefficient of binding matrices in tissue matrix |
| T_in | 298 | K | Ambient temperature of experimental condition |
| vD | 10 | mm | Diameter of the sample matrix dimension |
| vH | 17 | mm | Height of the sample matrix dimension |
| vW | 10 | mm | Width of the sample matrix dimension |
| Mw | 543.5 | g/mol | Molecular weight of DOX |
| Mb | 6.65E+04 | g/mol | Molecular weight of has |
| b | 145 | µm | SPME fiber outer coating diameter |
| a | 100 | µm | SPME fiber diameter |
| l | 15 | µm | Coating length |
| Ka | 6.20E+03 | L/mol | Binding constant of DOX with HSA |
| kr | 0.5 | 1/s | Rate of association of DOX with HSA matrix |
| kf | Ka*kr | L/(mol*s) | Rate of dissociation of DOX from HSA matrix |
| K | 468 | L/mol | Adsorption equilibrium constant |
| k_ads | 6.50E-05 | m/s | Adsorption rate constant of DOX on extraction surface |
| k_des | k_ads/K | mol/(m^2*s) | Desorption rate constant of DOX from extraction surface |
| Υ_s | 1.12E-05 | mol/m^2 | Maximum active site concentration |
| Af | 4.55E-04 | m^2 | Active surface area per fiber |

The numerical values used for simulation were obtained from experimental conditions, such as the SPME extraction phase dimensions – length of the extraction phase is 15 mm. Table 2.3 contains all the parameters used for three four different computational models (static extraction in agar gel, agitated extraction in PBS solution, agitated extraction in PBS with HSA, and static

extraction in tissue). Some parameters were inactive in respective computational model where it was not required, for example, linear velocity is not required in static extraction. It should be noted that the diffusion coefficient for binding matrix components in tissue is adjusted in comparison with the diffusion coefficient for HSA.[68]

### 2.3.5. Static extraction time profile of doxorubicin in agar gel

In this experiment, we evaluated the kinetic profile for static extraction of DOX in the absence of a binding matrix. Agar powder (0.8%, w/w) was added in PBS (1X, pH 7.4) spiked with 100 ng mL$^{-1}$ of DOX. The mixture was heated at 70$^{\circ}$C in a water bath for 30 min. Once the agar powder was completely dissolved, the solution was transferred to 2 mL glass vials and allowed to cool at room temperature until it attained a gel consistency. Then, a preconditioned SPME fiber was inserted into the vial containing 1.8 mL of agar gel. Static extraction was performed with five replicates and at eight different time points over 120 hrs. After each extraction time points, fibers were cleaned with Kimwipes and vortexed with 300 μL of LC-MS grade water for 10 s to remove matrix components from the coating. Desorption was performed with 300 μL of ACN/H2O (80/20 + 0.1% FA) for 60 min in a shaker at 1500 rpm.

**Mathematical model:** The 3D geometry was separated into two domains –the  sample matrix and the extraction phase (see the Figure 2.4). The objective was to calculate the mass transfer of a chemical species (DOX in this case) which is transported from one domain to another.
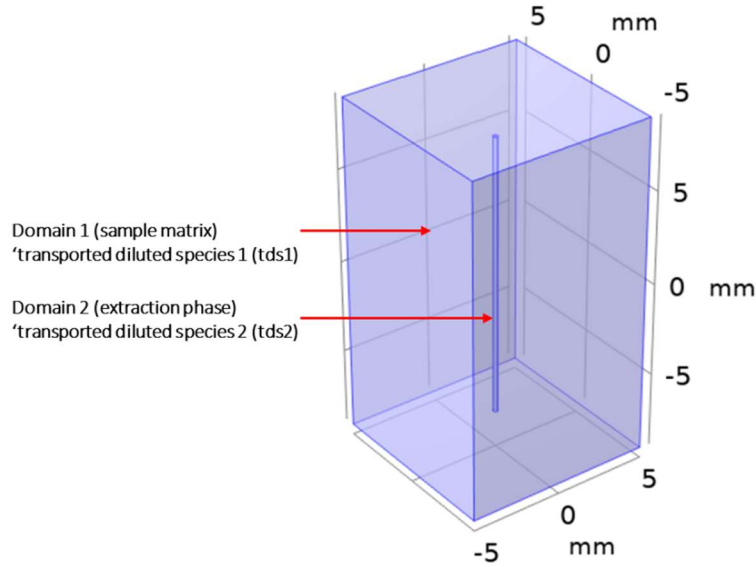
**Figure 2. 5** Two domains of 3D geometry of SPME extraction (static) in agar gel defined with 'transported diluted species (tds)' physics interface

That mass transport is driven by diffusion which can be defined by Fick's law. To determine the mass transport between the interface of the two domains, the 'transported diluted species (tds)' physics interface from COMSOL Multiphysics was selected for both domains. Under static extraction condition and without the presence of any binding matrix (agar is considered as a matrix lacking any binding affinity to the analyte), diffusion is the only governing force for mass transport. Therefore, the time-dependent mass balance equation for the bulk can be described according to eq. (1.6).

$$\frac{\partial c_A}{\partial t} - \nabla * (D_s \nabla c_A) = 0 \tag{2.18}$$

Where, $c_A$ (mol m$^{-3}$) is the concentration of DOX in agar gel, and $D_s$ (m$^2$s$^{-1}$) is the diffusivity in the bulk. It should be noted that the extraction phase is considered as a porous solid where the analyte partakes in surface reactions (adsorption and desorption). Therefore, the mass balance equation for the solid surface can be described by the following equation:

$$\frac{\partial c_s}{\partial t} - \nabla * (D_e \nabla c_s) = R \tag{2.19}$$

Where, $c_s$ (mol m$^{-2}$) is the analyte concentration in the extraction phase (solid surface), $D_e$ is the diffusivity in the extraction phase, and $R$ is the resultant of surface reactions. R can be defined as:

$$R = r_{ads} - r_{des}$$

According to eq. (2.6);

$$R = k_{ads} * [A] * \left(1 - \frac{cs}{\gamma_s}\right) - k_{des} * \frac{cs}{\gamma_s}$$

Where, Now, eq. (2.19) can be expressed as:

$$\frac{\partial c_s}{\partial t} - \nabla * (D_e \nabla c_s) = k_{ads} * [A] * \left(1 - \frac{cs}{\gamma_s}\right) - k_{des} * \frac{cs}{\gamma_s} \tag{2.20}$$

The variable $c_A$ in eq. (2.18) and $c_s$ in eq. (2.20) are both time and space dependent. Therefore, both the initial conditions and the boundary conditions are required to solve these equations.

**The initial conditions** for numerical models are given below:

$$c_A = A_{init} \quad \text{[bulk]}$$

$$c_s = 0 \quad \text{[surface]}$$

**Boundary conditions:** The boundary conditions for domain 1 (Figure 2.5) were set at the outer boundary and the interface of the two domains. The mass flux of the analyte across the outer boundary is zero. Which implies no analyte can cross the outer boundary. Therefore-

$$-\nabla * (D \nabla c_A) = 0 \quad \text{[at the outer surface of the sample]}$$

However, there is a mass flux at the interface of two domains due to surface reactions.

$$-\nabla * (D \nabla c_A) = -r_{ads} + r_{des} \quad \text{[sample-extraction phase interface]}$$

Or,

$$-\nabla * (D \nabla c_A) = -k_{ads} * [A] * \left(1 - \frac{cs}{\gamma_s}\right) + k_{des} * \frac{cs}{\gamma_s} \tag{2.21}$$

The negative sign of $-r_{ads}$ indicates that the concentration of the analyte in the bulk decreases due to adsorption onto the solid surface, whereas $r_{des}$ increases.

This boundary conditions for the domain 2 were set at the interface of two domains and the inner surface of the extraction phase which is connected to a metallic fiber (the extraction phase is coated onto a metallic fiber which does not contribute to the mass transfer). Therefore, the boundary condition at the inner surface is -

$$-\nabla * (D\nabla c_s) = 0$$

And the boundary condition at the interface of two domains-

$$-\nabla * (D\nabla c_s) = r_{ads} - r_{des}$$

$$\text{Or, } -\nabla * (D\nabla c_s) = k_{ads} * [A] * \left(1 - \frac{cs}{\gamma_s}\right) - k_{des} * \frac{cs}{\gamma_s}$$

The same boundary conditions for mass transfer of DOX were maintained for the rest of the mathematical models. Detailed mass transfer kinetics of DOX in r solid coating has been explained in the 'results ad discussion' section.

**Meshing:** User controlled meshing was performed using 'Free Tetrahedral' meshing elements. The geometry of SPME extraction is divided into two domains – Sample matrix (Domain-1) and the Extraction phase (Doman-2). Domain-1 was meshed with predefined size – '**Extra Fine**', and Domanin-2 was meshed with predefined '**Extremely Fine**' size. Since SPME extraction phase is very small compared to the sample matrix, the smallest possible meshing unit was used for the extraction phase to increase the meshing resolution.
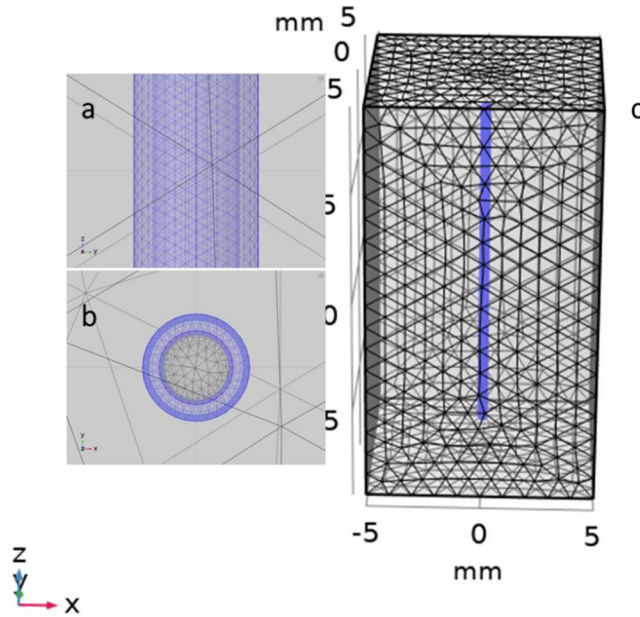
**Figure 2. 6** The meshing of SPME geometry in COMSOL –(a) side view of extraction phase domain; (b) top view of extraction phase domain; (c) the whole geometry

**Study:** In this section 'Time dependent' study was selected to calculate the time-dependent mass transport at the interface of two domains. Solvers were selected for time dependent study as 'Direct' and 'Fully coupled'. The 'Direct' solver corresponds to a linear solver -MUMPS and the 'Fully coupled solver' included both linear solver and nonlinear solver (constant Newton).
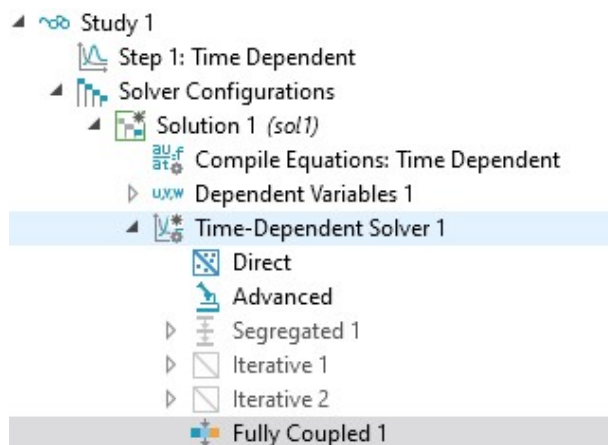


**Figure 2. 7** The solver sequence for Time-dependent' study of static extraction of DOX in agar gel

### 2.3.6. Agitated extraction time profile of doxorubicin in PBS

DOX was spiked in PBS (1X, pH 7.4) at the concentration of 100 ng mL$^{-1}$. Extraction was performed with preconditioned SPME C-8 mixed mode fibers with five replicates and at 1500 rpm vortex speed. The extraction time profile was obtained at eight different time points over 120 min. After each extraction, washing and desorption were performed followed by aforementioned method.

**Mathematical model:** The physics interfaces for sample matrix and the extraction phase were the same as for the static extraction condition. To simulate the convection in the sample domain, 'laminar flow (spf)' physics was selected. The fluid flow kinetics in the real experimental conditions is a vortex flow in finite volume. However, it is very difficult to develop such computational model due to the high number of degrees of freedom (number of mesh elements). To simplify the mathematical model, a single phase 'laminar flow (spf)' physics interface was chosen to simulate the fluid dynamics. The 'laminar flow (spf)' physics was coupled with sample domain physics 'transported diluted species 1 (tds1)' in order to provide the convection force for the transport of the diluted species (DOX) in the sample domain. Therefore, the mass transfer of DOX in the sample domain is controlled by convective-diffusion which can be defined by Fick's equation followed by eq. (1.7) and eq. (2.19).

Mass transfer in the sample matrix: $\frac{\partial c_A}{\partial t} - \nabla * (D_s \nabla c_A) + \boldsymbol{u} * \nabla c_A = 0$      [convective-diffusive]

Mass transfer in the extraction phase: $\frac{\partial c_S}{\partial t} - \nabla * (D_e \nabla c_S) = R$      [diffusive]

The initial conditions for analytes concentration in the sample matrix and the extraction phase are the same as for static extraction in agar gel. The boundary condition at the sample-extraction

phase interface was the same as for static extraction (eq. 2.19).

The 'laminar flow (spf)' physics interface is based on the Navier-Stokes equations for conservation of mass, momentum, and energy.

$$\frac{\partial \rho}{\partial t} + \nabla \left( \rho \boldsymbol{u} \right) = 0 \tag{2.22}$$

$$\rho \frac{\partial \boldsymbol{u}}{\partial t} + \rho \left( \boldsymbol{u}. \nabla \right) \boldsymbol{u} = \nabla. \left[ p\mathbf{I} + \mathbf{K} \right] + \mathbf{F} \tag{2.23}$$

$$\mathbf{F} = \mu \left( \nabla \boldsymbol{u} + (\nabla \boldsymbol{u})^T \right) \tag{2.24}$$

Where, $\rho$ is the density (kg m$^{-3}$), $\boldsymbol{u}$ is the velocity vector (m s$^{-1}$), $p$ is the pressure unit (Pa), $\mathbf{K}$ is the viscous stress tensor (Pa), $\mathbf{F}$ is the volume force vector (N m$^{-3}$), $\mu$ is the dynamic viscosity (Pa s) and $T$ is the temperature (K). Eq. (2.22) is a continuity equation which characterizes the conservation of mass. Eq. (2.23) is a vector equation which characterizes the conservation of momentum.
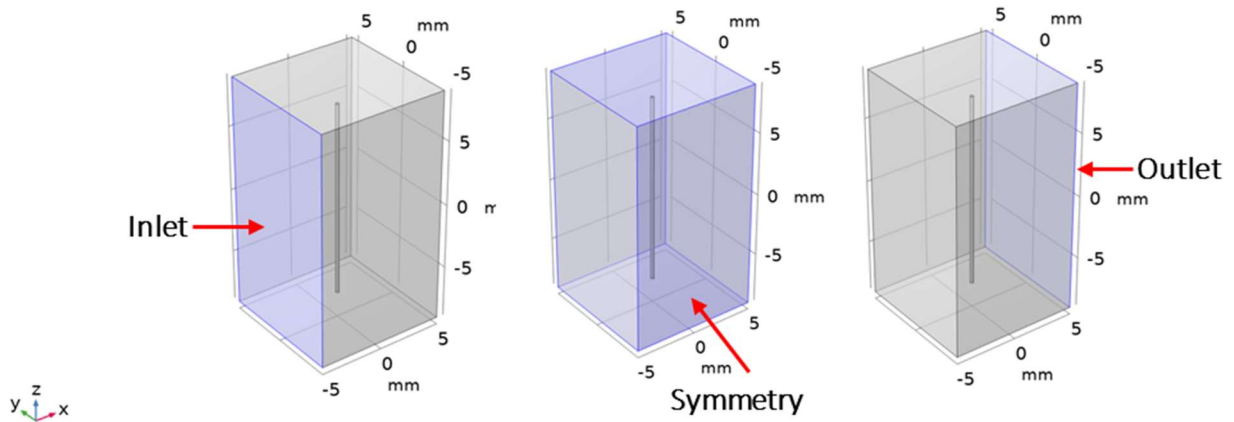


**Figure 2. 8  3D geometry of SPME extraction with boundary set up**

The boundary conditions for laminar fluid flow are shown in Figure 2.8. The solid wall boundary was 'No slip'. It is set for all boundaries except overridden by other conditions set particularly to any other boundaries.

Wall = No slip; where $\boldsymbol{u} = 0$.

Inlet: $\boldsymbol{u} = -\boldsymbol{n}U_0$          Outlet: $p = 0$       Initial condition: $U_0 = \text{u\_init}$

Where $\boldsymbol{n}$ is the boundary normal pointing out of the domain, $U_0$ is the linear flow velocity. The outlet condition can be set either pressure of velocity to specify the stress. A 'static' pressure option is select from the model to set the tangential stress component at zero. Also 'Suppress backflow' check is selected to reduce the amount of fluid entering the domain through the boundary. The other boundary walls of the sample domain were designated as symmetric walls to reduce their size for solving problem. The initial condition of the fluid flow is set by the linear velocity parameter.

**Mesh:** The meshing sequence is selected as 'User-controlled mesh'. The meshing sequence is given below:
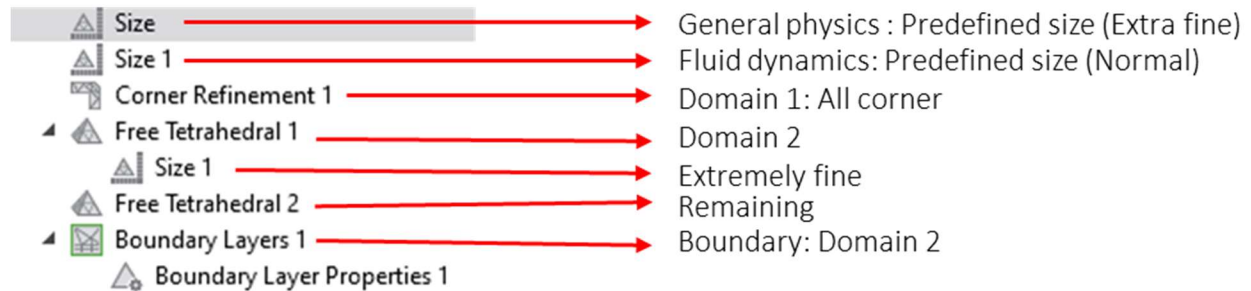


**Figure 2. 9** Meshing sequence of 3D SPME geometry in COMSOL for agitated extraction condition

**Study**: This node included both 'Stationary' for 'laminar flow (spf)' physics and 'Time dependent' for remaining physics. Both 'Stationary' and 'Time dependent' steps were subnode of 'Study'. The solvers for both 'Stationary' and 'Time dependent' were – 'Direct' and 'Fully coupled' (see Figure 2.10).
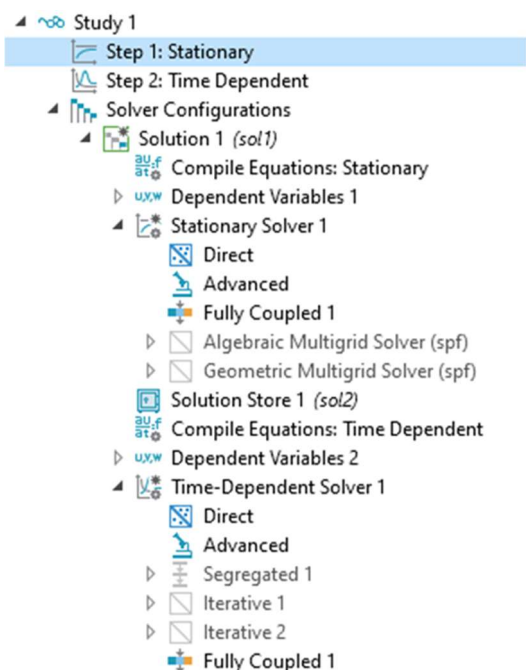
Figure 2. 10 'Study' sequence for SPME extraction kinetics in PBS under agitation

### 2.3.7. SPME extraction of DOX in presence of HSA binding matrix

Human Serum Albumin (HSA, 3.6%, w/w) was added in PBS at pH 7.4. Then 100 ng·mL$^{-1}$ of DOX was spiked into that mixture. In order to ensure the binding reaction reached equilibrium, the solution was incubated overnight at room temperature at 250 rpm. An extraction time profile was performed using preconditioned C-8 mixed mode SPME fibers for 10 different time points over 120 mins.

**Mathematical model:** The physics interfaces selected for this model were – 'reaction engineering (re)' to define the binding kinetics between the analyte (DOX) and the binding matrix HSA, 'transported diluted species (tds)' for the sample domain, 'transported diluted species 2 (tds2)' and laminar flow (spf)'. The 'reaction engineering (re)' physics is selected in a separate component while building the model in the wizard, because this physics interface is 0D in COMSOL by default, and the space dependent model can be generated according to the parameters defined by the .

56
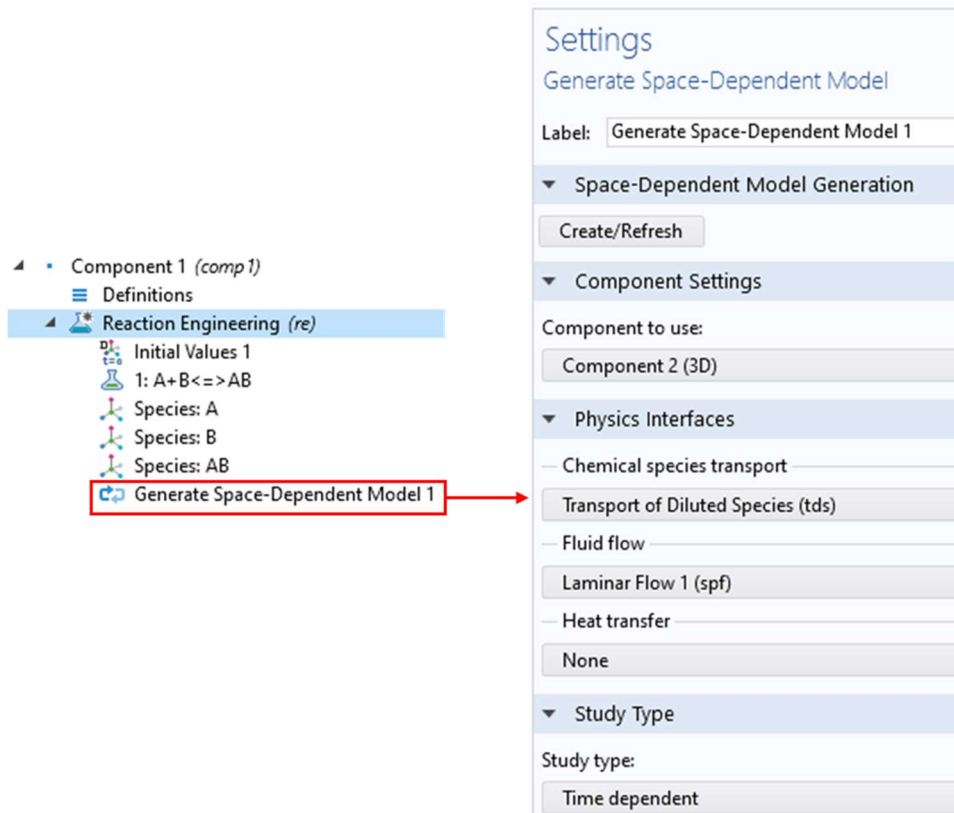
**Figure 2. 11 The 'reaction engineering (re)' physics interface in COMSOL Multiphysics 5.2**

The reaction for this study is defined as a reversible reaction between the analyte (DOX, A) and

the binding matrix (HSA, B):

$$A + B \iff AB$$
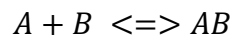
The reaction kinetics depends on temperature ($T$) and volume ($V$). The volume for this reaction

was constant, therefore the time-dependent mass balance equation can be defined as:

$$\frac{dc_i}{dt} = R_i^*$$

Where, $\frac{dc_i}{dt}$ denotes the change of concentration of species ($i$) with respect to time ($t$), $R_i^*$ is the

rate expression of species ($i$). The rate of expression can be defined as:

$$R_i^* = \sum_j v_{ij} r_j$$

Where, $v_{ij}$ is the activity coefficient of $j$ number of species $(i)$, and $r_j$ is the reaction rate which can be expressed as:

$$r_j = k_j^f \prod_{i \in react} c_i^{-v_{ij}} - k_j^r \prod_{i \in prod} c_i^{v_{ij}} \qquad (2.25)$$

Where, $k_j^f$ and $k_j^r$ denote the forward and backward reaction rate. The equilibrium constant for this reaction can be defined as binding association constant $K_A$ which is the ration of forward and backward reaction rates at equilibrium.

$$K_A = \frac{k_j^f}{k_j^r} \qquad (2.26)$$

The binding association constant, $K_A$ is determined experimentally from the slope of the binding isotherm (discussed in the Results section). For the mathematical modeling, the rate of dissociation of the analyte (DOX) from the binding matrix (HSA) is very fast and in the range of 0.1 to 1 [s⁻¹]. The assumption is true for many analytes.[17] In this case, it was considered 0.5 [s⁻¹] (since we have already determined the binding association constant $K_A$, the backward reaction rate only affects the time to reach equilibrium, and in our case is considered negligible unless the dissociation rate is extremely slow which may impact matrix assisted mass transfer). The initial conditions for this reaction are:

$$A = A_{\_init} \qquad B = B_{\_init} \qquad \text{and} \qquad AB = 0$$

Where, $A_{\_init}$ is the initial concentration of the analyte, $B_{\_init}$ is the initial concentration of binding matrix, and $AB$ is the initial concentration of the matrix-bound analyte at the beginning of the reaction. Since, this reaction kinetics affect the mass transport properties in the sample domain (we ignored the binding reaction in the extraction phase, since extraction phase material is

restricted to macromolecules like proteins),[34,35] a space-dependent-model was generated coupled with 'transported diluted species 1 (tds)' and 'laminar flow (spf)' physics.
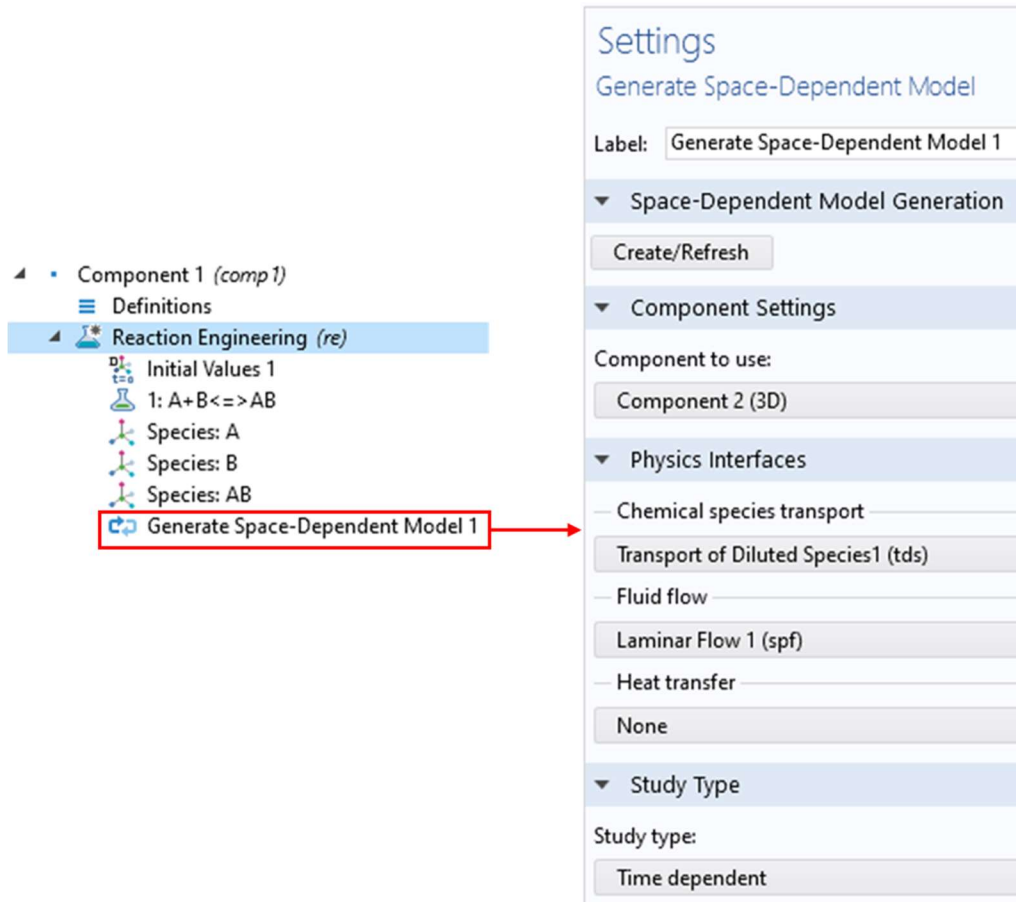


**Figure 2. 12** Space-Dependent Model for 'reaction engineering (re)' physics interface

The space-dependent model creates a new physics 'Chemistry (chem)' in component-2. 'Chemistry (chem)' under component-2 (3D) is now the space and time dependent physics for reaction engineering which contains all the variables and parameters of 'reaction engineering (re)' physics under defined properties. The 'reaction engineering (re)' physics also transfers the kinetic properties of the reaction to the sample domain since it affects the mass transfer (see Figure 2.13).
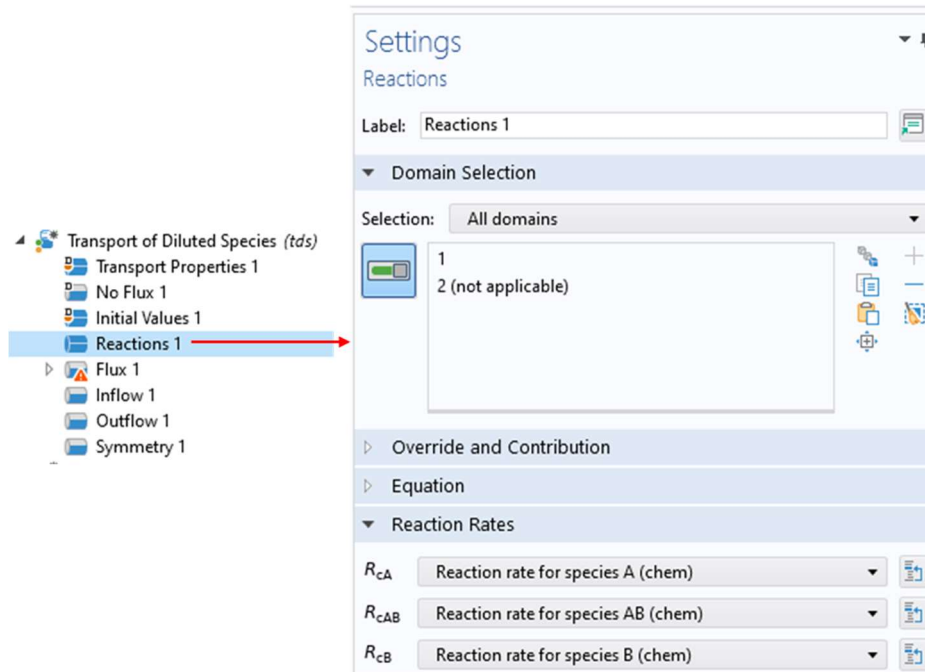
**Figure 2. 13 The physics interface of the sample domain (1) contains the reaction kinetic properties**

The time dependent mass balance equations and initial conditions for the physics interfaces – 'transported diluted species 1 (tds)' for mass transfer in the sample domain, 'transported diluted species 2 (tds2)' for mass transfer in the extraction phase, and the 'laminar flow (spf)' for fluid flow in the sample domain are the same as for the previous model explained for SPME extraction kinetics in PBS under agitation.

**Mesh:** The meshing was generated by 'User-controlled' configuration and the properties were the same as for the previous model – 'SPME extraction kinetics in PBS under agitation'.

**Study:** Two separate 'Study' nodes were developed – one for the 'reaction engineering (re)' physics in component-1 node, another for the remaining physics in component-2 (see Figure 2.14).
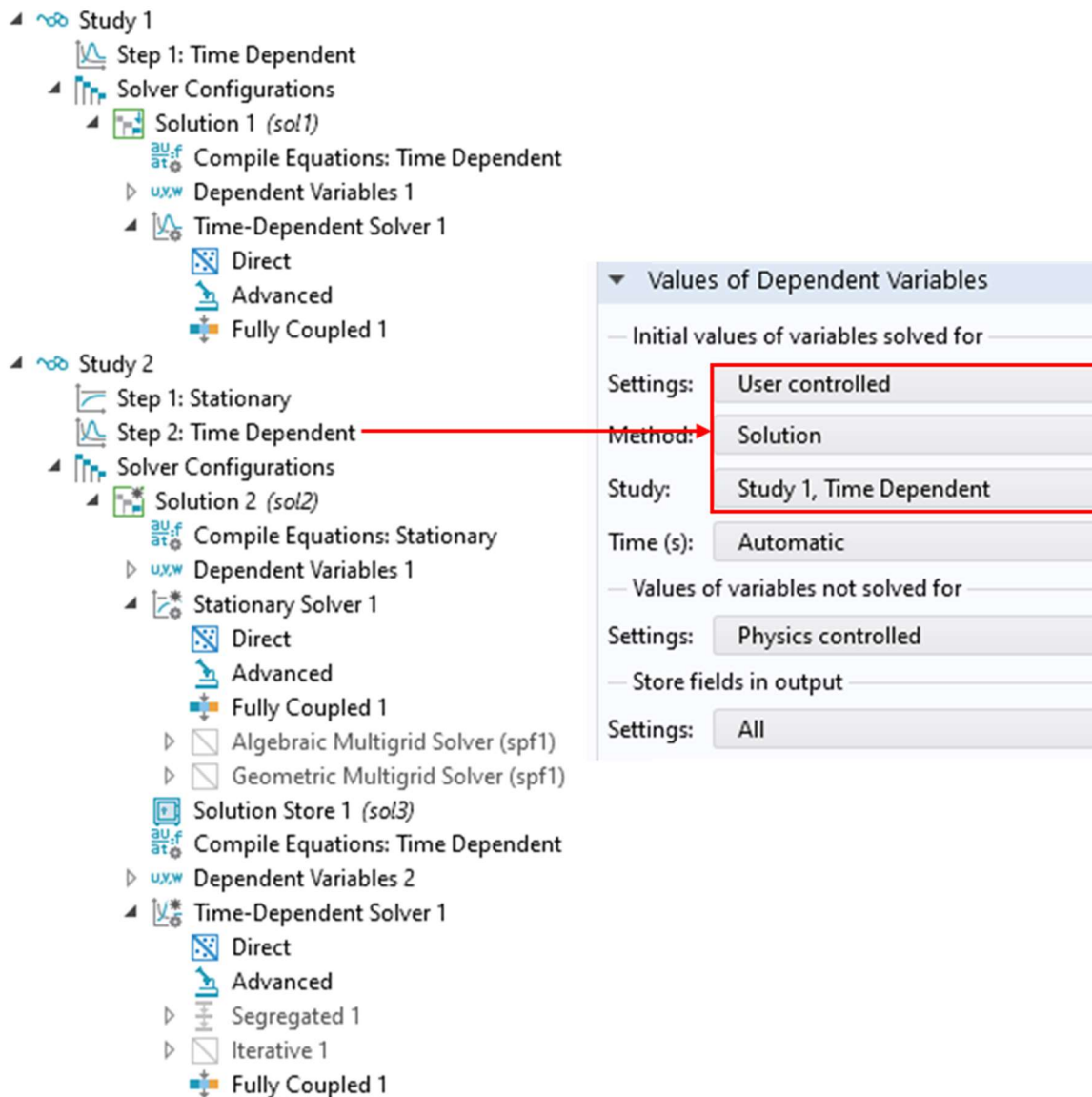
**Figure 2. 14 Study design for SPME extraction kinetics of DOX in presence of HSA binding matrix**

One of the important factors in the 'Study' node is to set the initial values and variables solved for 'Study 2' section as user controlled, and then solving of time dependent study-1 (according to Figure 2.13). This will allow the time dependent study-2 to take the initial values of the species in the sample matrix after equilibrium is established which is consistent with the experimental conditions.

### 2.3.8. Experimental measurement of binding constant $K_A$ of DOX with HSA

The binding constant $K_A$ for DOX was determined according to eq. (2.13).

$$K_A * [M]^{tot} = \frac{[A]^{tot}}{[A]^{free}} - 1$$

Where, $[M]^{tot}$, $[A]^{tot}$ are the initial concentrations of binding matrix (HSA) and DOX respectively. The superfix *tot* was used instead of *init*, to define the total matrix concentration in a sample matrix where multiple binding matrix components are present (such as tissue). $[A]^{free}$ is the free concentration of DOX experimentally determined by SPME extraction. In experimental study, five mixtures of DOX-HSA were prepared in PBS solution each of which was spiked with 100 ppb DOX and different concentration of HSA matrix (see Table 2.4 in Result and Discussion).

### 2.3.9. Extraction of DOX from homogenized lung tissue

Bovine lung was cut into small pieces and homogenized using dry ice and a meat blender. Doxorubicin was spiked into homogenized lung tissue (10g of each sample) at concentration levels 5, 10, 15, 25, and 50 µg·mL$^{-1}$. After spiking, samples were gently vortexed at 500 rpm for 2 hours and then stored at 4°C overnight for binding. The following day, each sample was equilibrated at room temperature for an hour. Extractions were performed from 1g of tissue sample for 25 mins under equilibrium conditions. After extractions, fibers were properly cleaned (wiped with Kimwipes) and rinsed with 300 µL of Milli Q water for 10 sec to remove attached tissue matrix and other unspecific matrix components, then submitted to desorption in a vial with 300 µL of desorption solvent (80% ACN + 20% H2O + 0.14% FA) for 60 minutes.

**Mathematical modeling:** A 3D mathematical model was developed (see Figure 2.15) using following physics interfaces – 'reaction engineering (re)' in Component-1 to demonstrate the reaction kinetics of DOX with the binding matrix components in the tissue, 'transported diluted species (tds)' and 'transported diluted species 2 (tds2) in Component-2 to define the mass transport in the tissue and the extraction phase, respectively. No convection was involved in mass transfer. The space-dependent reaction engineering physics - 'Chemistry (chem)' was generated in Component-2.
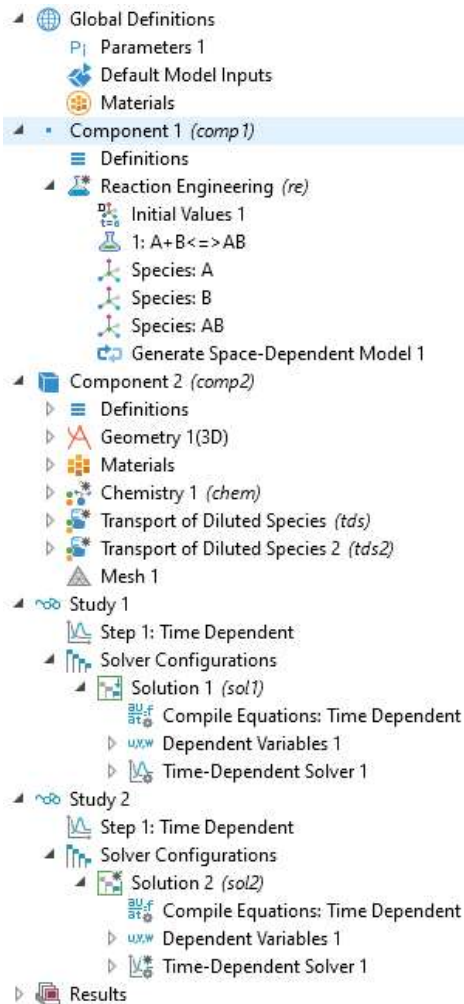


Figure 2. 15  The 'Model Builder' section of COMSOL Multiphysics 5.2 showing all the components, studies and physics included for simulation of SPME extraction of DOX from tissue

The binding reaction for DOX in the tissue matrix has been simplified in this model. There are different types of binding matrices present in the tissue and the initial (or total) concentration of each type of binding matrix is unknown (it is also practically very difficult to determine, if not impossible). To simplify this problem, all different types of binding matrices are considered as one and the binding affinity of DOX for each different matrix was considered as the apparent bind constant $K_{App}$. However, this oversimplification did not affect the determination of the value of $K_{App}$ which has been rationalized in the 'results and discussion' section.

**Mass transfer:** The mass transfer in the tissue matrix is controlled by the diffusion and matrix assisted mass transfer (the binding matrices contributes to the mass transfer). The time-dependent mass balance equation in tissue can be defined as:

$$\frac{\partial c}{\partial t} - \nabla * (D_s \nabla c_A) = R$$

Where, $R$ denotes the source term which defines if the analyte is consumed or produced in the system. Since the binding components near to the extraction phase surface release the analyte, $R > 0$.

The mass transfer in the extraction phase is only controlled by the diffusion and the mass balance equation is the same as for other cases explained before. The initial conditions for the binding reaction are the same as for DOX-HSA reaction (due to simplifications), however, the initial values are different. For the purpose of simulation the matrix concentration was extrapolated until it matched to the experimental extraction time profile (the detail has been explained in the 'results and discussion' section). The initial concentration DOX in the tissue was 25 ng mL$^{-1}$. The other initial conditions were the same as for the SPME extraction in agar gel (static). The boundary

conditions at the tissue-extraction phase interface were the same as for other extraction conditions described in eq. 2.19.

**Mesh:** The meshing was user controlled and designed in the same way as for the SPME extraction in agar gel (static extraction).

**Study:** Two separate studies were performed like Figure 2.14, except Study-2 did not include 'Stationary' solver required for 'laminar flow (spf)' physics.

### 2.3.10. LC-MS Characterization of Doxorubicin

DOX (MW: 543.4 Da) was characterized using a Thermo Ultima 3000 liquid chromatographic system coupled to a Quantiva (Thermo Scientific, San Jose, CA) triple quadrupole mass spectrometer. The LC-MS method was carried out according to recently published literature.[65] Briefly, liquid chromatographic separation was carried out using a C-18 (4.6 mm; 100mm, 5µm) Phenomenex column with mobile phase A (100% H2O +0.1% FA) and mobile phase B (100% ACN + 0.1% FA), as stated in the associated literature.[65] The instrumental limit of quantification (LOQ) under these conditions was 0.1 ppb.

### 2.4. Results and discussion

#### 2.4.1. In-Silico Study of Extraction Kinetics under Static Conditions (in Agar Gel)

Agar gel is considered as an ideal matrix for static (no convection) extractions without any binding matrix. Here, numerical simulations were based on the mass transfer kinetics of analytes that take place between the boundary layer of the SPME fiber coating and the sample matrix. The mass balance equation can be derived from eq. (1.8):[32]

$$N_i = \nabla * (D\nabla c) - \boldsymbol{u} * \nabla c + R \qquad (2.27)$$

Where $c$ is the concentration of the species (mol.m$^{-3}$), $D$ denotes the diffusion coefficient (m$^2$.s$^{-1}$), $R$ is the amount of any species produced or consumed in the system (mol m$^{-3}$ s$^{-1}$), and $\boldsymbol{u}$ is the velocity vector (m s$^{-1}$). The flux vector $N_i$ (mol m$^{-2}$ s$^{-1}$) is associated with the net change in mass transfer at the boundary layer.

In static extraction conditions for agar gel, $N_i$ is only controlled by diffusion and the binding equilibrium which can be expressed by eq. (1.9).

$$N_i = D\nabla c$$

For solid-coating adsorption kinetics, the flux vector $N_i$ for static extraction in agar gel can be expressed as:

$$N_i(mol\ m^{-2}\ s^{-1}) = r_{ads} - r_{des} \tag{2.28}$$

From eq. (2.7) and (2.28),

$$\frac{\partial cs}{\partial t}(mol\ m^{-2}\ s^{-1}) = k_{ads} * [A] * \left(1 - \frac{cs}{\gamma_s}\right) - k_{des} * \frac{cs}{\gamma_s} \tag{2.29}$$

Eq. (2.29) defines the mass transfer kinetics in static mode for solid coatings. The constant $k_{ads}$ was experimentally determined based on the assumption that $r_{des}$ can be considered negligible at the start of extraction, since the amount of extract on the fiber is infinitesimally small. In this case, eq. (2.29) can be expressed as:

$$\frac{\partial cs}{\partial t}(mol\ m^{-2}\ s^{-1}) = k_{ads} * [A]^{eq} * \left(1 - \frac{cs}{\gamma_s}\right) \tag{2.30}$$

Experimentally, $\frac{\partial c}{\partial t}$ can be obtained from the amount extracted on the fiber over time when the extraction rate is in the linear regime, which was experimentally observed to occur after 10 mins of extraction. Prior to this time point, the amount of extract on the fiber was below the instrumental LOQ. Therefore, $k_{ads}$ from eq. (2.30) can be derived as follows:

$$k_{ads} \left(\frac{m}{s}\right) = \frac{\frac{\partial c}{\partial t}}{[A]^t * (1 - \frac{cs}{\gamma s})} \tag{2.31}$$

Once $k_{ads}$ is attained via eq. (2.31), the value of $k_{des}$ can be obtained from eq. (2.7), followed by measurement of the adsorption equilibrium constant K. In this work, the specific surface area per fiber was 4.54e$^{-5}$ (m$^2$), while the saturated amount of DOX extracted per fiber was determined as 5.1e$^{-09}$ (mol) (Figure 2.2). The calculated value of $\gamma_s$ for DOX was 1.12E-04 (mol m$^{-2}$). From eq. (2.7), the estimated value of the adsorption equilibrium constant for DOX was ≈468 (m$^3$ mol$^{-1}$) (Table 2.2). Considering these parameters, the extraction kinetics were simulated using mathematical models and validated against experimental results. Simulation was performed using a 3D model designed in COMSOL Multiphysics 5.2, using the experimental parameters listed above to demonstrate the extraction kinetics in agar gel. The calculated results were then compared with the experimental extraction time profile. The simulation showed that the equilibrium time for static extraction was approximately 80 h, which is in good agreement with experimental results (see Figure 2.16).
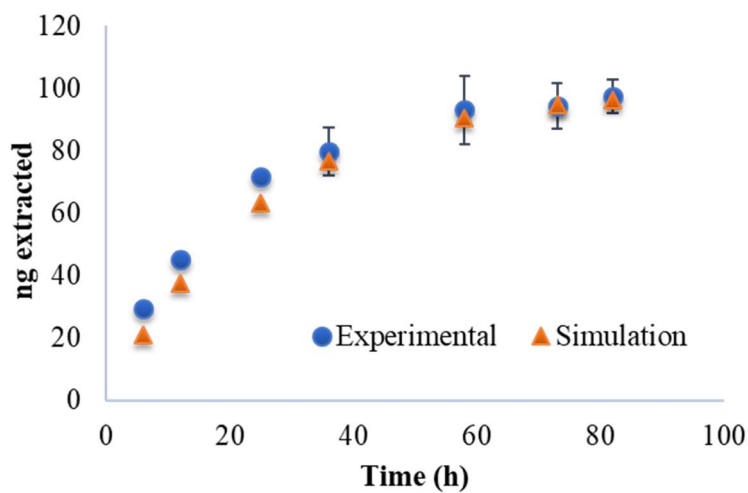


Figure 2. 16  Comparison of in-silico and experimental extraction time profiles of DOX with an initial concentration of 100 ng·mL$^{-1}$ in agar gel

**In-Silico Study of Extraction Kinetics using Agitated Conditions (in PBS).** Under agitation, the flux vector $N_i$ can be expressed as:

$$N_i = \nabla * (D\nabla c) - \boldsymbol{u} * \nabla c = r_{ads} - r_{des} \tag{2.32}$$

The mass transfer equation for solid coatings is the same as eq. (2.30), except that in this case, the flux $N_i$ changes rapidly due to the convection term $\boldsymbol{u}$, which enables equilibrium conditions to be established at a faster rate in comparison to the rate of equilibrium at static conditions.
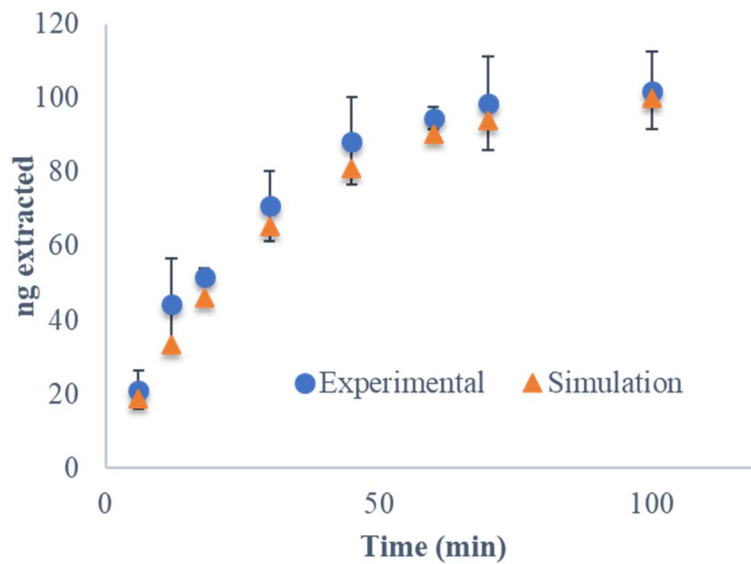


Figure 2. 17 Comparison of in-silico and experimental extraction time profiles of DOX, with initial concentration of 100 ng·mL$^{-1}$ in PBS

Simulated extraction kinetics under agitated conditions forecasted the time to reach equilibrium was approximately 100 min, which is in good agreement with experimental results (see Figure 2.17).

### 2.4.2. In-Silico Study of Extraction Kinetics under Agitated Conditions in the Presence of an HSA Binding Matrix.

In the presence of a binding matrix, the flux vector $N_i$ is defined by eq. (2.27). The reaction term $R$ of eq. (2.27) can be derived from eq. (2.12).

$$R = k_f * ([A]^{free} * [M]^{tot}) + k_r * ([A]^{tot} - [A]^{free} \tag{2.33}$$

Therefore, the flux for analyte in the presence of a binding matrix can be calculated as:

$$N_i = \nabla.(D\nabla c) - \boldsymbol{u}.\nabla c - k_f * ([A]^{free} * [M]^{tot}) + k_r * ([A]^{tot} - [A]^{free}) \tag{2.34}$$

This equation was used calculate extraction time profiles in the presence of a binding matrix are as follows:

$$\frac{\partial cs}{\partial t} = D\nabla c - \boldsymbol{u}.\nabla c - k_f * ([A]^{free} * [M]^{tot}) + k_r * ([A]^{tot} - [A]^{free}) \tag{2.35}$$

In order to simulate an extraction time profile in the presence of the HSA binding matrix, the value of the binding association constant $(K_A)$ was determined experimentally from Table 2.4 followed by using eq. (2.13). This calculated value was used to simulate an extraction time profile in the presence of a binding matrix, with good agreement found between simulated and experimental results. In this simulation, the value of the dissociation rate constant, $k_r$ with HSA for DOX was taken to be 0.5 (s$^{-1}$) based on a previously reported study that targeted similar drugs. [17]
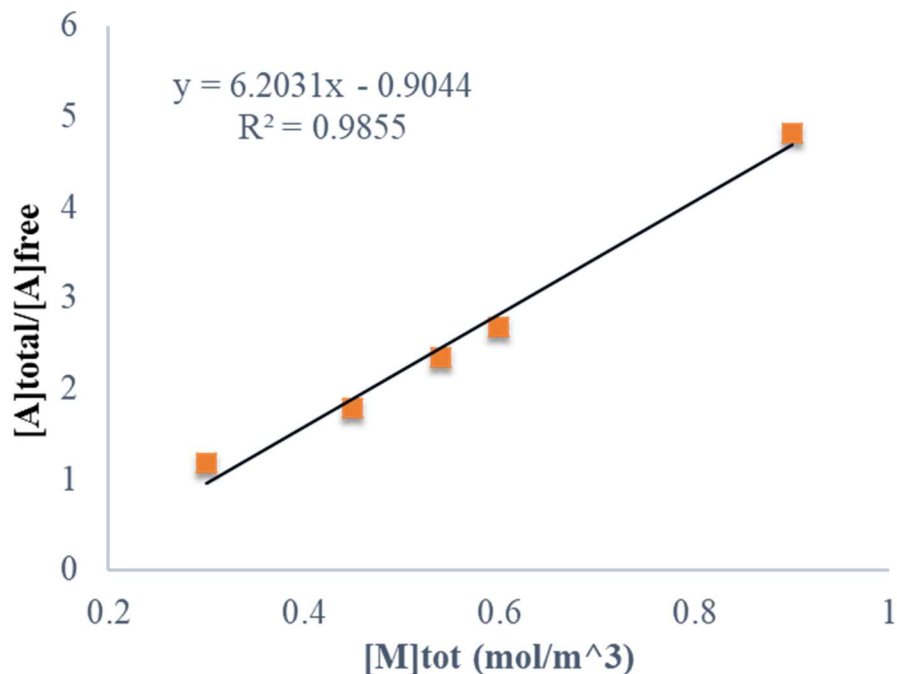
Figure 2. 18 The X axis represents the total HSA concentration and Y axis is the ration of total DOX concentration to free DOX concentration. Initial concentration of DOX was 100 ng·mL$^{-1}$

Table 2. 4 Experimentally calculated free DOX concentration at different HSA concentration

| $M^{tot}$ (mol m$^{-3}$) | $A^{tot}$ (mol m$^{-3}$) | $A^{free}$ (mol m$^{-3}$) |
|---|---|---|
| 0.15 | | 1.08E-04 |
| 0.3 | | 8.47E-05 |
| 0.45 | 0.0001841 | 6.63E-05 |
| 0.6 | | 5.01E-05 |
| 0.75 | | 4.39E-05 |
| 0.9 | | 3.16E-05 |

$K_A$ was calculated from the slope of the linear regression line presented in Figure 2.18, yielding a value of 6203 (l mol$^{-1}$), which agrees with the literature value.[47] The mass transfer kinetics of DOX in the presence of HSA was progressing faster than without HSA. This is due to the matrix assisted (HSA in this case) mass transfer. The equilibrium of DOX-HSA-PBS extraction kinetics was attained after approx. 60 min compared to the 82 min observed in DOX-PBS solution.
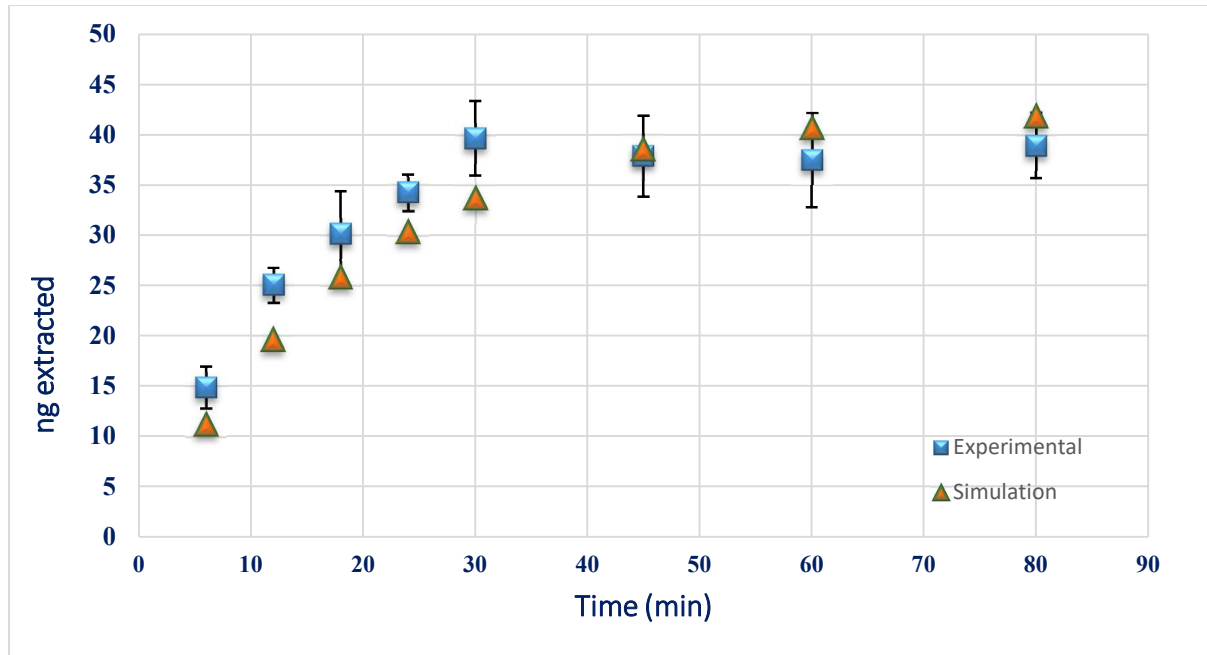
Figure 2. 19 In-Silico comparison of SPME extraction of DOX (100 ppb) in presence of HSA binding matrix (0.541 mol m$^{-3}$) in PBS

The amount extracted at equilibrium with HSA binding matrix was ≈40 ng significantly lower than without HSA binding matrix (≈100 ng) considering the same sample volume (1.7 mL) and the initial concentration of DOX (100 ppb). This indicates that a substantial amount of DOX was bound to HSA matrix. Figure 2.19 shows the in-silico comparison of SPME extraction of DOX in the presence of HSA binding matrix.

In-silico study of DOX in tissue: Given the extraction in tissue matrix occurs under static conditions, the kinetics of extraction are calculated using the following static conditions formulae. The mass balance equation for tissue can be derived from (2.35) as:

$$\frac{\partial cs}{\partial t} = D\nabla c - k_f * ([A]^{free} * [M]^{tot}) + k_r * ([A]^{tot} - [A]^{free})$$ (2.36)

In case of tissue matrix, there are different types of binding matrix components, and it is difficult to estimate their total concentration. If we assume that the stoichiometry of DOX with all binding

71

components in the extracellular space of the tissue is one, then the apparent binding constant for

DOX can be derived from eq. (2.14) as:

$$K_{App} = K_A * [M]^{tot} \tag{2.37}$$

The product of $K_A * [M]^{tot}$ in eq. (2.37) is a unitless factor, and a constant for a given matrix. Here,

$[M]^{tot}$ defines the total concentration of different binding matrices. Since DOX has binding affinity

to DNA, serum albumin, cell membrane, and other binding agents presents in the tissue matrix,

calculating the true concentration of the binding matrix in the tissue is therefore impractical due

to the complex nature of the binding mechanism.[69,70] Therefore, we consider $K_{App}$ as an apparent

binding constant, which can be predicted in a well-defined mathematical model by changing the

total matrix concentration $[M]^{tot}$. As the value of $K_A$ for DOX with HSA matrix has been

experimentally determined and validated by mathematical simulation (Figure 2.19; in-silico

comparison of extraction time profile using experimentally determined $K_A$. Now in eq. (2.37), if

we change the concentration of total matrix $[M]^{tot}$ value of $K_{App}$ will increase. The trend of the

extraction time profile with a 3D mathematical model was developed for DOX extraction in the

tissue matrix under static conditions.
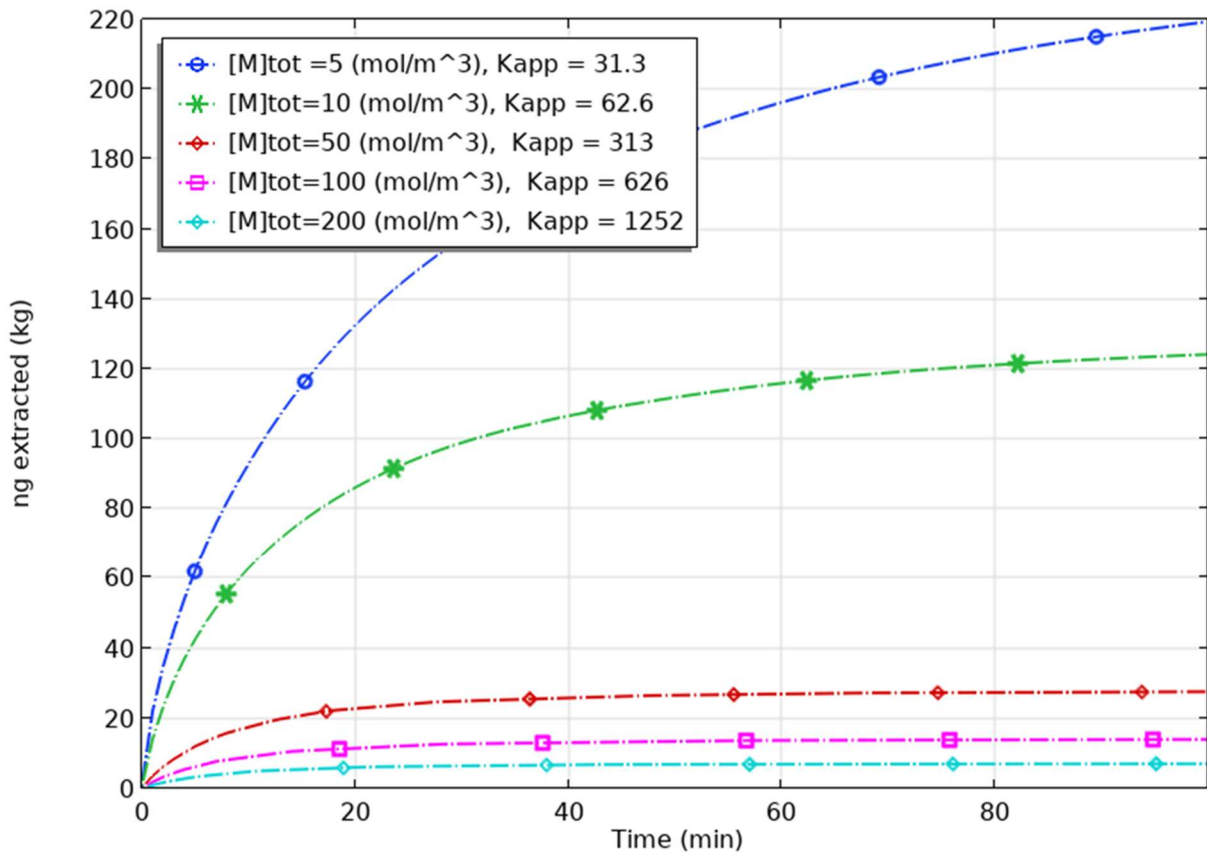
**Figure 2. 20** Change of extraction time profile for DOX in tissue with changing the binding matrix concentration $[M]^{tot}$

These findings indicate that it is possible to determine the apparent binding constant for an analyte in a tissue or any complex biological matrix (where multiple binding components are present) by developing a well-defined mathematical model and performing all relevant experiments to validate it. However, this theoretical approximation is only valid for those compounds which bind univalently to the matrix components. The novelty of this concept was the experimental and mathematical approach to determine the apparent binding constant $K_{App}$ for DOX in the tissue matrix and the measurement of free analyte concentration in the tissue matrix. The data oprovided by the mathematical simulation simplified the complexities associated with

the experimental conditions, particularly when it becomes cumbersome to differentiate the binding association constant for each different binding matrix present in the sample. The extraction kinetic profiles behaved similarly despite using different matrix concentrations [M] and binding association constants $K_A$ for the same $K_{App}$. The initial concentration $[A]^{tot}$ was 25 µg g$^{-1}$.
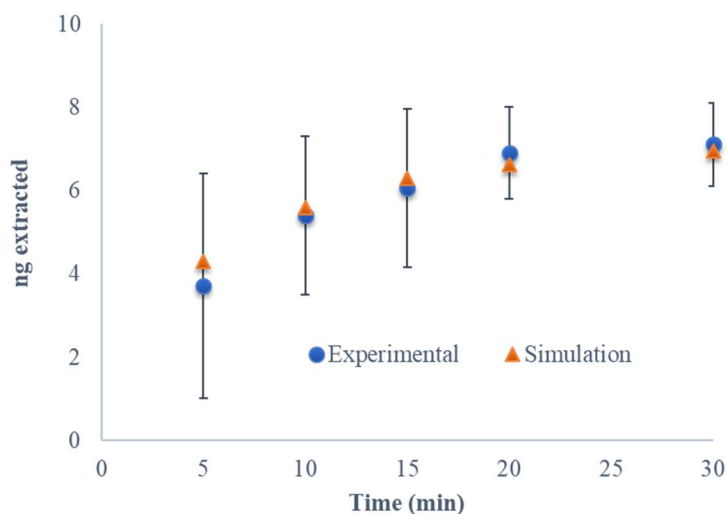


Figure 2. 21  Comparison of in-silico and experimental extraction time profiles of doxorubicin (25 µg g$^{-1}$) in homogenized bovine lung tissue

Experimental results from tissue showed that approximately 7 ng of DOX are extracted when an initial concentration of 25 µg·g$^{-1}$ is spiked into the tissue. Extraction reached equilibrium after 25 min (equilibration time was herein defined as the time needed for 95% of the total equilibrium concentration to be extracted onto the coating), which is reasonable given the high binding affinity of DOX for lung tissue components. Simulated results were well-fitted with experimental results despite the fact that experimental errors are higher at lower time points due to the proximity of

the experimentally extracted amount to LOQ values. For all other studied initial concentrations in tissue matrix, the amount of extract at equilibrium were identical (within error) to in-silico extracted amounts, while the analytical concentration of the sample was observed in the range studied. In-silico results were in agreement with the attained experimental results.[65] Finally, the free concentration of DOX from lung tissue was estimated from eq. (2.14), yielding a value of $1.25e^{-05}$ (mol m$^{-3}$) for 25 µg g-1. These results indicate that DOX is heavily bound to the tissue matrix, at an estimated binding percentage of 99.97%. The experimentally attained value was very close to the value generated by numerical simulations.

### 2.4.3. Negligible depletion of free concentration and spatial resolution

To determine the free concentration of analyte in the presence of binding matrix components, negligible depletion of the free concentration surrounding the SPME fiber is imperative. Figure 2.9 (a) describes how the free concentration DOX depletes over the time around the SPME fiber during static extraction in agar gel. The X axis represents the distance from the SPME fiber in millimeter while the Y axis is the concentration of DOX in the sample matrix in mol m$^{-3}$. At the beginning of extraction time profile, the depletion of concentration in the proximity of the fiber is higher (the green line graph at 1h). The total length of the X axis represents the dimension of the sample matrix which is the diameter of the glass vial (10 mm) used in the experiment. From that figure, we can assume that the boundary layer thickness is approximately 8 mm after 1h of extraction. However, close to the equilibrium (the blue line graph at 82 h) there is no gradient of concentration around the fiber. On the other hand, extraction from tissue matrix apparently exhibited negligible depletion of the free concentration at equilibrium conditions, as seen in Figure 2.9 (b). Therefore, although the C-8 mixed mode SPME fiber enabled significant

depletion of the free concentration of DOX at equilibrium, estimated at approximately 60 percent of the initial concentration, extraction from tissue matrix apparently exhibited negligible depletion of the free concentration at equilibrium conditions. Such a phenomenon is caused by the rapid release of DOX from the matrix-bound complex, indicating that the binding matrix and the SPME extraction phase compete for DOX. In fact, the binding matrix works as a buffer to maintain the free form of DOX surrounding the fiber while it is being extracted onto the extraction phase. It should be noted as well that the free concentration of DOX will likely not change in the matrix system unless the dissociation rate constants $k_r$ are slow. This also indicates that successive extractions from the same place within the sample matrix should not matter particularly if the matrix bound fraction of the analyte is significantly higher than that of unbound analyte, as the matrix replenishes the free concentration rapidly. Figure 2.9 (c) evidences the spatial resolution of the SPME sampling by showing the depleted DOX concentration volume surrounding the fiber at equilibrium. This indicates that placing multiple SPME fibers in a small region of sample matrix should not interfere in the extraction kinetics. Therefore, experimental results should incur less bias relative to the matrix.
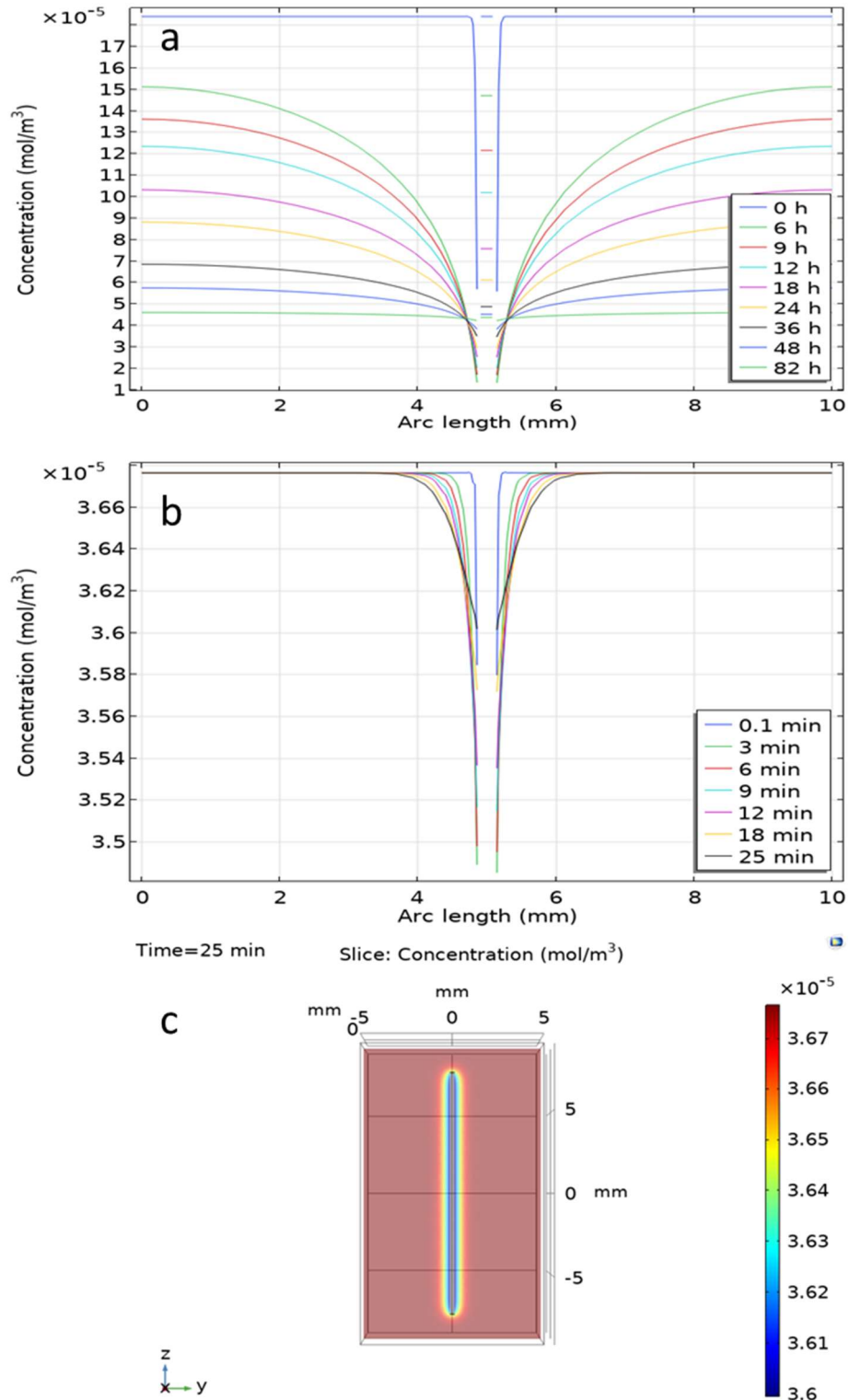
Figure 2. 22 (a) COMSOL simulation shows the change of DOX concentration in agar gel across a line drawn through the center of the SPME fiber at different extraction times. The X axis shows the distance from the fiber, and the Y axis represents concentration. The initial concentration was 0.1 μg·mL⁻¹ (b) The change in the free concentration of DOX in tissue at equilibrium, indicating that the

gradient in concentration is negligible. The initial concentration was 25 μg·g$^{-1}$. (c) The spatial resolution of the concentration gradient of DOX in tissue across a 2D line cut through the SPME fiber

## 2.5. Conclusion

This chapter theoretically studies the extraction dynamics of molecules from bovine lung tissue using solid-phase microextraction, further presenting experimental validation of the COMSOL simulation models using a well-known chemotherapeutic drug, doxorubicin (DOX) as a model compound. In this context, a novel technique was introduced for measurement of free drug concentration in bovine tissue homogenate by using biocompatible C-8 mixed mode SPME fiber. Also, theoretical studies were discussed and defined to interpret several crucial concepts on mass transfer kinetics that take place in tissue matrix. To validate the established mathematical models, a novel SPME technique to determine free and bound concentrations from tissue by either in vivo or ex vivo sampling was theoretically developed and experimentally established, using DOX. The attained experimental results were explained and cross-validated by mathematical COMSOL simulations, which described in detail the mass transfer kinetics of DOX in lung tissue matrix. Moreover, derived from this primary work, several relevant concepts concerning tissue sampling, such as apparent binding constant, spatial resolution, and local depletion, were developed and discussed. Of note, the attained results help to shed light on the principle of SPME tissue extraction, including in vivo extraction scenarios. As part of this investigation, the unbound free concentration of analyte is shown to remain constant when a thin coating SPME fiber is used, as the amount of analyte that is transferred to the coating is replaced from the reservoir of analyte bound to the tissue matrix. In addition, the presented work represents the first attempt to measure free drug concentrations in tissue matrix with the assistance of mathematical models.

The key attributes of the herein presented numerical models include estimation of the apparent binding constant $K_{App}$ of DOX in tissue matrix, demonstration of negligible depletion, and spatial resolution for multiple ex vivo or in vivo samplings. Here, $K_{App}$ is defined as a unitless constant that describes the binding properties of an analyte in a specific sample matrix; in this work, the $K_{App}$ for DOX in bovine lung tissue was estimated as **1252**. The value of $K_{App}$ is difficult to estimate experimentally since the total concentration of binding species [M] is unknown in a given tissue matrix. This limitation is herein addressed by taking advantage of the mathematical models established in this work. Although this study was performed using homogenized tissue, future research efforts may include estimation of in vivo free concentrations in the extracellular space of tissue matrix. The developed simulation approach thus substantiates that SPME can be used as a valuable tool for accurate measurements of free drug concentrations in tissue matrix. Of note, we could have selected BSA as a binding matrix to estimate the binding association constant $K_A$ instead of HSA. However, given that the ultimate goal of this ongoing research concerns future implementation of this technique for in vivo determinations in human lung tissue, HSA was herein selected as binding matrix. Finally, the output of this article is not only limited to DOX or lung tissue, but also paves the way for quantitation of free and conjugated forms of other drugs in any complex biological matrix. In fact, this study will allow for exploration of completely new horizons in biomedical sciences, such as in vivo monitoring of drug pharmacodynamics in tissue, without the need of correlative investigations using surrounding biofluids or biopsies.

# Chapter 3     Investigation of binding characteristics of fatty acids with human serum albumin
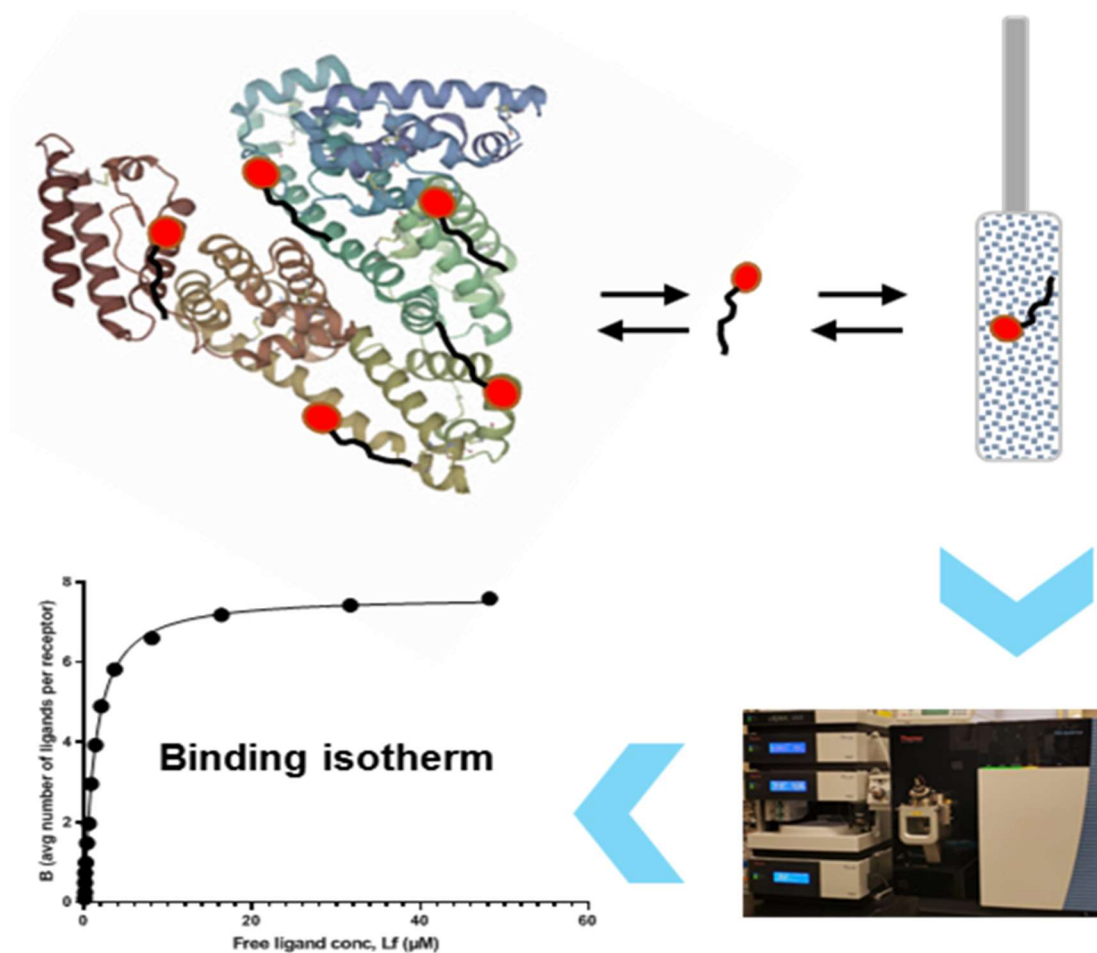


## 3.1. Preamble

This chapter has been submitted as a manuscript in the journal Analytical Chemistry. Mohammad Huq, Hernando Rosales, Janusz Pawliszyn; *Investigation of fatty acids binding to human serum albumin to determine free concentration: experimental and in-silico approaches*. The contribution of co-author Hernando Rosales pertained to sample preparation and characterization.

## 3.2. Introduction

There is mounting evidence that solid-phase microextraction (SPME) is a suitable tool for extracting lipophilic compounds from tissues *in-vivo*. In this chapter, we employ SPME to investigate the multiphase equilibria of fatty acids in complex samples, such as human serum albumin.[71,72,73] Fatty acids (FA) are a lipid class that can be readily found throughout the human body due to their key role in physiological processes. Some of the major functions of FAs include providing a source of energy because of metabolic reactions via β-oxidation in the heart and skeletal muscles; serving as key constituents of phospholipids, which provide fluidity and flexibility to cell membranes; and as cellular signaling molecules, such as those responsible for reducing tyrosine phosphorylation in the insulin receptor substrate (IRS)-I/II. Fatty acids can be supplied to the body through diet; and they can also be synthesized in the body via desaturation and elongation of dietary FAs, also from carbohydrate catabolism. Linoleic acid (LA) and alpha-Linolenic acid (aLA), which are available in different vegetable oils, are the primary precursors of the biosynthesis of longer ω-6 and ω-3 polyunsaturated fatty acids (PUFAs), respectively. FAs acquired through one's diet are deposited in the adipose tissue, where they are stored as triglycerides until being released into the body through lipolysis.[74,75] When FAs are released into the blood, they strongly bind to human serum albumin (HSA) to be transported to the muscle tissue, and to the liver for ketone synthesis. HSA is the most abundant protein in blood plasma, and functions as a cargo/or transport vehicle for FAs in addition to controlling oncotic pressure. Furthermore, it is unique in that it is able to bind up to 99% of non-esterified fatty acids (NEFAs) under normal physiological conditions.[76] Excessive abundance of NEFAs in a person's blood plasma can have major consequences for their health; for example, elevated NEFA levels have been causally linked

to obesity and other health-related risks, such as type 2 diabetes mellitus (T2DM), cardiovascular diseases, myocardial infarction, and inflammatory diseases like rheumatoid arthritis (RA).[75,77,78,79] Not all FAs adversely affect one's health, however; some play a central role in ameliorating health risks, most notably ω-3 and ω-6 PUFAs. ω-3 and ω-6 PUFAs also play a vital role in the normal growth of brains and retinas in newborn humans, as well as functioning as precursors for a plethora of signaling lipids with anti-inflammatory properties.[80,81,82]

Aside from their immense biological and pathological importance, FAs also play a critical role in interaction of human serum albumin (HSA) with other molecules. Many studies have revealed that HSA's affinity to drugs and other endogenous molecules may be modulated by the number of FAs bound to the HSA.[83,84] This characteristic interplay between FAs and HSA has attracted scientific interest in drug development studies.[85,11,76] Under normal physiological conditions, almost 99% of NEFAs are heavily bound to HSA, with an FA-to-HSA molar ratio of <1. However, there are multiple binding sites for FAs on HSA, and the number of FAs that bind to HSA will vary as the FA-to-HSA molar ratio changes.[87] The binding pattern of FAs to HSA can also be altered due to allosteric effects, such as proteins or peptides released by cancerous cells, which compete with specific FA binding sites.[76] The investigation of FA-HSA binding is therefore important, as it can further develop our understanding of their dynamic behavior as a lipid transport mechanism, their role in pharmacokinetic and pharmacodynamic (PK/PD) studies of drug molecules, and their regulatory function in many physiological reactions. However, the mechanism responsible for FA-HSA binding is not as straightforward as the mechanism governing the binding of other small molecules, because HSA offers numerous binding sites for FAs. High-resolution X-ray crystallographic analysis of HSA-palmitate complexes reveals that there are at least seven FA binding sites heterogeneously

distributed across three structurally similar HSA domains.[88] Furthermore, recent two-dimensional

nuclear magnetic resonance (2D NMR) studies of HSA-palmitate complexes have identified at least

nine FA binding sites in HSA; of these, three have high affinity, one has medium affinity, and the

others have low affinity.[89] Although multiple FA binding sites have been identified and categorized,

we know of no prior studies that have attempted to determine the binding affinity of FAs to a

*specific* site. However, the site-specific binding affinities are variable not fixed.[87,90,91] In an attempt

to understand the complex characteristics FA-HSA binding, Goodman *et al.* first experimentally

determined the stoichiometric and site-specific binding constants of long chain FAs to HSA, and

then applied the Scatchard equation for multiple ligand-receptor interactions.[92]

### 3.2.1. Theoretical approach

For a multivalent receptor R with b number of binding sites for a ligand L, the stepwise

stoichiometric equilibria can be formulated as:[93]

$$R + L \rightleftarrows RL_1$$

$$RL_1 + L \rightleftarrows RL_2$$

$$RL_{b-1} + L \rightleftarrows RL_b$$
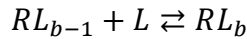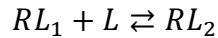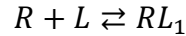
The equilibrium binding constants $K_i$ for each stoichiometric step can be formulated as follows:

$$K_1 = \frac{[RL_1]}{[R]*[L]} \quad \text{or, } [RL_1] = K_1 * [R] * [L]$$

$$K_2 = \frac{[RL_2]}{[RL_1] * [L]}$$

$$[RL_2] = K_2 * [RL_1] * [L] = K_1 * K_2 * L^2$$

$$[RL_b] = K_1 * K_2 \ldots K_b * L^b \tag{3.1}$$

The number of ligand (L) molecules bound per receptor molecules (R) can be expressed as the degree of binding (B) of ligand to receptor at a given ligand concentration, or the saturation fraction. B can be expressed as a function of free ligand ($C_f = [L]$) and total ligand ($C_t$) and total receptor ($C_r$) concentrations:

$$B = \frac{(C_t - C_f)}{C_r} = \frac{moles\ of\ bound\ ligand}{moles\ of\ total\ recptor} \quad \text{、} \tag{3.2}$$

From stoichiometric equilibrium steps, eq. (3.2) can be formulated as:

$$B = \frac{[RL_1] + 2[RL_2] + \cdots + b[RL_b]}{[RL_1] + [RL_2] + \cdots + [RL_b]}$$

$$\text{Or, } B = \frac{K_1*[L] + 2K_1*K_2*[L]^2 \ldots + b(K_1*K_2*\ldots K_b)[L]^b}{1 + K_1*[L] + *K_2*[L]^2 \ldots + (K_1*K_2*\ldots K_b)[L]^b} \tag{3.3}$$

Eq. (3.3) demonstrates the stoichiometric binding interactions in terms of ligand concentrations. In case of site-oriented approach, the total number of site binding constants is determined by $b * 2^{b-1}$ number of different binding constants where $2^{b-1}$ are independent. For site-oriented interactions,

$$R_i + L \rightleftarrows R_i L_1$$
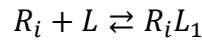
Where, $R_i$ represents the i$^{th}$ binding site of the receptor. For each binding site, eq. (3.2) can be formulated as:

$$B = \frac{k_i * [L]}{1 + k_i * [L]}$$

Then the receptor as a whole,

$$B = \frac{(C_t - C_f)}{C_r} = \sum_{i=1}^{b} B_i = \sum_{i=1}^{b} \frac{k_i*[L]}{1 + k_i*[L]} \tag{3.4}$$

Eq. (3.4) is defines the site-oriented binding approach for multiple sets of binding sites. A special case that is often assumed to be applicable is a system with two classes of binding sites, each with

identical invariant affinities that differ from the identical invariant affinities of the other class.[94]

Under this circumstances, Eq4 can be simplified as:

$$B = \frac{(C_t - C_f)}{C_r} = \frac{b_1 * k_1 * [L]}{1 + k_1 * [L]} + \frac{b_2 * k_2 * [L]}{1 + k_2 * [L]} \tag{3.5}$$

Where $b_1$ and $b_2$ represents respective classes; $b_1 + b_2 = b$, and $k_1$ and $k_2$ are corresponding site binding constants. Eq. (3.4) and eq. (3.5) are nonlinear and used to study FAs to HSA in terms of site-oriented approach. However, interactions between binding sites (cooperation) make it difficult to interpret the binding isotherm in terms of site-oriented scrutiny. Therefore, the stoichiometric binding constant approach is the appropriate way to investigate FAs binding to HSA.[94]

### 3.2.2. Site-specific vs. stoichiometric binding affinities

The principles underlying the stoichiometric and site-specific binding constants are illustrated below. If we consider a receptor (R) with two binding sites, b1 and b2, four equilibria are established in a site-oriented approach. The corresponding binding constants for the ligand, L, are $k_{b1}$, $k_{b2}$, $k_{b1,b2}$, and $k_{b2,b1}$. If the two binding sites are identical (invariant affinity), there will be one site-binding constant, which will be equal to $k_{b1}$. If the binding sites are not identical, but the binding interactions are independent of each other (noncooperative), there will be two site-binding constants: $k_{b1}$ and $k_{b2}$. $k_{b1}$ is equivalent to $k_{b2,b1}$, and $k_{b2}$ is equivalent to $k_{b1,b2}$ because the binding of one site does not interfere with the other. On the other hand, stoichiometric binding constants do not distinguish between the intermediates, $R_{b1}$ and $R_{b2}$; rather, they comprise both constants, $k_{b1}$ and $k_{b2}$, in first equilibrium constant. Similarly $k_{b1,b2}$ and $k_{b2,b1}$ are incorporated in the second equilibrium constant. If the binding sites are not independent, all site-binding constants

will be different, but the number of stoichiometric binding constants will be the same. As the number of non-identical binding sites and their respective cooperativity increases, it becomes more difficult to interpret a site-oriented binding approach. In such cases, a stoichiometric binding approach is more practical.
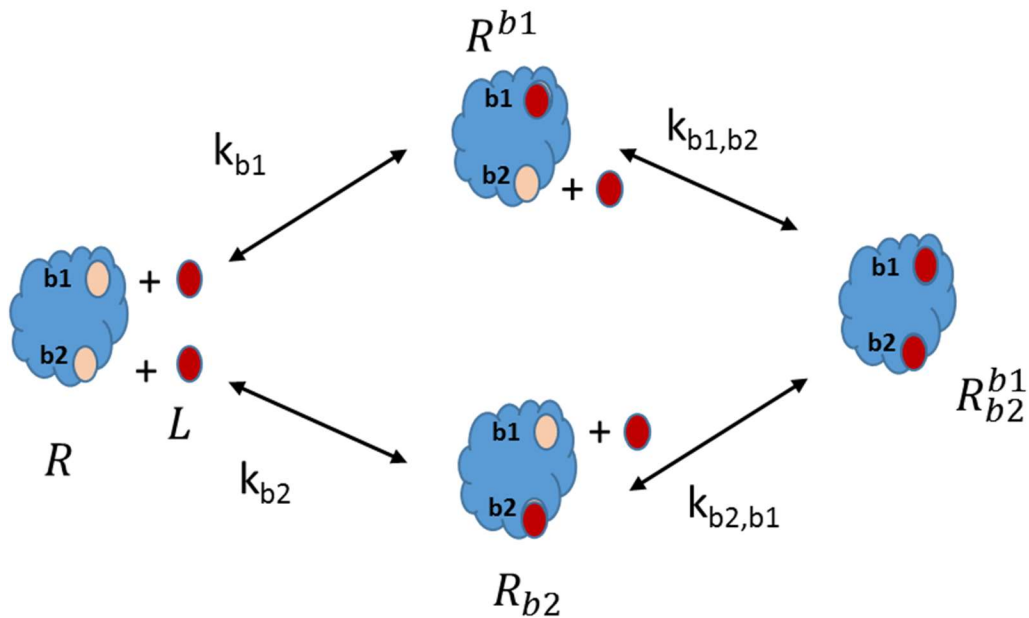


**Figure 3. 1 Schematic diagram of ligand-bivalent receptor binding interactions**

The cooperation among the binding sites can be clearly observed by measuring the stoichiometric binding affinities, and the degree of cooperativity is determined by the Hill equation, which is given for a single set of binding sites ($b$) and $k$ intrinsic binding constant as follows:[95]

$$B = \frac{b(k*[L])^n}{(1+k*[L])^n}$$
(3.6)

Where $n$ is the Hill coefficient, which represents the degree of cooperation between binding sites ($n = 1$: no cooperation; $n > 1$: positive cooperation; and $n < 1$: negative cooperation). There are multiple statistical software programs that use nonlinear curve fitting equations to solve eq. (3.6).[96]

In the present study, we used the GraphPad Prism software tool to determine the apparent binding affinity and the Hill coefficient, which determines the cooperation between binding sites.

### 3.2.3.  Binding constant by Scatchard plot

The binding constant for a single set of binding sites where all binding affinities are considered similar can be measured using a Scatchard plot. In this case, eq. (3.4) can be simplified as below:

$$\frac{B}{L} = (b - B)K \tag{3.7}$$

The binding constant, $K$, is the slope and can be measured by plotting $\frac{B}{L}$ vs $B$ (Figure 3.2)
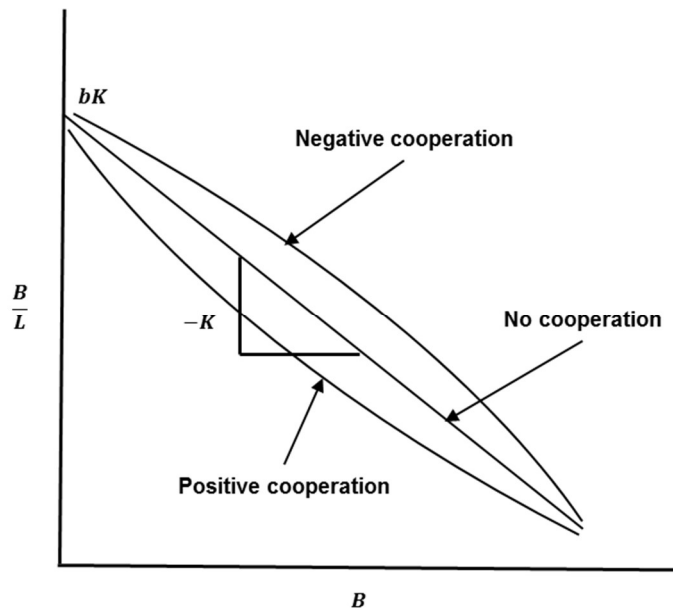


**Figure 3. 2  Schematic diagram of Scatchard plot for identical and one-set of binding sites**

If there is cooperation, the slope becomes nonlinear.

### 3.2.4. Experimental techniques

For this study, it is critical to obtain accurate measurements of the free (unbound) concentration of FAs ($L$) in eqs. 4 and 5. However, FAs have very low solubility in aqueous phases, which results in experimental difficulties when attempting to accurately measure their free concentrations, while also not disturbing the equilibrium between the ligands and receptors.[97] Goodman et al. first studied the binding isotherm of FAs with HSA receptors by using radio-isotope-labelled FAs to determine the free concentration of FAs. To this end, they partitioned the FAs in a water-heptane two-phase system to circumvent the low solubility of FAs. The distribution of free FAs between the water and heptane was dependent on their partition coefficients, which were known. The free FAs were then collected from the aqueous phase and quantified using a radiation detector. The major drawback of this method is the very low solubility of long-chain fatty acids, which results in poor quantitative results. Recent studies have more commonly employed equilibrium dialysis (ED) and isothermal titration calorimetry (ITC) to study the binding characteristics of FAs to HSA.[97,98,99,100] However, ED has several shortcomings, such as possible analytes loss of analytes to the dialysis interface, its time-consuming nature, and poor quantitative results when the free concentration is very low.[101] On the other hand, ITC has multiple advantages. For example, it is nondestructive, which means that a sample can be reused, and it can measure many thermodynamic parameters (e.g., binding affinity, binding enthalpy, and stoichiometry) in a single experiment. However, ITC is limited by low sensitivity and requires a high amount of samples; therefore, it is commonly considered a complementary method. Another sensitive technique capable of measuring the binding affinity of ligand receptors is surface plasmon resonance (SPR), wherein the receptor (in this case HSA) is tagged into a gold-coated surface by a covalent linker.

The introduction of the ligand changes the surface SPR signal, which is detected by an optical detector. Although SPR is highly sensitive, it requires high-purity samples and has high experimental costs.[102,103] Other possible techniques include 2D NMR analysis, fluorescence measurement, and electron paramagnetic resonance; however, these techniques are quite sophisticated, require high technical expertise and high purity standards in order to avoid background noise, are limited to lower ranges of ligand concentration, and are unable to measure the free concentration of FAs *in vivo* or *ex vivo*.[104,97,105] Recently, Andrew H. Huber *et al.* developed an antibody tagged fluorescent probe that enables the *ex vivo* measurement of the unbound fraction of free fatty acids in blood plasma.[106] This technique provides more comprehensive results due to its use of *ex vivo* sampling, and it has been increasingly gaining acceptance by biological scientists.[106] However, the development of antibody tagged probes is not straightforward, as it requires specific antibody probes for specific FAs, which is expensive. To overcome the limitations associated with existing separation techniques, we propose the use of solid-phase microextraction (SPME) coupled with GraphPad Prism software and Scatchard plot to study the characteristics of FA-HSA binding. Developed by Arthur and Pawliszyn in the early 90s, SPME is a separation tool that uses a thin layer of extraction phase to separate target analytes based on their affinity for the selected coating.[31] SPME extracts *via* free concentration, with its extraction kinetics being predominantly driven by diffusion, convection, and binding matrix components. The use of a biocompatible extraction phase makes it is possible to separate small molecules from complex matrix components, which are essentially large biomolecules. In addition, the small amount analyte extracted means the changes to the free concentration will be negligible in the presence of binding matrices, which does not the affect the dynamic conditions of the native environment.[26]

Furthermore, calibration can be performed in either equilibrium or pre-equilibrium regimes, which significantly shortens experimental time. SPME's unique characteristics make it an ideal choice for measuring the free concentration of analytes in complex biological matrices, both *in vivo* and *ex vivo*.[53] Musteata et al. have already successfully applied SPME in order to explain multiple binding interactions between the pharmaceutical drug diazepam and HSA.[93] In this article, we apply SPME to analyze more complex ligand molecules, such as FAs, and obtain more detailed characterizations of the attendant binding characteristics using GraphPad Prism software. We also introduced mathematical models in order to illustrate the extraction kinetics of SPME in the presence of a binding matrix.

### 3.2.5. *In-silico* studies

Simulation can be a great supportive tool in many scientific research areas, as it allows researchers to reduce the cost of materials and the amount of time required. Furthermore, simulation allows researchers to gain a more in-depth understanding of many complex physics that may be difficult to grasp using just common sense. In the present study, we investigate mass transfer by developing mathematical models for the kinetics of extractions of FA using SPME with a solid coating. In addition to advancing our understanding of the mass transfer of FAs, a validated mathematical model can help to reduce the number of experimental steps required for similar analytes. Most importantly, when a sample consists of multiple complex matrices (e.g., biological tissue), simulations are extremely useful in demonstrating the mass transfer kinetics.[26] The mathematical models in this research were developed using COMSOL Multiphysics 5.5 simulation

software. The extraction kinetics of FAs onto an SPME extraction phase were consistent with the adsorption kinetics onto a solid surface. The mathematical equations for mass transfer onto a solid extraction phase have been detailed elsewhere in the literature.[26] The objective for investigation of mass transfer of aLA and LA using mathematical models is to develop well-defined computational models which can determine the free concentration of other FAs with similar properties.

## 3.3. Experimental section

### 3.3.1. Materials and supplies

Human serum albumin (HSA, essentially fatty acid free), α-Linolenic acid (aLA), γ-Linolenic acid (glA), and chloroform (CHCl$_3$, LC grade) were purchased from Sigma–Aldrich (Oakville, ON, Canada), while linoleic acid (LA) and tridecanoic acid were acquired from Cayman chemicals (Burlington, ON, Canada). LC-MS-grade methanol (MeOH), isopropyl alcohol (IPA), and water were purchased from Fisher Scientific (Mississauga, ON, Canada). C18-coated SPME fibers were kindly provided by Millipore–Sigma (Oakville, ON, Canada). Standard stock solutions were prepared daily in MeOH from a stock prepared in CHCl$_3$: MeOH (2:1, v/v) and stored at-30 ºC in amber silanized vials.

### 3.3.2. Measurement of active surface area of SPME extraction phase

BET (Brunauer–Emmett–Teller) is an experimental technique to estimate the active surface area of solid material (the theory of BET was explained in chapter 2). The experiment was performed to determine the surface area of C-18 fiber by physical adsorption of N$_2$. However, this

measurement is a rough estimation, since the pore area is considered for $N_2$ molecule which is much smaller than our target analyte. Therefore, we only considered the pores larger than 100 Å, which will be able to bind with our target analyte aLA and LA considering their size and shape. It is difficult to determine the accurate active surface area for each analyte, since it requires BET measurement of that specific analyte which is experimentally not possible (since BET technique requires inert gas molecule to calculate specific surface area). Based on this consideration we estimated the active surface area of C-18 fiber is app. 2.0 $m^2$ g-1 from Table 3.1.

Table 3. 1  BET analysis of pore surface area of C18 SPME fiber

| Average Pore Width (Å) | Incremental Pore Volume (cm³/g) | Cumulative Pore Volume (cm³/g) | Incremental Pore Area (m²/g) | Cumulative Pore Area (m²/g) |
|---|---|---|---|---|
| 2335.820 | 0.000 | 0.000 | 0.000 | 0.000 |
| 1754.945 | 0.000 | 0.000 | 0.004 | 0.004 |
| 1329.692 | 0.000 | 0.000 | 0.003 | 0.008 |
| 1051.384 | 0.000 | 0.000 | 0.002 | 0.010 |
| 902.340 | 0.000 | 0.000 | 0.003 | 0.012 |
| 797.678 | 0.000 | 0.000 | 0.003 | 0.015 |
| 710.907 | 0.000 | 0.001 | 0.002 | 0.018 |
| 625.532 | 0.000 | 0.001 | 0.007 | 0.024 |
| 542.974 | 0.000 | 0.001 | 0.004 | 0.028 |
| 467.420 | 0.000 | 0.001 | 0.006 | 0.034 |
| 411.828 | 0.000 | 0.001 | 0.009 | 0.042 |
| 365.583 | 0.000 | 0.001 | 0.008 | 0.050 |
| 324.368 | 0.000 | 0.001 | 0.010 | 0.061 |
| 288.465 | 0.000 | 0.001 | 0.013 | 0.074 |
| 254.816 | 0.000 | 0.001 | 0.033 | 0.106 |
| 226.426 | 0.000 | 0.002 | 0.054 | 0.161 |
| 198.395 | 0.001 | 0.002 | 0.120 | 0.281 |
| 173.434 | 0.001 | 0.003 | 0.186 | 0.467 |
| 154.157 | 0.001 | 0.004 | 0.256 | 0.723 |
| 136.106 | 0.001 | 0.005 | 0.420 | 1.143 |
| 120.213 | 0.001 | 0.007 | 0.475 | 1.619 |
| 107.587 | 0.001 | 0.008 | 0.428 | 2.046 |

### 3.3.3. Measurement of maximum surface concentration of aLA ($\gamma_s$).

This physical parameter is required in order to develop the mathematical model in COMSOL Multiphysics. Accordingly, the maximum occupancy of α-Linolenic acid on the surface of the extraction phase was measured following the method described below. $\gamma_s$ was determined experimentally by performing extractions from initial concentrations of aLA in PBS of 0.01, 0.1, 0.2, 0.5, 0.75, 1, 2, 3, 4, 5, 6, 7, 8, 9, 10, 15, and 20 µg·mL$^{-1}$ under agitation at 1500 rpm. The active surface area of the fiber coating was determined via Brunauer–Emmett–Teller (BET) analysis. Therefore, the value of maximum surface concentration ($\gamma_s$) can be obtained by following eq. (2.5):

$$\gamma_s \left(\frac{mol}{m^2}\right) = \frac{\text{saturated amount extracted on the fiber}}{\text{active surface area per fiber}} = \frac{cs_{sat}}{A} \qquad (2.5)$$

To measure saturated aLA amount experimentally, SPME extractions were performed with increasing conc. of aLA spiked in PBS (Phosphate Buffer Saline) solution. The extracted amount of aLA was plotted against initial concentration in the sample matrix.
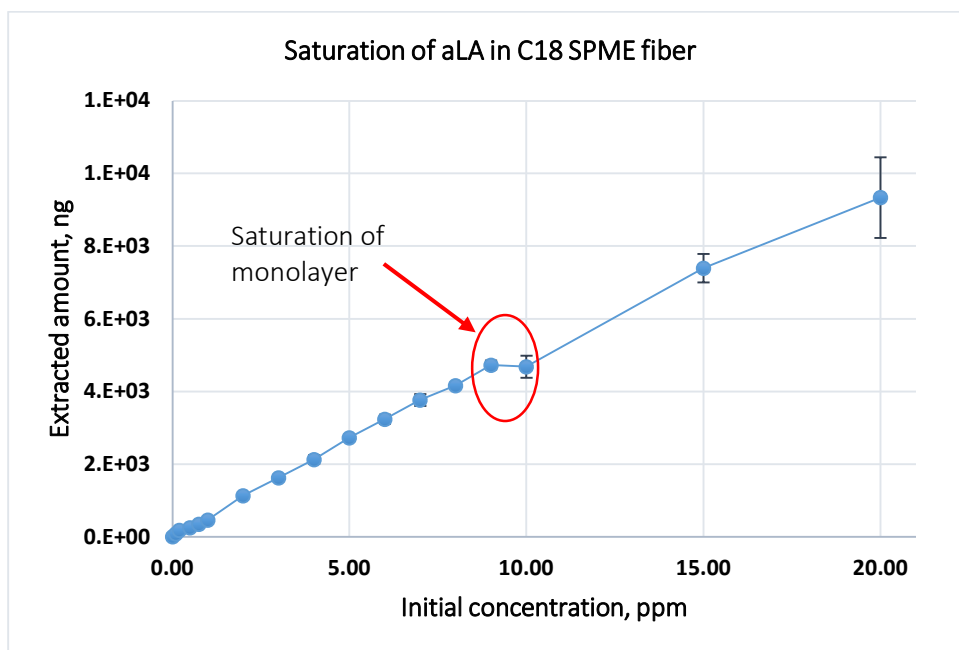


Figure 3. 3   Amount of aLA concentration on the extraction phase with increasing initial

concentration. A plateau was observed at which aLA concentration on the extraction phase reached at saturation of monolayer according to Langmuir's isotherm

The amount of aLA extracted at saturation point is 4683 ng which is equivalent to $1.7e^{-08}$ mole of aLA. The value of maximum surface concentration, $\gamma_s$ was determined from eq. (2.5).

$$\gamma_s \left(\frac{mol}{m^2}\right) = \frac{1.7e - 7(\text{mol})}{9.2e - 4(\text{m}^2)} = 1.8e^{-5} \left(\frac{mol}{m^2}\right)$$

Table 3. 2  Experimentally measured physical properties of SPME extraction phase

| Parameters (unit) | Value |
| --- | --- |
| Specific surface area (m^2/g) | 2.0 |
| Amount of particle per fiber (g) | 4.5E-04 |
| Specific surface area per fiber (m^2) | 9.2E-04 |

### 3.3.4.  Measurement of the adsorption equilibrium constant ($K_{ads}$) for aLA.

This physical parameter is also necessary in order to develop the mathematical model in COMSOL Multiphysics. The equilibrium constant for the adsorption of aLA onto the C18-coated SPME fibers was determined by performing agitated extractions at 100 ng·mL$^{-1}$ aLA in PBS at 15 different time points within a 180 min time period, for four independent replicates. After each extraction, the fibers were rinsed for 10 s with 400 µL of LC-MS grade water to remove salts and nonspecific attachments, and then desorbed for 60 min at 1500 rpm in 200 µL of IPA: MeOH: H$_2$O (45:45:10) containing 100 ng/µL of tridecanoic acid as an internal standard. The adsorption equilibrium constant, $K_{ads}$  was experimentally determined using following equation:

94

$$K_{ads} = \frac{k\_ads}{k\_des} = \frac{cs^{eq}/\gamma_s}{[A]^{eq} * (1 - cs/\gamma_s)}$$

Table 3. 3  Calculation of $K_{ads}$

| [A]init (mol.m-3) | $\gamma_s(\frac{mol}{m^2})$ | [A]eq (mol.m-3) | cseq (mol.m-2) | $K_{ads}$ (m3.mol-1) | K (m3.mol-1) Average |
|---|---|---|---|---|---|
| Static extraction | 1.8e-5 | 2.00e-04 | 2.59e-07 | 71.9 | ≈70 |
| Agitated extraction | | 2.04e-04 | 2.49e-07 | 67.1 | |

### 3.3.5.  Static extraction time profile of aLA in agar gel.

The kinetic profile for the static extraction of aLA was assessed by performing static extractions in the absence of a binding matrix. An agar gel solution in PBS (0.8%, w/v) was prepared by heating the mixture in a conventional/commercial microwave oven in 1 min increments until the agar was completely dissolved. Next, the agar solution was spiked with aLA (100 µg·mL-1) and placed in a water bath at 45°C for 30 min. After the water bath, 1.5 mL aliquots of the solution were poured into 2 mL silanized glass vials and allowed to cool at room temperature until they had attained a gel-like consistency. Once the solution had gelled, preconditioned SPME fibers were inserted into the vials, and static extraction was performed at twenty different time points up to 210 hours. After each extraction step, the fibers were cleaned with Kim wipes, rinsed with water, and desorbed as described above.

### 3.3.6. Agitated extraction time profile of aLA with HSA binding matrix.

Human serum albumin (HSA) was added (20 µM) to PBS (pH 7.4) that had been spiked with 100 ng·mL$^{-1}$ of aLA. To ensure sufficient binding between the analyte and matrix, the solution was incubated overnight at room temperature with agitation at 500 rpm. The ensuing extraction profile was performed at 500 rpm for up to 300 min at different time points over a 180-minute time period. After each extraction step, the above-described fiber treatment procedure was followed.

### 3.3.7. Development of mathematical models.

3D simulation models were developed in COMSOL Multiphysics 5.5 software. The purpose of 3D models was to implement *in vivo* in future. Three different mathematical models were developed in order to simulate the mass transfer properties in following extraction conditions:

a) **Extraction of FAs in agar gel (static extraction)** – the computational model for this extraction kinetics is similar to the DOX in agar gel. The mass transfer is controlled by only diffusion. The mass balance equation, initial conditions, boundary conditions are same as for DOX in agar gel. The physics interfaces for both sample matrix and the extraction phase were 'transported diluted species (tds)'. However, the physical properties of the extraction phase for FAs extraction was C-18 instead of C-8 mixed mode. Therefore, respective physical parameters different.

b) **Extraction of FAs in PBS solution under agitation** – This computational model was similar to the DOX extraction in PBS. The mass transfer is controlled by the diffusion and convection. The mass balance equation, boundary conditions, initial conditions and the components of the model were same as for DOX in PBS under agitated extraction.

c) **Extraction in PBS with HSA binding matrix** – The computational model for this experiment was similar to the DOX extraction in PBS-HSA. The mass transfer is controlled by diffusion, convection, and matrix components.

The parameters for extraction kinetics were determined experimentally, with the exception of the diffusion coefficient of FAs, which were adjusted into the simulation based on values obtained from the literature.[107] Because the diffusion coefficient for our target analytes – aLA and LA are not available in the literature, however similar compound to aLA and LA are available , such as oleate.

### 3.3.8. Binding isotherm of FAs with HSA.

100 mL of 100 µM defatted HSA stock was prepared in PBS, while 500, 1000, 5000 ppm stocks of LA and aLA were prepared in MeOH. The LA and aLA stocks were then transferred into 20 mL silanized amber vials containing 7.5 mL of 20µM HSA solution with FA:HSA ratios of 0.1:1, 0.25:1, 0.5:1, 1:1, 1.5:1, 2:1, 3:1, 4:1, 4:1, 5:1, 6:1, 7:1, 8:1, 9:1, 10:1, 15:1, and 20:1. The spiked solutions were gently agitated at 500 rpm in a shaker for 18h at room temperature to achieve equilibration. Subsequently, 1.5 mL aliquots of each sample were transferred into 2 mL silanized amber vials, and equilibrium extraction was performed using preconditioned C18 SPME fibers (15 mm coating length) for 5h at 500 rpm. Following extraction, the fibers were removed and washed with 200 µL of LCMS-grade water for 5 s in a vortex to ensure no matrix components remained. Finally, desorption was performed in 200 µL of desorption solvent for 1h at 1500 rpm.

### 3.3.9. LC-MS/MS quantitation of aLA.

aLA (MW: 278.43 Da) was characterized using either a Dionex UltiMate 3000 UHPLC system coupled to a TSQ Quantiva (Thermo Scientific, San Jose, CA) triple quadrupole mass spectrometer,

or a Vanquish Flex UHPLC system coupled to a TSQ Vantage (Thermo Scientific, San Jose, CA). Chromatographic separation was carried out on a Waters Xselect CSH C18 column (2.1 mm; 100mm, 2.5μm) using mobile phase A ($H_2O$:MeOH, 3:2 v/v, 0.05% Acetic acid) and mobile phase B (MeOH:IPA, 4:1 v/v, 0.05% Acetic acid). MS/MS was operated in SRM mode, and the monitored transition was *m/z* 277.3 > 259.3, which is a dehydration product. The heated-ESI source was operated in positive ionization mode under the following conditions: a capillary voltage of 2500 V; a vaporizer temperature of 350 °C; and a transfer capillary temperature of 325 °C. These conditions enabled an instrumental limit of quantification (LOQ) of 5 ng/mL. The The dehydration product ion is considered a non-specific transition ion and therefore not suitable for quantification in a complex sample. However, the ionization of long chain FAs is not efficient in ESI (electrospray ionization) source. In many cases, derivatization is employed to render these compounds labile and use GC-MS for quantification. However, within the scope of this study we tried to avoid derivatization in order to minimize the loss of the analyte. Since SPME extracts negligible amounts of the analyte present in the sample, and the method requires accurate quantification of FAs, we have chosen LC-MS/MS analysis using triple quadrupole mass spectrometer. Optimization of the ion source parameters was conducted in order to obtain selective product ions (such as loss of hydrogen, or carbon dioxide in this case) to a quantification range. However, we have been able to acquire the intensity of selective transition ions at barely three order of magnitude for six order magnitude of parent ion.

## 3.4. Results and discussion

### 3.4.1. Binding isotherm of FAs with HSA

The binding isotherm curves for aLA and LA were obtained by measuring free concentration at the different FA:HSA ratios detailed in the experimental section. The occupancy of binding sites, B, was calculated for each FA:HSA ratio following eq. (3.2), while the total ligand and receptor concentrations were known from initial concentration spiked into PBS solution. After binding equilibrium was established at a given ligand-receptor ratio, the free ligand concentration, $L$, was determined via SPME extractions of free ligand.
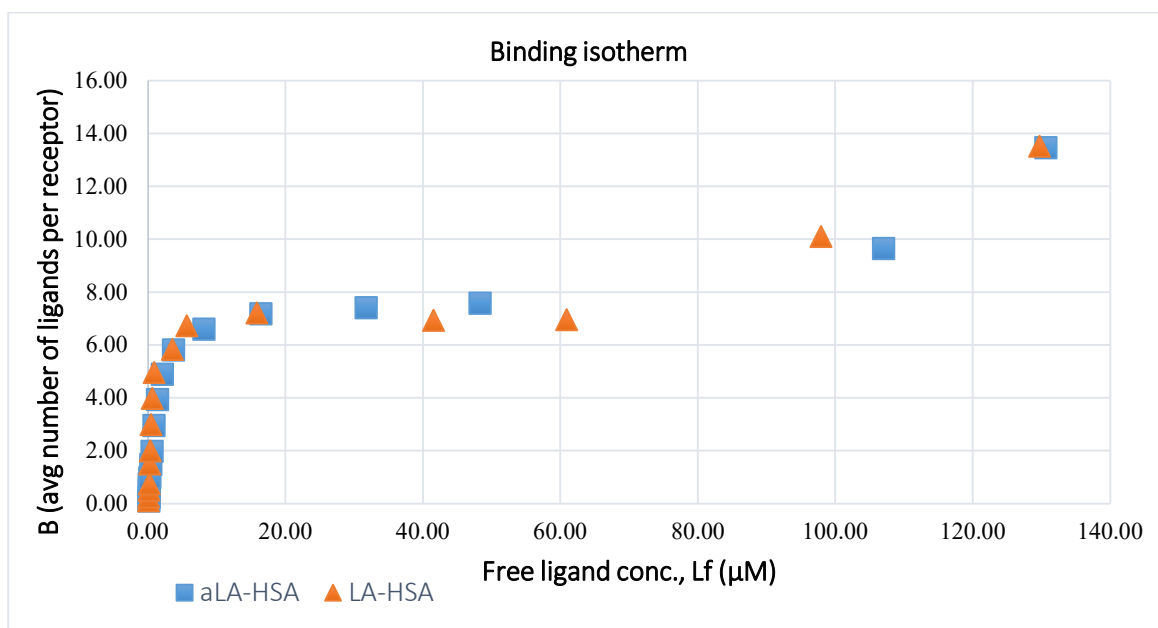


Figure 3. 4 Binding occupancy, B, isotherm plotted against free ligand concentration of aLA and LA with HSA

Figure 3.4 demonstrates how ligand molecules occupy multiple binding sites of HSA receptors as the molar ratio of ligands increases. The binding isotherm experiments were followed by a titration experiment wherein the receptor concentration was constant at 20 μM, and respective ligands

were added to the receptors at different molar ratio. The ligand-to-receptor molar ratio range was

set from 0.1 to 20 with 17 different data points (see Table 3.4 & 3.5). Equilibration was followed by

SPME extractions to measure free ligand concentrations. Once the SPME extractions were

completed, the B values for the respective ligand-to-receptor ratios were calculated. At the

beginning of the isotherm, the B value increased sharply with the addition of ligands, which

indicates that almost all ligands were bound to the receptor. The isotherm of both ligands reached

saturation for B≈7 at a ligand-to-receptor ratio of 7:1, where the free concentrations of aLA and LA

were calculated to be 8.1 and 5.6 µM, respectively (see Table 3.4 & 3.5). After saturation had been

reached, the addition of more ligands to the receptor did not increase the value of B, which shows

that HSA receptors have seven specific and high-affinity binding sites. As the ligand molar ratio

increased, the isotherm curve showed further escalation of the B value, which is presumably due

to the nonspecific interaction of FAs and the HSA receptor.[108]

Table 3. 4  Calculation of B values for aLA-HSA binding isotherm

| Ratio (aLA:HSA) | Ext. amt (ng) | Free conc. Lf (µM) | B |
|---|---|---|---|
| 0.10 | 9 | 0.051 | 0.099 |
| 0.25 | 16 | 0.087 | 0.246 |
| 0.50 | 19 | 0.103 | 0.495 |
| 0.75 | 25 | 0.123 | 0.744 |
| 1.00 | 37 | 0.208 | 0.990 |
| 1.50 | 63 | 0.352 | 1.482 |
| 2.00 | 96 | 0.535 | 1.973 |
| 3.00 | 145 | 0.808 | 2.960 |
| 4.00 | 238 | 1.327 | 3.934 |
| 5.00 | 362 | 2.017 | 4.899 |
| 6.00 | 651 | 3.623 | 5.819 |
| 7.00 | 1448 | 8.065 | 6.597 |
| 8.00 | 2934 | 16.337 | 7.183 |
| 9.00 | 5689 | 31.679 | 7.416 |
| 10.00 | 8665 | 48.248 | 7.588 |
| 15.00 | 19211 | 106.970 | 9.651 |
| 20.00 | 23450 | 130.576 | 13.471 |

Table 3. 5  Calculation of B values for LA-HSA binding isotherm

| Ratio (LA:HSA) | Ext. amt (ng) | Free conc. Lf (μM) | B |
|---|---|---|---|
| 0.10 | 4 | 0.023 | 0.099 |
| 0.25 | 9 | 0.052 | 0.247 |
| 0.50 | 18 | 0.100 | 0.495 |
| 0.75 | 26 | 0.145 | 0.743 |
| 1.50 | 38 | 0.211 | 1.489 |
| 2.00 | 48 | 0.264 | 1.987 |
| 3.00 | 68 | 0.378 | 2.981 |
| 4.00 | 100 | 0.551 | 3.972 |
| 5.00 | 156 | 0.860 | 4.957 |
| 6.00 | 630 | 3.484 | 5.826 |
| 7.00 | 766 | 5.600 | 6.720 |
| 8.00 | 2860 | 15.816 | 7.209 |
| 9.00 | 7507 | 41.510 | 6.925 |
| 10.00 | 11010 | 60.877 | 6.956 |
| 15.00 | 17705 | 97.892 | 10.105 |
| 20.00 | 23458 | 129.706 | 13.515 |

Under normal physiological conditions, the molar ratio of FAs to HSA is usually <1, which indicates that almost all FAs are bound to the HSA. Although the binding isotherms for aLA and LA look very similar, they have different binding characteristics. These characteristics are explained via Scatchard plot below. We used nonlinear curve fitting to obtain the binding affinity constants for each ligand to the HSA receptor.

### 3.4.2.  Measurement of site binding constant using Scatchard plot

Determination of binding constant was determined from the slop of the Scatchard equation (eq8) using nonlinear curve fitting in GraphPad Prism 9.0 software. Experimentally measured of free ligand concentrations using SPME were used to calculate B value (see Table 3.4 & 3.5) which were used for nonlinear fitting using the model of specific binding with Hill's coefficient in the

software. Obtained results for characteristics binding parameters shown in Table 3.6, whereas

Figure 3.5 shows the nonlinear fitting of binding isotherms for respective ligands.

Table 3. 6  Binding parameters obtained using GraphPad Prism software.

| Best-fit values | aLA | LA |
|---|---|---|
| $B_{max}$ | 7.634 (95% CI: 7.447 to 7.835) | 6.849 (95% CI: 6.564 to 7.150) |
| h (Hill's coefficient) | 1.098 (95% CI: 1.020 to 1.184) | 1.551 (95% CI: 1.264 to 1.907) |
| $K_d$ (binding dissociation constant, μM) | 1.263 (95% CI: 1.160 to 1.382) | 0.4695 (95% CI: 0.4109 to 0.5489) |
| Goodness of fit | | |
| Degrees of Freedom | 12 | 12 |
| R Squared | 0.9985 | 0.9927 |
| Sum of Squares | 0.1666 | 0.8175 |
| Sy.x | 0.1178 | 0.261 |
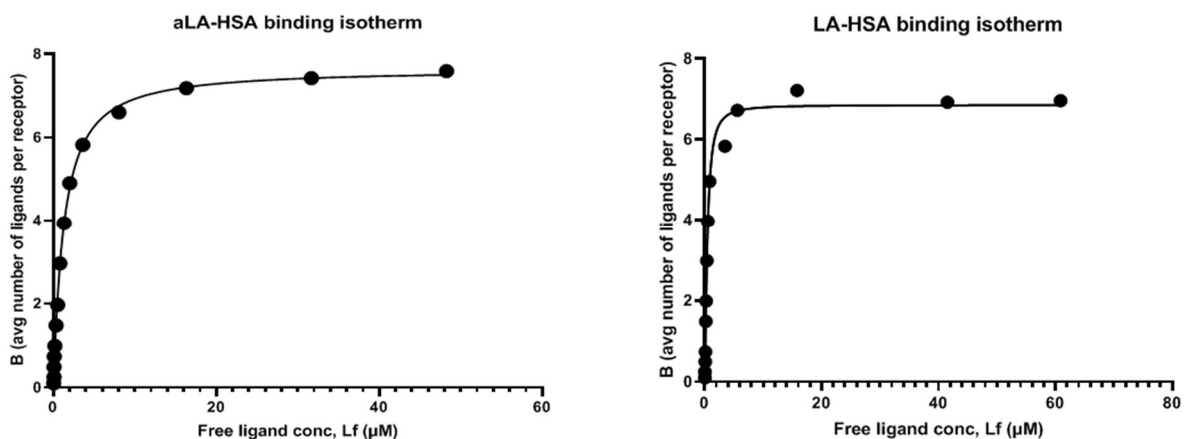


Figure 3. 5  Curve fitting of aLA and LA with HSA binding isotherm using GraphPad Prism software

In Table 3.6, $B_{max}$ denotes the highest occupancy of ligands for specific receptor binding

sites, which was roughly 7 for both ligands. This result indicates that an HSA receptor has seven

specific binding sites for both ligands. The binding dissociation constant, $K_d$,  for aLA and LA was

1.26 and 0.46 µM, respectively. In many cases, the binding affinity is interpreted as a binding association constant, which is simply the reciprocal of the binding dissociation constant. In this case, the binding association constants were $K_{aLA} = 7.7\,E^{05}$ L/mol and $K_{LA} = 2.1\,E^{06}$ L/mol. A comparison of the obtained results to those of other methods used to measure similar fatty acids yielded comparable results; any discrepancies in the results were due to the fact that the previous study focused on ester derivatives of FAs rather than FAs specifically.[97] LA had a significantly higher binding affinity than aLA, which is presumably due to their structural differences. Specifically, LA's binding affinity is known to increase as the higher number of hydrocarbons.[97] The Hill coefficient value for LA is higher than for aLA, which indicates that cooperation is more prominent in LA binding sites than it is in aLA binding sites. The $R^2$ values also showed very good fit with the experimental data, which indicates that the model offers a high level of accuracy.

### 3.4.3.  Characteristics and cooperativity of binding sites via Scatchard plot

Scatchard plots for both ligand-receptor binding experiments were constructed using eq. 2. As shown in Figure 3.6 both positive and negative cooperation were observed for both ligands. The upward curve indicates negative cooperation, and the downward curve indicates positive cooperation.[95] Both isotherms indicated positive and negative cooperation; conversely, the LA:HSA binding interaction was more curved, which indicates greater cooperativity than in the case of the aLA:HSA complex.
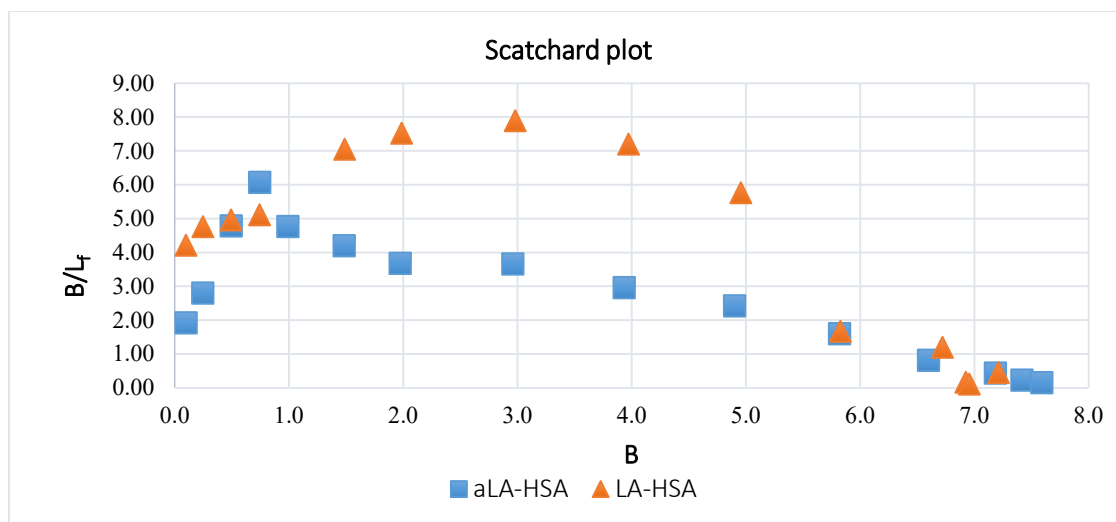
**Figure 3. 6 Scatchard plot analysis of aLA and LA ligands with HSA receptor**

### 3.4.4.  Stoichiometric binding constants

We determined the stoichiometric binding constants, $K_i$ (stepwise binding reactions), for aLA and LA through the nonlinear fitting of experimentally obtained data using the least-squares fitting (LSF) method in Microsoft Excel solver. The calculated stoichiometric binding constants are summarized in Table 3.7. The accuracy of LSF method depends on the square sum of residuals (SSR). In this case, we obtained SSR value app. 0.36.

**Table 3. 7  Calculated stoichiometric binding association constants for aLA and LA using least squares fitting of the experimental data.**

| $i^{th}$ binding site | $K_i$ (aLA-HSA), M$^{-1}$ | $K_i$ (LA-HSA), M$^{-1}$ |
|---|---|---|
| 1 | 2.52E+06 | 4.61E+06 |
| 2 | 4.42E+06 | 1.14E+05 |
| 3 | 1.82E+06 | 1.96E+08 |
| 4 | 6.29E+01 | 2.61E+03 |
| 5 | 3.78E+09 | 4.49E+06 |
| 6 | 1.24E+06 | 4.41E+08 |
| 7 | 4.81E+04 | 9.99E+04 |

It should be noted that the stoichiometric binding constants calculated using nonlinear regression fitting are approximate values. Since there are a lot of free parameters to fit a single curve, this may lead to overfitting or high flexibility – which means the graph will nicely fit with experimental data but fail to predict unseen values. This can be overcome by generating a lot of experimental data. Similar experiment was performed by other researchers for laureate binding study with human serum albumin.[109],[110] In their experiments, they obtained similar graph with plenty of experimental data. Besides, the main purpose of this study was to show the cooperativity among binding sites. Because, in practical most of the binding studies includes drug-receptor interactions where the number of binding sites is very limited and for simplicity, those binding sites are categorized into 'strong' and 'weak' binding sites. Therefore, the number of degrees of freedom is reduced to the extent where reliable binding studies are performed using above mentioned methods. The sensitivity of the LSF method for LA compound was performed by changing the stoichiometric binding constant values presented in Table 3.7. The stoichiometric binding constants were determined using nonlinear solver in Microsoft excel followed by eq. (3.3). The solver calculates the coefficients (which are stoichiometric binding constants) to obtain the lowest square sum of residuals (SSR). The SSR is the residuals between the true B values (experimentally determined) and the adjusted B values (calculated by the solver). The obtained SSR value of LA-HSA study was 0.03 which depends on the accuracy of the experimental results. This results show that experimental results were satisfactory. To justify this claim, a sensitivity test was performed which is presented in Table 3.8.  In this table, some results of the test analysis were displayed.  The test analysis involved the manual changing of stoichiometric constants and observe the desired results.

**Table 3. 8** The  SSR values determined by the solver with respect to stoichiometric binding constants

| $L_f$ (µM) | B (estimated) | B (adjusted) | Test-1 ($K_2$*10) | Test-2 ($K_2$*100) | Test-3 ($K_3$/10) |
|---|---|---|---|---|---|
| 0.023 | 0.10 | 0.10 | 0.13 | **0.35** | 0.10 |
| 0.052 | 0.25 | 0.23 | **0.44** | **1.54** | 0.20 |
| 0.100 | 0.50 | 0.50 | **1.32** | **2.68** | **0.34** |
| 0.145 | 0.74 | 0.83 | **2.14** | **3.05** | **0.46** |
| 0.211 | 1.49 | 1.40 | **2.89** | **3.34** | **0.64** |
| 0.264 | 1.99 | 1.87 | **3.27** | **3.54** | **0.81** |
| 0.378 | 2.98 | 2.83 | **3.80** | **3.90** | **1.35** |
| 0.551 | 3.97 | 4.08 | 4.30 | 4.33 | **2.53** |
| 0.860 | 4.96 | 5.32 | 4.79 | 4.79 | 4.17 |
| 3.484 | 5.83 | 6.25 | 6.09 | 6.09 | 6.09 |
| 5.600 | 6.72 | 6.37 | 6.48 | 6.48 | 6.48 |
| 15.816 | 7.21 | 6.67 | 6.89 | 6.89 | 6.89 |
| 41.510 | 6.92 | 6.96 | 6.98 | 6.98 | 6.98 |
| 60.877 | 6.96 | 7.07 | 7.00 | 7.00 | 7.00 |
| | | | | | |
| SSR | | 0.03 | 8.38 | 65.27 | 1.41 |

Table 3.8 shows how the SSR values changes in Test runs due to change in stoichiometric binding constant values of LA-HSA in Table 3.7. 'B (estimated)' indicates the values determined experimentally followed by eq. (3.2) whereas 'B (adjusted)' are the values adjusted by the solver followed by eq. (3.3). It should be noted that, eq. (3.2) requires the value of free concentration of analyte to determine B value, On the other hand, eq. (3.3) requires both free analyte concentration of analyte as well as the stoichiometric binding constants which are determined by the solver. Table 3.7 shows that, the stoichiometric binding constants of LA with HSA are cooperative, such as negative cooperation between $K_1$ and $K_2$ which indicates that the second stoichiometric binding constant negatively affects the first stoichiometric binding affinity. Therefore, the value of B (number of bound analytes per receptor) will decrease compare to no –cooperativity condition. In our test analyses (Test-1 and Test-2) in Table 3.8, an increase in B values were observed (highlighted

with bold) when the value of K2 was increased one and two order of magnitude. The increase in B

values in Test-1 and Test-2 indicates that the cooperativity is turning towards the positive direction.

In Test-3, the value of $K_3$ was decreased one magnitude of order which resulted in lower B values

(highlighted in bold). This is because K3 shows positive cooperation.

To illustrate the cooperativity among binding sites, Klotz affinity model can be plotted

graphically using stoichiometric binding constants (Figure 3.7). In Fig. 3.7, the Y-axis represents the

logarithmic value of stoichiometric binding affinity corresponding to the $i^{th}$ binding site on the X-

axis. The trend shows how binding affinity changes according to the binding sites. For positive

cooperation, binding affinities incline upwards (e.g., the cooperation between the $4^{th}$ and $5^{th}$

stoichiometric binding affinities for both aLA and LA); for negative cooperation, the binding

affinities decline (e.g., the $5^{th}$ and $6^{th}$ binding affinities of aLA).
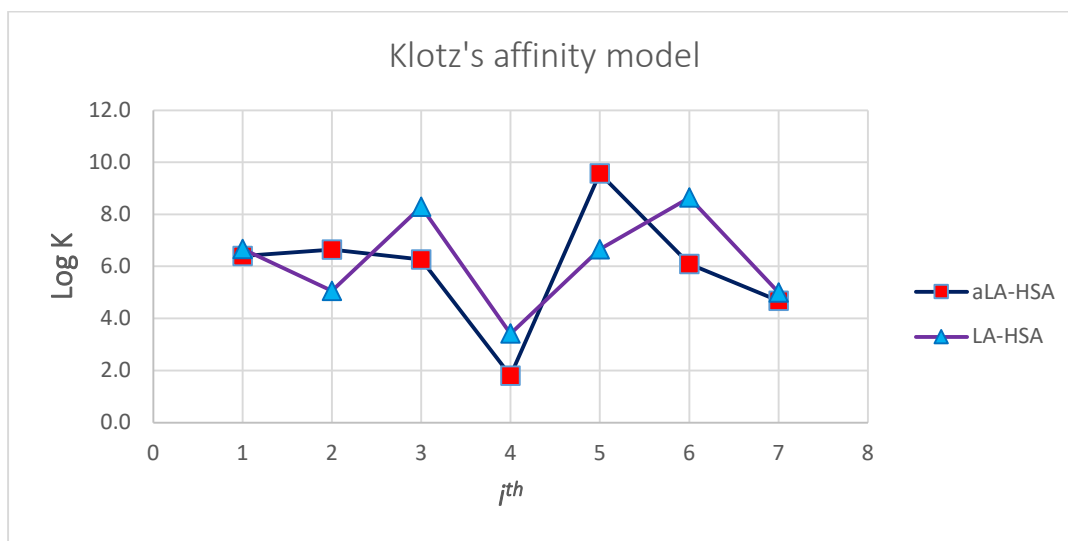


Figure 3. 7 Klotz affinity model. The X axis represents the stoichiometric binding constants for $i^{th}$ binding stoichiometry and the Y axis represents the respective binding constant. This graph indicates how each stoichiometric binding association constant interacts positively (upward) and negatively (downward) with the others.
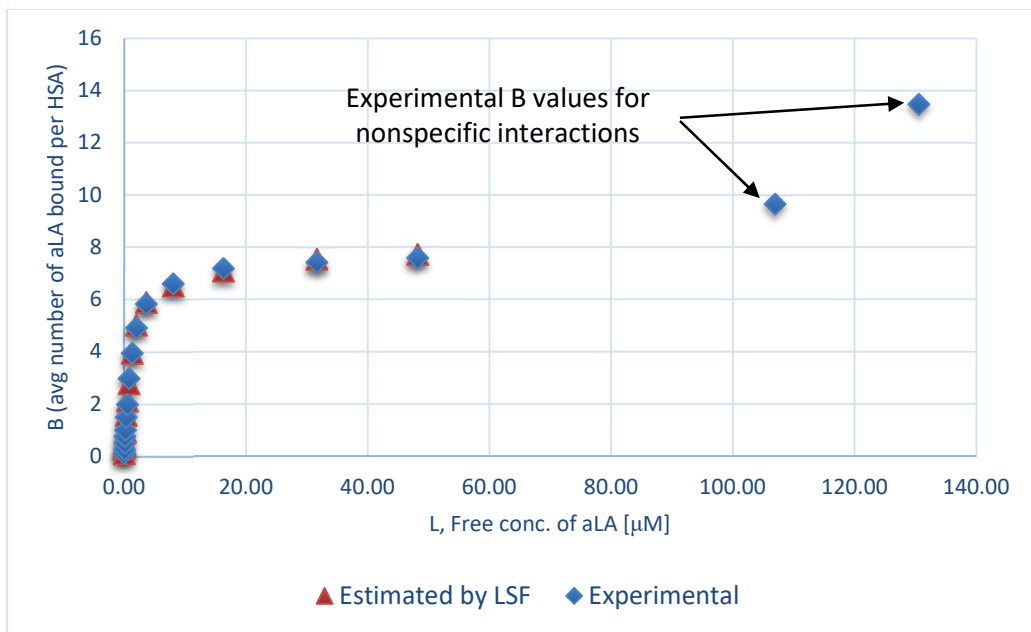
**Figure 3. 8** Nonlinear fitting of binding isotherm of aLA-HSA using least-square fitting (LSF) method in Microsoft Excel

Figure 3.8 shows the nonlinear fitting of aLA-HSA binding isotherm considering stoichiometric binding equation (eq. 3.3). Experimental B values for $L$ over 50μM concentration were not taken into account for curve fitting, because those observed B values are considered for nonspecific interactions. For nonspecific interactions B value increases slowly with linear gradient.

### 3.4.5. *In silico* studies of SPME extraction kinetics of FAs

*In silico* studies were performed to investigate the mass transfer kinetics of FAs onto the SPME extraction phase under equilibrium extraction condition. Mass transfer is driven by three factors: diffusion, agitation (convection), and any reaction that produces or consumes the target in the system. The basic design of the computational models used for investigation of mass transfer of FAs in agar gel, PBS solution and with HSA binding matrix are similar to that for DOX in

chapter 2. Detailed mathematical explanations for these respective models have been provided in chapter 2. The primary objective computational models were to develop well-defined mathematical models that can be used to study other FAs which are similar in properties, such as stearic acid (18:0), oleic acid (18:1), linoleic acid (18:2) and alpha-linoleic acid (18:3) have many similar physical properties.
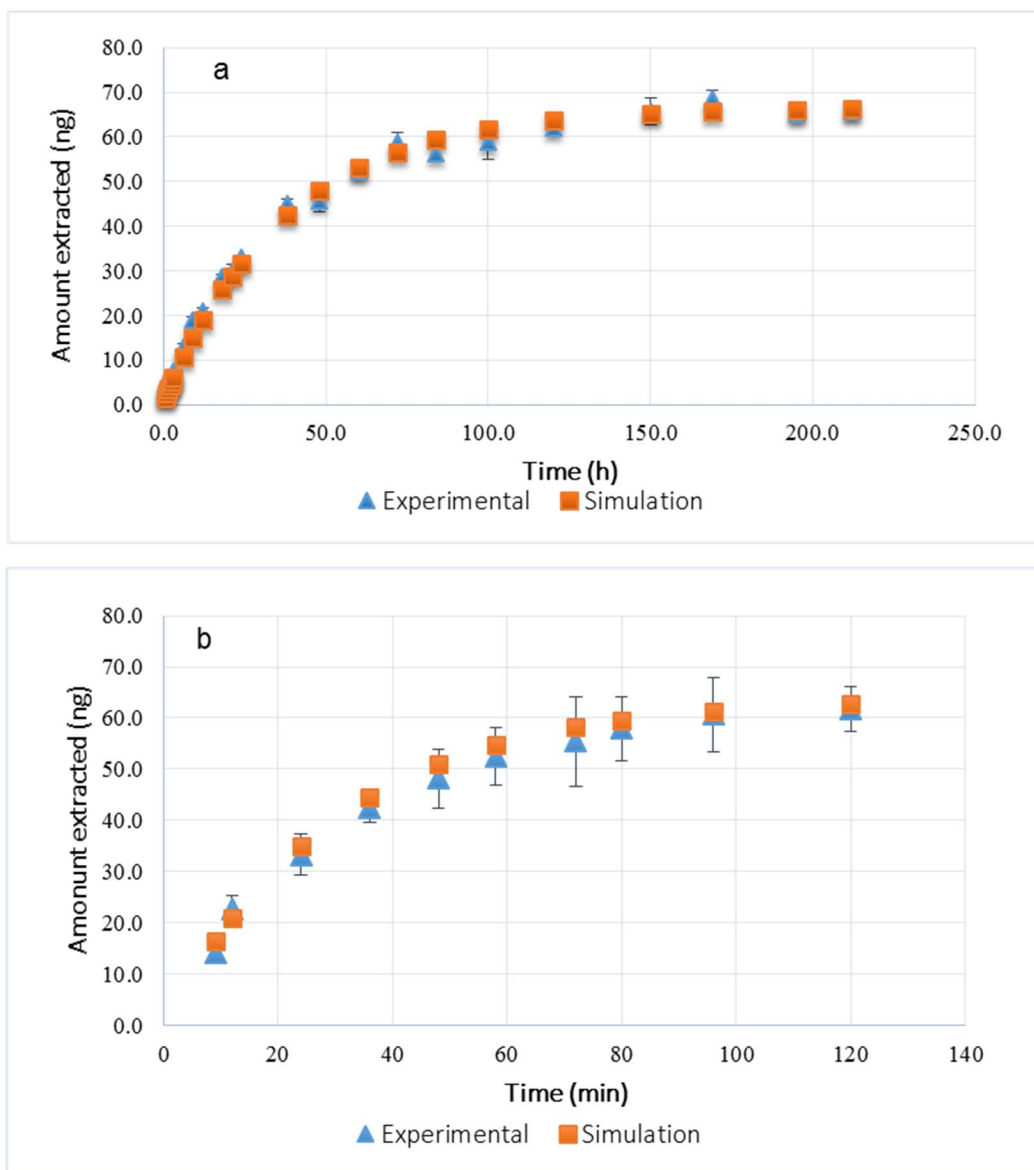


Figure 3. 9  In-silico comparison of extraction time profile for (a) static extraction of 100 ppm aLA spiked in PBS-agar gel, and (b) agitated (500 rpm) extraction of 100 ppm aLA in PBS solution

Figure 3.9 shows that, in both the static and agitated conditions, around 65 μg out of 150 μg (100 μg/mL, 1.5 mL) of aLA was extracted at equilibrium. Since there was no binding matrix in these extraction conditions, all aLA is considered to be free (the concentration of aLA in this case was lower than the CMC value, and silanized vials were used to avoid the nonspecific adsorption of FAs to the surface of the sample vial) and measurable based on the $K_{ads}$ value.[26] The amount of aLA extracted at equilibrium on a solid SPME coating can be defined as the adsorption equilibrium constant, $K_{ads}$, which is a thermodynamic parameter that does not depend on the properties of the sample matrix or the convection conditions. Figure 3.9 shows that approximately the same amount of aLA was extracted using these two extraction conditions and sample matrices. The $K_{ads}$ value of $\sim 70\ m^3/mol$ for aLA was determined by measuring its equilibrium concentration on the solid extraction phase and in the sample matrix. To obtain the surface concentration, we determined the active surface area of the extraction phase via BET analysis (*Section 3.3.2*). For the *in-silico* studies, a 3D mathematical model for the static extraction kinetics was first developed using experimentally obtained values, and the convection conditions were then applied to simulate the agitated extraction kinetics. The experimentally measured binding affinity of aLA to HSA ($K_{aLA} = 7.9E^{05} L/mol$), followed by Scatchard plotting, was used to simulate agitated extraction kinetics in the presence of an HSA binding matrix. The results of this simulation showed good agreement with the experimental results (Figure 3.10), which validates the accuracy and efficiency of the technique used to determine the binding constant of aLA with HSA. Notably, the amount of aLA extracted at equilibrium in the presence of an HSA matrix (20 μM) was 37.3 ng (approximately 0.4% of the total initial concentration). It should be noted that these mathematical

models developed for aLA and LA can be used to determine the free concentration and mass transfer properties in blood plasma.
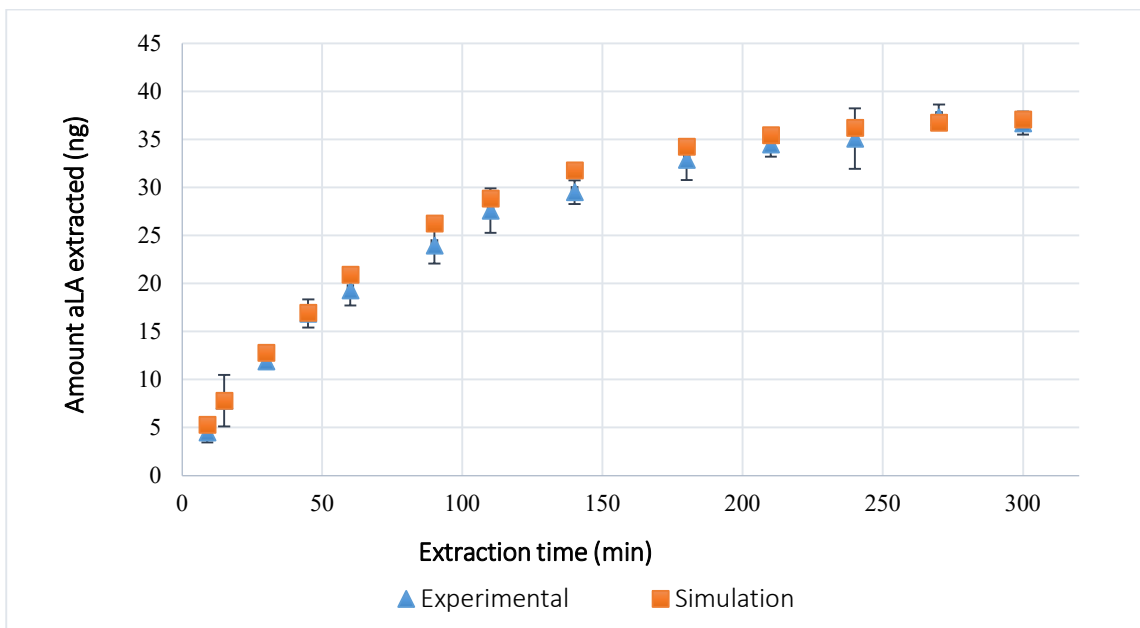


Figure 3. 10  In-silico modeling compared to experimental of extraction-time profile of aLA from PBS solution in the presence of HSA (20 μM) with an aLA:HSA molar ratio of (1:1)

## 3.5. Conclusion

The binding of FAs to HSA plays a vital role in the transport of fatty acids in the circulation. However, this binding interaction is not straightforward since HSA has multiple high-affinity binding sites for FAs, which results in multiple binding equilibria under given physiological conditions. This binding can be explained using site-oriented or stoichiometric approaches, depending on how the interaction takes place with a specific fatty acid. Regardless, the binding effects determine the concentration of free fatty acids. Appropriate analytical methods are required to obtain reliable and accurate free analyte concentrations, with or without disturbance of the native environment. Since SPME extracts via free concentration and can accomplish it with negligible depletion under

the appropriate conditions, the binding equilibrium will not be affected by the mass transfer kinetics of the extraction phase, which is a key criterion in the study of ligand-receptor binding. In this investigation, SPME was able to successfully and efficiently determine the ligand-receptor binding characteristics. The binding association constant for aLA was determined according to Scatchard plot, which was used to develop mathematical model to simulate the extraction kinetics of aLA in the presence of an HSA binding matrix. It should be mentioned that the apparent binding constant is not possible to determine followed by site-oriented and stoichiometric approach if the binding sites are not independent and they cooperate with each other. The purpose of the Scatchard plot is to determine the apparent binding constant, it can not explain the dynamics of the binding characteristics like the other two approaches – site specific binding and stoichiometric binding. The results of the *in-silico* comparisons were satisfactory, which demonstrates the usefulness of mathematical models in validating SPME experimental data. In addition, the developed mathematical models can be applied to in-silico investigations of similar interactions between ligands including lipids and HSA receptors, thereby reducing time, effort, and cost. The presented results illustrate principles of non-exhaustive microextraction, specifically those of SPME, from a highly bounding matrix. Moreover, they advance our understanding of how this technique can be used to obtain information about multiphase equilibria in complex systems, as well as how to optimize microextraction conditions and interpret SPME data involving matrix specific binding sides.

## Chapter 4:    Summary and future perspectives

This study demonstrates the dynamics of mass transfer kinetics on SPME in complex biological samples, such as blood plasma, solid tissue. In chapter 2, a well-known chemotherapeutic drug, doxorubicin (DOX) was chosen as a model drug, while bovine lung tissue was selected as model matrix. DOX is frequently used as a local chemotherapeutic agent for cancer therapy and is currently under pre-clinical trial for treatment of human lung cancer through in vivo lung perfusion (IVLP). In this regard, a novel analytical technique to determine free and bound concentrations from tissue by either *in vivo* or *ex vivo* sampling is demanded. In this study, we addressed a novel SPME technique for measurement of DOX from bovine lung tissue by direct sampling.

In these investigations, a model analyte doxorubicin (DOX) was spiked into homogenized tissue matrix at transient and equilibrium extraction conditions, with subsequent assessment of obtained experimental results by an *in-silico* approach using mathematical models developed in COMSOL Multyphysics. *In-silico* studies were performed based on transported diluted species (*tds*) and reaction engineering (*re*) modules from COMSOL Multiphysics, using the same conditions as those used to attain experimental results. To determine the apparent binding affinity of DOX to the tissue matrix which contains multiple binding species, the experimentally determined binding affinity of DOX with human serum albumin (HSA) was considered to simplify the mathematical calculations. Here, the value of the binding affinity was considered for single binding site and adjusted by fitting the experimental results with the mathematical models. The developed mathematical model allows for measurements of free drug concentrations inside tissue matrix and facilitates calculations of local depletion of DOX by a solid SPME coating. Results of the

113

investigations indicate that local depletion of the free form of DOX, even at the kinetic stage, is negligible for tissue extraction, as the release of the heavily bound analyte (over 99% binding to tissue matrix) is very rapid, thus easily compensating for the loss of the drug to the SPME coating. This indicates that the dissociation rate constant of DOX from lung tissue components is very rapid; therefore, the mass transfer of drug to the fiber coating via free from is very efficient. Our results also indicate that thin coating SPME fibers provide a good way to measure drug distribution after dosing, as extractions via thin coating SPME fibers do not affect the free concentration of drug, which is responsible for drug distribution in tissue.

This thesis studies the dynamics of solid phase microextraction extraction in tissue with the presence of a binding matrix, providing further experimental validation of the theoretical findings and mathematical models. In this context, the presented work is introduced as a novel technique for measurement of free drug concentration in biological tissue via biocompatible solid-phase microextraction (SPME). In addition, the presented theoretical studies greatly contribute to the literature on SPME by discussing and defining several crucial concepts for *in vivo* SPME sampling, an emerging technique with great potential in bioanalysis.

Moreover, derived from this primary work, many important concepts in tissue sampling, such as apparent binding constant, spatial resolution, and local depletion, were developed and discussed. The results of this line of investigation help to shed light on the principles of SPME tissue extraction, including *in vivo* extraction, by demonstrating that when a thin coating SPME fiber is used as extraction phase in tissue matrix, the unbound free concentration of analytes in the sampling area remains constant as analytes transferred to the coating are rapidly replaced from the reservoir of analytes bound to the tissue matrix. Despite its higher extraction capacity, the

SPME probe is herein shown to behave similarly to an electrochemical probe, allowing for monitoring of drug concentrations at particular locations and enabling measurements of drug distribution following dosing in tissue, while additionally facilitating multicomponent determinations at the same time.

The conclusions from this thesis are not limited to only DOX or lung tissue, but also paves the way for quantitation of free and conjugated forms of other drugs in any complex biological matrix. In fact, this study will allow for exploration of completely new horizons in biomedical sciences, such *in vivo* monitoring of drug pharmacodynamics in tissue, without the need for costly and invasive correlative investigations, such as determinations in surrounding biofluids and biopsies.

In chapter 3, SPME technique was employed to investigate the binding characteristics of fatty acids (FA) to human serum albumin (HSA) have been garnering increased attention due to the importance of FAs in numerous in clinical and biological fields. In that study, binding characteristics of two long-chain FAs—linoleic acid (LA; FA 18:2) and alpha-linoleic acid (aLA; FA 18:3, n-3) with HSA, was investigated followed by binding isotherm studies. HSA has multiple binding sites for FAs, and these binding sites are involved in a complex and dynamic binding equilibrium with FAs. The binding dynamics changes with initial concentration of FAs and their length. In this study we explained these complex binding interactions in terms of site-oriented and stoichiometric approaches. It is very important to understand these binding characteristics to determine the free concentration of FAs, because the correlation between the free concentration of and matrix components are nonlinear. Computational models were developed to determine free concentration and subsequently validate experimental results.

**ACS** Publications
Most Trusted. Most Cited. Most Read.

**Measurement of Free Drug Concentration from Biological Tissue by Solid-Phase Microextraction: In Silico and Experimental Study**

**Author:** Mohammad Huq, Marcos Tascon, Emir Nazdrajic, et al

**Publication:** Analytical Chemistry

**Publisher:** American Chemical Society

**Date:** Jun 1, 2019

*Copyright © 2019, American Chemical Society*

## Quick Price Estimate

# References

(1)     Varchanis, S.; Dimakopoulos, Y.; Wagner, C.; Tsamopoulos, J. How Viscoelastic Is Human

Blood Plasma? *Soft Matter* **2018**, *14* (21), 4238–4251.

https://doi.org/10.1039/c8sm00061a.

(2)     Benjamin, R. J.; McLaughlin, L. S. Plasma Components: Properties, Differences, and Uses.

*Transfusion* **2012**, *52* (SUPPL. 1). https://doi.org/10.1111/j.1537-2995.2012.03622.x.

(3)     Yang, H.; Wang, G.; Zhang, T.; Beattie, J. H.; Zhou, S. Establishing an Optimized Method for

the Separation of Low and High Abundance Blood Plasma Proteins. *PeerJ Anal. Chem.*

**2020**, *2*, e6. https://doi.org/10.7717/peerj-achem.6.

(4)     Schaller, J. *Human Blood Plasma Proteins : Structure and Function*; John Wiley & Sons:

Chichester, West Sussex, England, 2008.

(5)     Varshney, A. Ligand Binding Strategies of Human Serum Albumin: How Can the Cargo Be

Utilized? *Chirality* **2010**, *22* (1), 77–87. https://doi.org/https://doi-

org.proxy.lib.uwaterloo.ca/10.1002/chir.20709.

(6)     Ha, C.-E.; Bhagavan, N. V. Novel Insights into the Pleiotropic Effects of Human Serum

Albumin in Health and Disease. *Biochim. Biophys. Acta - Gen. Subj.* **2013**, *1830* (12), 5486–

5493. https://doi.org/10.1016/j.bbagen.2013.04.012.

(7)     Atala, A.; Lanza, R. Handbook of Stem Cells. *Handb. Stem Cells* **2013**, *1*.

https://doi.org/10.1016/C2010-0-66893-3.

(8)     Alberts, B.; Johnson, A.; Lewis, J.; Raff, M.; Roberts, K.; Walter, P. The Extracellular Matrix

of Animals. In *Molecular Biology of the Cell*; Garland Science: New York, 2002.

(9)     Kusindarta, D. L.; Wihadmadyatami, H. The Role of Extracellular Matrix in Tissue

Regeneration. In *Tissue Regeneration*; Kound, H. A. E., Ed.; IntechOpen, 2018; pp 65–73. https://doi.org/10.5772/intechopen.70922.

(10)  Moody, M. T.; Diaz, S.; Shah, P.; Papsun, D.; Logan, B. K. Analysis of Fentanyl Analogs and Novel Synthetic Opioids in Blood, Serum/Plasma, and Urine in Forensic Casework. *Drug Test. Anal.* **2018**, *10* (9), 1358–1367. https://doi.org/10.1002/dta.2393.

(11)  Kim, H.; Choi, Y.; An, Y.; Jung, Y.-R.; Lee, J.-Y.; Lee, H.-J.; Jeong, J.; Kim, Z.; Kim, K. Development of P-Coumaric Acid Analysis in Human Plasma and Its Clinical Application to PK/PD Study. *J. Clin. Med.* **2020**, *10* (1), 108. https://doi.org/10.3390/jcm10010108.

(12)  Miyauchi, E.; Furuta, T.; Ohtsuki, S.; Tachikawa, M.; Uchida, Y.; Sabit, H.; Obuchi, W.; Baba, T.; Watanabe, M.; Terasaki, T.; Nakada, M. Identification of Blood Biomarkers in Glioblastoma by SWATH Mass Spectrometry and Quantitative Targeted Absolute Proteomics. *PLoS One* **2018**, *13* (3), 1–22. https://doi.org/10.1371/journal.pone.0193799.

(13)  Germain, A.; Ruppert, D.; Levine, S. M.; Hanson, M. R. Metabolic Profiling of a Myalgic Encephalomyelitis/Chronic Fatigue Syndrome Discovery Cohort Reveals Disturbances in Fatty Acid and Lipid Metabolism. *Mol. Biosyst.* **2017**, *13* (2), 371–379. https://doi.org/10.1039/c6mb00600k.

(14)  Simão; Gonçalves; Duarte; Barroso; Cristóvão; Gallardo. Toxicological Aspects and Determination of the Main Components of Ayahuasca: A Critical Review. *Medicines* **2019**, *6* (4), 106. https://doi.org/10.3390/medicines6040106.

(15)  Alvarez, M. J.; Shen, Y.; Giorgi, F. M.; Lachmann, A.; Ding, B. B.; Hilda Ye, B.; Califano, A. Functional Characterization of Somatic Mutations in Cancer Using Network-Based Inference of Protein Activity. *Nat. Genet.* **2016**, *48* (8), 838–847.

https://doi.org/10.1038/ng.3593.

(16) Parviainen, V.; Joenväärä, S.; Tukiainen, E.; Ilmakunnas, M.; Isoniemi, H.; Renkonen, R. Relative Quantification of Several Plasma Proteins during Liver Transplantation Surgery. *J. Biomed. Biotechnol.* **2011**, *2011*. https://doi.org/10.1155/2011/248613.

(17) Alam, M. N.; Ricardez-Sandoval, L.; Pawliszyn, J. Numerical Modeling of Solid-Phase Microextraction: Binding Matrix Effect on Equilibrium Time. *Anal. Chem.* **2015**, *87* (19), 9846–9854. https://doi.org/10.1021/acs.analchem.5b02239.

(18) Alam, M. N.; Pawliszyn, J. Effect of Binding Components in Complex Sample Matrices on Recovery in Direct Immersion Solid-Phase Microextraction: Friends or Foe? *Anal. Chem.* **2018**, *90* (4), 2430–2433. https://doi.org/10.1021/acs.analchem.7b05436.

(19) Gonzalez, D.; Schmidt, S. Importance of Relating Efficacy Measures to Unbound Drug Concentrations for Anti-Infective Agents. **2013**, *26* (2), 274–288. https://doi.org/10.1128/CMR.00092-12.

(20) Pawliszyn, J. *Handbook of Solid Phase Microextraction*; 2012. https://doi.org/10.1016/B978-0-12-416017-0.00003-6.

(21) Reyes-Garcés, N.; Gionfriddo, E.; Gómez-Ríos, G. A.; Alam, M. N.; Boyacl, E.; Bojko, B.; Singh, V.; Grandy, J.; Pawliszyn, J. Advances in Solid Phase Microextraction and Perspective on Future Directions. *Anal. Chem.* **2018**, *90* (1), 302–360. https://doi.org/10.1021/acs.analchem.7b04502.

(22) Bahrami, N.; Yonekura, L.; Linforth, R.; Carvalho da Silva, M.; Hill, S.; Penson, S.; Chope, G.; Fisk, I. D. Comparison of Ambient Solvent Extraction Methods for the Analysis of Fatty Acids in Non-Starch Lipids of Flour and Starch. *J. Sci. Food Agric.* **2014**, *94* (3), 415–423.

https://doi.org/10.1002/jsfa.6449.

(23) Morais, D. R. de; Visentainer, J. E. L.; Santos, L. P. dos; Matsushita, M.; Souza, N. E. de; Visentainer, J. V. Evaluation of Lipid Extraction and Fatty Acid Composition of Human Plasma. *Rev. Bras. Hematol. Hemoter.* **2010**, *32* (6), 439–443. https://doi.org/10.1590/s1516-84842010000600006.

(24) Berendsen, B. J. A.; Stolker, L. A. A. M.; Nielen, M. W. F.; Nielen, M. W. F. Selectivity in the Sample Preparation for the Analysis of Drug Residues in Products of Animal Origin Using LC-MS. *TrAC - Trends Anal. Chem.* **2013**, *43*, 229–239. https://doi.org/10.1016/j.trac.2012.09.019.

(25) Vuckovic, D. Current Trends and Challenges in Sample Preparation for Global Metabolomics Using Liquid Chromatography-Mass Spectrometry. *Anal. Bioanal. Chem.* **2012**, *403* (6), 1523–1548. https://doi.org/10.1007/s00216-012-6039-y.

(26) Huq, M.; Tascon, M.; Nazdrajic, E.; Roszkowska, A.; Pawliszyn, J. Measurement of Free Drug Concentration from Biological Tissue by Solid-Phase Microextraction: In Silico and Experimental Study. *Anal. Chem.* **2019**, *91* (12), 7719–7728. https://doi.org/10.1021/acs.analchem.9b00983.

(27) Gómez-Ríos, G. A.; Tascon, M.; Pawliszyn, J. Coated Blade Spray: Shifting the Paradigm of Direct Sample Introduction to MS. *Bioanalysis* **2018**, *10* (4), 257–271. https://doi.org/10.4155/bio-2017-0153.

(28) Mirabelli, M. F.; Wolf, J. C.; Zenobi, R. Direct Coupling of Solid-Phase Microextraction with Mass Spectrometry: Sub-Pg/g Sensitivity Achieved Using a Dielectric Barrier Discharge Ionization Source. *Anal. Chem.* **2016**, *88* (14), 7252–7258.

https://doi.org/10.1021/acs.analchem.6b01507.

(29)    Gómez-Ríos, G. A.; Liu, C.; Tascon, M.; Reyes-Garcés, N.; Arnold, D. W.; Covey, T. R.;

        Pawliszyn, J. Open Port Probe Sampling Interface for the Direct Coupling of Biocompatible

        Solid-Phase Microextraction to Atmospheric Pressure Ionization Mass Spectrometry. *Anal.*

        *Chem.* **2017**, *89* (7), 3805–3809. https://doi.org/10.1021/acs.analchem.6b04737.

(30)    Onat, B.; Rosales-Solano, H.; Pawliszyn, J. Development of a Biocompatible Solid Phase

        Microextraction Thin Film Coating for the Sampling and Enrichment of Peptides. *Anal.*

        *Chem.* **2020**, *92* (13), 9379–9388. https://doi.org/10.1021/acs.analchem.0c01846.

(31)    Arthur, C. L.; Pawliszyn, J. Solid Phase Microextraction with Thermal Desorption Using

        Fused Silica Optical Fibers. *Anal. Chem.* **1990**, *62* (19), 2145–2148.

        https://doi.org/10.1021/ac00218a019.

(32)    COMSOL Multiphysics. Comsol Multiphysics Reference Manual: Version 5.6. *Manual* **2014**.

(33)    Musteata, M. L.; Musteata, F. M.; Pawliszyn, J. Biocompatible Solid-Phase Microextraction

        Coatings Based on Polyacrylonitrile and Solid-Phase Extraction Phases. *Anal. Chem.* **2007**,

        *79* (18), 6903–6911. https://doi.org/10.1021/ac070296s.

(34)    Mullett, W. M.; Pawliszyn, J. Direct Determination of Benzodiazepines in Biological Fluids

        by Restricted-Access Solid-Phase Microextraction. *Anal. Chem.* **2002**, *74* (5), 1081–1087.

        https://doi.org/10.1021/ac010747n.

(35)    Mullett, W. M.; Pawliszyn, J. The Development of Selective and Biocompatible Coatings for

        Solid Phase Microextraction. *J. Sep. Sci.* **2003**, *26* (3–4), 251–260.

        https://doi.org/10.1002/jssc.200390031.

(36)    Alam, M. N.; Nazdrajić, E.; Singh, V.; Tascon, M.; Pawliszyn, J. Effect of Transport

Parameters and Device Geometry on Extraction Kinetics and Efficiency in Direct Immersion Solid-Phase Microextraction. *Anal. Chem.* **2018**, *90* (19), 11548–11555. https://doi.org/10.1021/acs.analchem.8b02855.

(37)   Thirukumaran, M.; Singh, V.; Arao, Y.; Fujito, Y.; Nishimura, M.; Ogura, T.; Pawliszyn, J. Solid-Phase Microextraction- Probe Electrospray Ionization Devices for Screening and Quantitating Drugs of Abuse in Small Amounts of Biofluids. *Talanta* **2021**, *231* (January), 122317. https://doi.org/10.1016/j.talanta.2021.122317.

(38)   Tascon, M.; Singh, V.; Huq, M.; Pawliszyn, J. Direct Coupling of Dispersive Extractions with Magnetic Particles to Mass Spectrometry via Microfluidic Open Interface. *Anal. Chem.* **2019**, *91* (7), 4762–4770. https://doi.org/10.1021/acs.analchem.9b00308.

(39)   Rizk, M. L.; Zou, L.; Savic, R. M.; Dooley, K. E. Importance of Drug Pharmacokinetics at the Site of Action. *Clin. Transl. Sci.* **2017**, *10* (3), 133–142. https://doi.org/10.1111/cts.12448.

(40)   Schmidt, S.; Banks, R.; Kumar, V. Clinical Microdialysis in Skin and Soft Tissues : An Update. **2008**, 351–364. https://doi.org/10.1177/0091270007312152.

(41)   Revue, L.; Industries, P.; Metabolic, T.; Commission, T. E.; European, T. The Effect of Plasma Protein Binding on in Vivo Efficacy : Misconceptions in Drug Discovery. **2010**, *9* (DECEmbER), 929–939. https://doi.org/10.1038/nrd3287.

(42)   Reck, P.; Sakamoto, J.; Chen, M.; Linacre, V.; Arce, C.; Liu, M.; Waddell, T. K.; Keshavjee, S.; Cypel, M. Modi Fi Ed In Vivo Lung Perfusion for Local Chemotherapy : A Preclinical Study With Doxorubicin. *Ann. Thorac. Surg.* **2016**, *101* (6), 2132–2140. https://doi.org/10.1016/j.athoracsur.2015.12.043.

(43)   Collins, J. M.; Klecker, R. W. Evaluation of Highly Bound Drugs : Interspecies , Intersubject ,

and Related Comparisons. **2002**, *902*, 971–975.

(44)   Hoseyni, H.; Xu, Y.; Zhou, H. Therapeutic Drug Monitoring of Biologics for Inflammatory

Bowel Disease : An Answer to Optimized Treatment ? **2018**, No. January.

https://doi.org/10.1002/jcph.1084.

(45)   Microdialysis- an Alternative for in Vitro and in Vivo Protein Binding Studies.Pdf.

(46)   Liu, P.; Müller, M.; Grant, M.; Obermann, B.; Derendorf, H. Tissue Penetration of

Cefpodoxime and Cefixime in Healthy Subjects. **2005**, 564–569.

https://doi.org/10.1177/0091270004273679.

(47)   Finlay, G. J.; Baguley, B. C. Effects of Protein Binding on the in Vitro Activity of Antitumour

Acridine Derivatives and Related Anticancer Drugs. *Cancer Chemother. Pharmacol.* **2000**,

*45*, 417–422. https://doi.org/10.1007/s002800051011.

(48)   Dale, N.; Hatz, S.; Tian, F.; Llaudet, E. Listening to the Brain : Microelectrode Biosensors for

Neurochemicals. **2005**, *23* (8). https://doi.org/10.1016/j.tibtech.2005.05.010.

(49)   Bloedow, D. C.; Ph, D.; Piepho, R. W. SerumBinding of Diltiazemin Humans. **1982**, 201–

205.

(50)   Colussi, D. M.; Parisot, C. Y.; Lefèvre, G. Y. Plasma Protein Binding of Letrozole, a New

Nonsteroidal Aromatase Enzyme Inhibitor. *J. Clin. Pharmacol.* **1998**, *38* (8), 727–735.

https://doi.org/10.1002/j.1552-4604.1998.tb04813.x.

(51)   Pawliszyn, J. *Solid Phase Microextraction*; 2001. https://doi.org/10.1007/978-1-4615-

1247-9_6.

(52)   Musteata, F. M. Monitoring Free Drug Concentrations : Challenges. **2011**, 1753–1768.

(53)   Lord, H. L.; Zhang, X.; Musteata, F. M.; Vuckovic, D.; Pawliszyn, J. In Vivo Solid-Phase

Microextraction for Monitoring Intravenous Concentrations of Drugs and Metabolites. *Nat. Protoc.* **2011**, *6* (6), 896–924. https://doi.org/10.1038/nprot.2011.329.

(54)    Musteata, F. M.; de Lannoy, I.; Gien, B.; Pawliszyn, J. Blood Sampling without Blood Draws for in Vivo Pharmacokinetic Studies in Rats. *J. Pharm. Biomed. Anal.* **2008**, *47* (4–5), 907– 912. https://doi.org/10.1016/j.jpba.2008.03.028.

(55)    Lord, H. L.; Grant, R. P.; Walles, M.; Incledon, B.; Fahie, B.; Pawliszyn, J. B. Development and Evaluation of a Solid-Phase Microextraction Probe for in Vivo Pharmacokinetic Studies. **2003**, *75* (19), 5103–5115. https://doi.org/10.1021/ac0343230.

(56)    Bojko, B.; Gorynski, K.; Gomez-rios, G. A.; Matthias, J.; Machuca, T.; Nikolaus, V.; Cudjoe, E.; Hsin, M.; Cypel, M.; Selzner, M.; Liu, M.; Keshavjee, S.; Pawliszyn, J. Analytica Chimica Acta Solid Phase Microextraction Fills the Gap in Tissue Sampling Protocols. *Anal. Chim. Acta* **2013**, *803*, 75–81. https://doi.org/10.1016/j.aca.2013.08.031.

(57)    Cudjoe, E.; Bojko, B.; Delannoy, I.; Saldivia, V.; Pawliszyn, J. Solid-Phase Microextraction: A Complementary InVivo Sampling Method to Microdialysis. *Angew. Chemie - Int. Ed.* **2013**, *52* (46), 12124–12126. https://doi.org/10.1002/anie.201304538.

(58)    Ouyang, G.; Vuckovic, D.; Pawliszyn, J. Nondestructive Sampling of Living Systems Using in Vivo Solid-Phase Microextraction. **2011**, 2784–2814. https://doi.org/10.1021/cr100203t.

(59)    Musteata, F. M.; Pawliszyn, J. Study of Ligand-Receptor Binding Using SPME: Investigation of Receptor, Free, and Total Ligand Concentrations. *J. Proteome Res.* **2005**, *4* (3), 789–800. https://doi.org/10.1021/pr049768z.

(60)    Alam, M. N.; Ricardez-Sandoval, L.; Pawliszyn, J. Calibrant Free Sampling and Enrichment with Solid-Phase Microextraction: Computational Simulation and Experimental

Verification. *Ind. Eng. Chem. Res.* **2017**, *56* (13), 3679–3686.

https://doi.org/10.1021/acs.iecr.7b00131.

(61)     Dukhin, S. S.; Labib, M. E. Theory of Effective Drug Release from Medical Implants Based

on the Higuchi Model and Physico-Chemical Hydrodynamics. *Colloids Surfaces A*

*Physicochem. Eng. Asp.* **2012**, *409*, 10–20. https://doi.org/10.1016/j.colsurfa.2012.04.040.

(62)     Zhou, S. N.; Zhang, X.; Ouyang, G.; Es-haghi, A.; Pawliszyn, J. On-Fiber Standardization

Technique for Solid-Coated Solid-Phase Microextraction. *Anal. Chem.* **2007**, *79* (3), 1221–

1230. https://doi.org/10.1021/ac061626w.

(63)     Tacar, O.; Sriamornsak, P.; Dass, C. R. Doxorubicin : An Update on Anticancer Molecular

Action ,. **2013**, 157–170. https://doi.org/10.1111/j.2042-7158.2012.01567.x.

(64)     Carvalho, C.; Santos, R. X.; Cardoso, S.; Correia, S.; Oliveira, P. J.; Santos, M. S.; Moreira, P.

I. Doxorubicin : The Good , the Bad and the Ugly Effect Doxorubicin : The Good , the Bad

and the Ugly Effect. **2009**, No. October. https://doi.org/10.2174/092986709788803312.

(65)     Roszkowska, A.; Tascon, M.; Bojko, B.; Goryński, K.; dos Santos, P. R.; Cypel, M.; Pawliszyn,

J. Equilibrium Ex Vivo Calibration of Homogenized Tissue for in Vivo SPME Quantitation of

Doxorubicin in Lung Tissue. *Talanta* **2018**, *183* (November 2017), 304–310.

https://doi.org/10.1016/j.talanta.2018.02.049.

(66)     Reck dos Santos, P.; Sakamoto, J.; Chen, M.; Linacre, V.; Arce, C.; Liu, M.; Waddell, T. K.;

Keshavjee, S.; Cypel, M. Modified In Vivo Lung Perfusion for Local Chemotherapy: A

Preclinical Study With Doxorubicin. *Ann. Thorac. Surg.* **2016**, *101* (6), 2132–2140.

(67)     Alam, M. N.; Nazdrajić, E.; Singh, V.; Tascon, M.; Pawliszyn, J. Effect of Transport

Parameters and Device Geometry on Extraction Kinetics and Efficiency in Direct

Immersion Solid-Phase Microextraction. *Anal. Chem.* **2018**, acs.analchem.8b02855.

https://doi.org/10.1021/acs.analchem.8b02855.

(68)    Gaigalas, A. K.; Hubbard, J. B.; McCurley, M.; Woo, S. Diffusion of Bovine Serum Albumin in

Aqueous Solutions. *J. Phys. Chem.* **1992**, *96* (5), 2355–2359.

https://doi.org/10.1021/j100184a063.

(69)    Wop, F. A. De; Demep, R. A.; Bet, D.; Katsz, V.; Kruijff, B. De. Characterization of the

Interaction of Doxorubicin with ( Poly ) Phosphoinositides in Model Systems Evidence for

Specific Interaction with Phosphatidylinositol-Monophosphate And. **1991**, *288* (1), 237–

240.

(70)    Awasthia, S.; Frenkel, P.; Bellib, A. The Relationship Drug Resistance of Doxorubicin

Binding to Membrane Lipids With. **1992**, *63*, 109–116.

(71)    Birjandi, A. P.; Bojko, B.; Ning, Z.; Figeys, D.; Pawliszyn, J. High Throughput Solid Phase

Microextraction: A New Alternative for Analysis of Cellular Lipidome? *J. Chromatogr. B*

*Anal. Technol. Biomed. Life Sci.* **2017**, *1043*, 12–19.

https://doi.org/10.1016/j.jchromb.2016.09.034.

(72)    Roszkowska, A.; Yu, M.; Bessonneau, V.; Bragg, L.; Servos, M.; Pawliszyn, J. Tissue Storage

Affects Lipidome Profiling in Comparison to in Vivo Microsampling Approach. *Sci. Rep.*

**2018**, *8* (1), 1–10. https://doi.org/10.1038/s41598-018-25428-2.

(73)    Birjandi, A. P.; Mirnaghi, F. S.; Bojko, B.; Wąsowicz, M.; Pawliszyn, J. Application of Solid

Phase Microextraction for Quantitation of Polyunsaturated Fatty Acids in Biological Fluids.

*Anal. Chem.* **2014**, *86* (24), 12022–12029. https://doi.org/10.1021/ac502627w.

(74)    Nagy, K.; Tiuca, I.-D. Importance of Fatty Acids in Physiopathology of Human Body. In *Fatty*

*Acids*; Catala, A., Ed.; IntechOpen, 2017; Vol. 32, pp 137–144.

https://doi.org/10.5772/67407.

(75)    Boden, G. Fatty Acid - Induced Inflammation and Insulin Resistance in Skeletal Muscle and

Liver. *Curr. Diab. Rep.* **2006**, *6* (3), 177–181. https://doi.org/10.1007/s11892-006-0031-x.

(76)    Haeri, H. H.; Schunk, B.; Tomaszewski, J.; Schimm, H.; Gelos, M. J.; Hinderberger, D. Fatty

Acid Binding to Human Serum Albumin in Blood Serum Characterized by EPR

Spectroscopy. *ChemistryOpen* **2019**, *8* (5), 650–656.

https://doi.org/10.1002/open.201900113.

(77)    Brouwers, H.; Von Hegedus, J.; Toes, R.; Kloppenburg, M.; Ioan-Facsinay, A. Lipid

Mediators of Inflammation in Rheumatoid Arthritis and Osteoarthritis. *Best Pract. Res.*

*Clin. Rheumatol.* **2015**, *29* (6), 741–755. https://doi.org/10.1016/j.berh.2016.02.003.

(78)    Visioli, F.; Poli, A. Fatty Acids and Cardiovascular Risk. Evidence, Lack of Evidence, and

Diligence. *Nutrients* **2020**, *12* (12), 1–19. https://doi.org/10.3390/nu12123782.

(79)    Huber, A. H.; Kampf, J. P.; Kwan, T.; Zhu, B.; Adams, J.; Kleinfeld, A. M. Usefulness of

Serum Unbound Free Fatty Acid Levels to Predict Death Early in Patients with St-Segment

Elevation Myocardial Infarction (from the Thrombolysis in Myocardial Infarction [TIMI] II

Trial). *Am. J. Cardiol.* **2014**, *113* (2), 279–284.

https://doi.org/10.1016/j.amjcard.2013.08.057.

(80)    Kidd, P. M. Omega-3 DHA and EPA for Cognition, Behavior, and Mood: Clinical Findings

and Structural-Functional Synergies with Cell Membrane Phospholipids. *Altern. Med. Rev.*

**2007**, *12* (3), 207–227.

(81)    Uauy, R.; Calderon, F.; Mena, P. Essential Fatty Acids in Somatic Growth and Brain

Development. *World Rev. Nutr. Diet.* **2001**, *89* (9), 134–160.

https://doi.org/10.1159/000059785.

(82)   Sureda, A.; Martorell, M.; Bibiloni, M. del M.; Bouzas, C.; Gallardo-Alfaro, L.; Mateos, D.;

Capó, X.; Tur, J. A.; Pons, A. Effect of Free Fatty Acids on Inflammatory Gene Expression

and Hydrogen Peroxide Production by Ex Vivo Blood Mononuclear Cells. *Nutrients* **2020**,

*12* (1). https://doi.org/10.3390/nu12010146.

(83)   Lee, P.; Wu, X. Review: Modifications of Human Serum Albumin and Their Binding Effect.

*Curr Pharm Des.* **2015**, *21* (14), 1862–1865.

https://doi.org/10.2174/1381612821666150302115025.

(84)   Kitamura, K.; Takegami, S.; Tanaka, R.; Omran, A. A.; Kitade, T. Effect of Long-Chain Fatty

Acids on the Binding of Triflupromazine to Human Serum Albumin: A Spectrophotometric

Study. *Sci. Pharm.* **2014**, *82* (2), 233–245. https://doi.org/10.3797/scipharm.1310-23.

(85)   Yamasaki, K.; Hyodo, S.; Taguchi, K.; Nishi, K.; Yamaotsu, N.; Hirono, S.; Tuan, V.; Chuang,

G.; Seo, H.; Maruyama, T.; Otagiri, M. Long Chain Fatty Acids Alter the Interactive Binding

of Ligands to the Two Principal Drug Binding Sites of Human Serum Albumin. **2017**, 1–15.

(86)   Paál, K.; Müller, J.; Hegedûs, L. High Affinity Binding of Paclitaxel to Human Serum

Albumin. *Eur. J. Biochem.* **2001**, *268* (7), 2187–2191. https://doi.org/10.1046/j.1432-

1327.2001.02107.x.

(87)   Petitpas, I.; Gru, T.; Bhattacharya, A. A.; Curry, S. Crystal Structures of Human Serum

Albumin Complexed with Monounsaturated and Polyunsaturated Fatty Acids. **2001**, 955–

960. https://doi.org/10.1006/jmbi.2001.5208.

(88)   Simard, J. R.; Zunszain, P. A.; Ha, C. E.; Yang, J. S.; Bhagavan, N. V.; Petitpas, I.; Curry, S.;

Hamilton, J. A. Locating High-Affinity Fatty Acid-Binding Sites on Albumin by x-Ray Crystallography and NMR Spectroscopy. *Proc. Natl. Acad. Sci. U. S. A.* **2005**, *102* (50), 17958–17963. https://doi.org/10.1073/pnas.0506440102.

(89)   Krenzel, E. S.; Chen, Z.; Hamilton, J. A. Correspondence of Fatty Acid and Drug Binding Sites on Human Serum Albumin: A Two-Dimensional Nuclear Magnetic Resonance Study. **2013**. https://doi.org/10.1021/bi301458b.

(90)   Fujiwara, S. I.; Amisaki, T. Identification of High Affinity Fatty Acid Binding Sites on Human Serum Albumin by MM-PBSA Method. *Biophys. J.* **2008**, *94* (1), 95–103. https://doi.org/10.1529/biophysj.107.111377.

(91)   Curry, S.; Mandelkow, H.; Brick, P.; Franks, N. Crystal Structure of Human Serum Albumin Complexed with Fatty Acid Reveals an Asymmetric Distribution of Binding Sites. *Nat. Struct. Biol.* **1998**, *5* (9), 827–835. https://doi.org/10.1038/1869.

(92)   Goodman, D. W. S. The Interaction of Human Serum Albumin with Long-Chain Fatty Acid Anions. *J. Am. Chem. Soc.* **1958**, *80* (15), 3892–3898. https://doi.org/10.1021/ja01548a024.

(93)   Musteata, F. M.; Pawliszyn, J. Study of Ligand-Receptor Binding Using SPME: Investigation of Receptor, Free, and Total Ligand Concentrations. *J. Proteome Res.* **2005**, *4* (3), 789–800. https://doi.org/10.1021/pr049768z.

(94)   PEDERSEN, A. O.; HUST, B.; ANDERSEN, S.; NIELSEN, F.; BRODERSEN, R. Laurate Binding to Human Serum Albumin: Multiple Binding Equilibria Investigated by a Dialysis Exchange Method. *Eur. J. Biochem.* **1986**, *154* (3), 545–552. https://doi.org/10.1111/j.1432-1033.1986.tb09433.x.

(95)    Hamacek, J.; Piguet, C. How to Adapt Scatchard Plot for Graphically Addressing

Cooperativity in Multicomponent Self-Assemblies. *J. Phys. Chem. B* **2006**, *110* (15), 7783–

7792. https://doi.org/10.1021/jp056932c.

(96)    Jeon, J.; Lee, K. H.; Rao, J. A Strategy to Enhance the Binding Affinity of Fluorophore–

Aptamer Pairs for RNA Tagging with Neomycin Conjugation. *Chem. Commun.* **2012**, *48*

(80), 10034–10036. https://doi.org/10.1039/c2cc34498j.

(97)    Richieri, G. V.; Ogata, R. T.; Kleinfeld, A. M. A Fluorescently Labeled Intestinal Fatty Acid

Binding Protein. Interactions with Fatty Acids and Its Use in Monitoring Free Fatty Acids. *J.

Biol. Chem.* **1992**, *267* (33), 23495–23501. https://doi.org/10.1016/s0021-9258(18)35866-

6.

(98)    Fredholm, B. B.; Rane, A.; Persson, B. Diphenylhydantoin Binding to Proteins in Plasma and

Its Dependence on Free Fatty Acid and Bilirubin Concentration in Dogs and Newborn

Infants. *Pediatr. Res.* **1975**, *9* (1), 26–30. https://doi.org/10.1203/00006450-197501000-

00005.

(99)    Ebden, P.; Leopold, D.; Smith, A. P.; Buss, D.; Routledge, P. A. Free and Total Plasma

Theophylline Concentrations in Chronic Airflow Obstruction. *Thorax* **1984**, *39* (5), 352–

355. https://doi.org/10.1136/thx.39.5.352.

(100)   Zhu, T. T.; Zhang, Y.; Luo, X. A.; Wang, S. Z.; Jia, M. Q.; Chen, Z. X. Difference in Binding of

Long- and Medium-Chain Fatty Acids with Serum Albumin: The Role of Macromolecular

Crowding Effect. *J. Agric. Food Chem.* **2018**, *66* (5), 1242–1250.

https://doi.org/10.1021/acs.jafc.7b03548.

(101)   Pawliszyn, J. *Handbook of Solid Phase Microextraction*, 1st editio.; Chemical Industry

Press: Beijing, 2009. https://doi.org/10.1016/C2011-0-04297-7.

(102) Capelli, D.; Parravicini, C.; Pochetti, G.; Montanari, R.; Temporini, C.; Rabuffetti, M.; Trincavelli, M. L.; Daniele, S.; Fumagalli, M.; Saporiti, S.; Bonfanti, E.; Abbracchio, M. P.; Eberini, I.; Ceruti, S.; Calleri, E.; Capaldi, S. Surface Plasmon Resonance as a Tool for Ligand Binding Investigation of Engineered GPR17 Receptor, a G Protein Coupled Receptor Involved in Myelination. *Front. Chem.* **2020**, *7* (January), 1–14. https://doi.org/10.3389/fchem.2019.00910.

(103) Rowland, A.; Hallifax, D.; Nussio, M. R.; Shapter, J. G.; Mackenzie, P. I.; Houston, J. B.; Knights, K. M.; Miners, J. O. Characterization of the Comparative Drug Binding to Intra- (Liver Fatty Acid Binding Protein) and Extra- (Human Serum Albumin) Cellular Proteins. *Xenobiotica* **2015**, *45* (10), 847–857. https://doi.org/10.3109/00498254.2015.1021403.

(104) Maclek-Jurczyk, M.; Sułkowska, A.; Bojko, B.; Równicka-Zubik, J.; Szkudlarek-Haśnik, A.; Zubik-Skupień, I.; Góra, A.; Dubas, M.; Korzonek-Szlacheta, I.; Wielkoszyński, T.; Urawiński, W.; Sosada, K. The Influence of Fatty Acids on Theophylline Binding to Human Serum Albumin. Comparative Fluorescence Study. *Spectrochim. Acta - Part A Mol. Biomol. Spectrosc.* **2012**, *89*, 270–275. https://doi.org/10.1016/j.saa.2011.12.035.

(105) Richieri, G. V.; Kleinfeld, A. M. Unbound Free Fatty Acid Levels in Human Serum. *J. Lipid Res.* **1995**, *36* (2), 229–240. https://doi.org/10.1016/s0022-2275(20)39899-0.

(106) Huber, A. H.; Kleinfeld, A. M. Unbound Free Fatty Acid Profiles in Human Plasma & the Unexpected Absence of Unbound Palmitoleate. *J. Lipid Res.* **2017**, *58* (3), 578–585. https://doi.org/10.1194/jlr.M074260.

(107) Stewart, J. M.; Driedzic, W. R.; Berkelaar, J. A. M. Fatty-Acid-Binding Protein Facilitates the

Diffusion of Oleate in a Model Cytosol System. *Biochem. J.* **1991**, *275* (3), 569–573.

https://doi.org/10.1042/bj2750569.

(108)  Zenei, T.; Hiroshi, T. Specific and Non-Specific Ligand Binding to Serum Albumin. *Biochem.*

*Pharmacol.* **1985**, *34* (11), 1999–2005. https://doi.org/10.1016/0006-2952(85)90322-3.

(109)  PEDERSEN, A. O.; HUST, B.; ANDERSEN, S.; NIELSEN, F.; BRODERSEN, R. Laurate Binding to

Human Serum Albumin: Multiple Binding Equilibria Investigated by a Dialysis Exchange

Method. *Eur. J. Biochem.* **1986**, *154* (3), 545–552. https://doi.org/10.1111/j.1432-

1033.1986.tb09433.x.

(110)  Spector, A. A. Fatty Acid Binding to Plasma Albumin. *J. Lipid Res.* **1975**, *16* (3), 165–179.